University of Alabama
Bureau of Engineering Research
University, Alabama

AN EXPERIMENTAL STUDY OF MOLECULAR SURFACE INTERACTIONS AT VELOCITIES UP TO AND EXCEEDING SPACE PROBE ESCAPE VELOCITIES

Final Report
Contract NAS8-5326
June 15, 1966

by

Dr. Walter J. Schaetzle
Professor of Mechanical Engineering
Project Director

Prepared for

George C. Marshall Space Flight Center
Huntsville, Alabama

TABLE OF CONTENTS

LIST OF FIGURES

LIST OF FIGURES (Continued)

LIST OF FIGURES (Continued)

LIST OF TABLES

LIST OF SYMBOLS

= Areas

= Mean square molecule velocity

= Average molecule velocity

= Modulus of elasticity

= Momentum

= Molecule mass

= Molecule density per unit time and area

= Pressure due to incoming molecules

= Pressure due to reflected molecules

= Pressure due to reflected molecules if in equilibrium with surface

= Probability of molecule transmission through nozzle

= Pressure differential

= Radius (tank, flange, etc.)

= Skin thickness

= Molecule distribution angle at exit of nozzles

= Poisson's ratio

= Solid angle

= Tensile stress

= Tangential accommodation coefficient

= Normal accommodation coefficient

= Incidence angle of molecules on surface (Fig. 61)

I. INTRODUCTION

Essentially no data exists on the momentum accommodation coefficients. Experimental data of this type is required to calculate the drag on space probes, boosters, and even to calibrate instrumentation to accurately control these vehicles. References 1 through 6* give a survey of experimental work towards this type of data. The only accommodation coefficients directly measured to date are the thermal coefficients. To determine momentum coefficients only, the directions of the reflected molecules have been measured. There was no data presented in the area of directly measuring the momentum accommodation coefficients at the Fourth International Symposium held at Toronto, Canada, in 1964. To the best of the author's knowledge, this is still the only work directly orientated in this direction.

In order to acquire date of this type in the proper velocity ranges, the Bureau of Engineering Research at the University of Alabama proposed to set up experimental apparatus to acquire this type of data (7,8,9). The original proposal recommended a three year program, and the program was actively funded for two and one-half years with a six-month-no-cost extension. This report discusses the effort made on the project, describing the equipment and results. Over 90% of the original criteria have been completed and the equipment constructed and operating.

*Numbers refer to references at the end of the report.

The basic object of the project was to measure the statistical interaction of forces between individual molecules and surfaces, and reduce the results to accommodation coefficients. This is to be done by impinging a molecular beam on surfaces and by measuring the normal forces and tangential forces independently through a unique probe setup.

The design criteria for the project, appreciably upgraded from the original proposal, are

a. Particle velocities from 4 km/sec. to 50 km/sec.

b. Particle energies from 4 to 1000 ev/molecule

c. Beam intensity of 10^{10} to 10^{16} molecules/sec.

d. Beam density of 10^{12} to 10^{18} molecules/sec. cm^2

e. Beam diameter of 0.2 mm to 1 mm

f. Beam current of 10^{-11} to 10^{-4} amperes

g. Pumping rates in excess of 25,000 liters/sec.

h. Pressures in the primary tank to be below 10^{-8} mm Hg.

To match these requirements, improvements are still required in the lower velocity and energy ranges. Minimum energies attained were approximately 60 ev/molecule. Accurate measurements of actual beam diameters have not been made and the minimum attainable pressure has been 1.5×10^{-8} mm Hg. In all other areas the original equipment goals have been exceeded.

The final data is limited due to the project cutoff date, but some low speed data is included. During the project, three papers directly related to problems and progress in the development of the project were presented (10, 11, 12). Also, one paper in the field

indirectly related to the project was presented (13). A fifth paper in preparation will be submitted for publication in the near future (14).

An indirect result of the project is the technical knowledge and financial support received by students working on the project. The list of students employed by the project is given in Appendix I. Otherwise, a number of students benefited through use of the equipment and knowledge towards work on undergraduate papers, master's theses, and a doctoral dissertation. A large percentage of the work by these students was basically a donation to the project. At present, a student is at work turning out a set of production data for accommodation coefficients as a master's thesis. A doctoral dissertation for the final instrumentation and production data for the high velocity molecules is being initiated. The data from the last two student studies will be published and would exceed all the goals of the project.

The total technical hours spent on the project are:

Project Director (Dr. Walter J. Schaetzle)	2128 hours
Graduate Student Research Assistants	3659 hours
Undergraduate Research Assistants	5655 hours
TOTAL	11442 hours

The following sections describe the tankage, pumping systems, the force probes, the low velocity calibration flows, the molecular accelerator and the results.

II. TANKAGE AND PUMPING SYSTEMS

The tankage and pumping systems are designed to reach the required pressures, be capable of providing the required pumping rates, be sufficiently large to contain the apparatus, and be suitable for some expansion. The basic tankage is broken into two parts; the first part containing the apparatus for forming a molecular beam, and the second part containing the equipment for measuring the forces. The setup is shown in Fig. 1.

Since two independent tanks are utilized, specific pressure requirements are required for each tank. The primary tank with the measuring equipment requires a pressure which will allow the surfaces to decontaminate of surface gases and remain in the decontaminated state for long periods of time. The gaseous layer normally does not form under 10^{-7} mm Hg, so the final design pressure chosen is below 10^{-8} mm Hg. As a result this tank is designed for fairly high temperature ranges to allow degassing. The temperature chosen for this purpose was 500°F. (Discussed in degassing section II.B.). The pressure in the secondary tank has to be designed so negligible collisions occur between gas molecules to eliminate interference with the molecular beams. The mean free path length for air molecules is approximately 8 cm at 1 micron. Desiring a mean free path over ten times the maximum beam length of approximately 150 cm results in a pressure of 5×10^{-6} mm Hg or less. To achieve this pressure no degassing is required. The upper temperature limit set for this tank was 120°F, which could occur when the second tank is being degassed in the adjacent position.

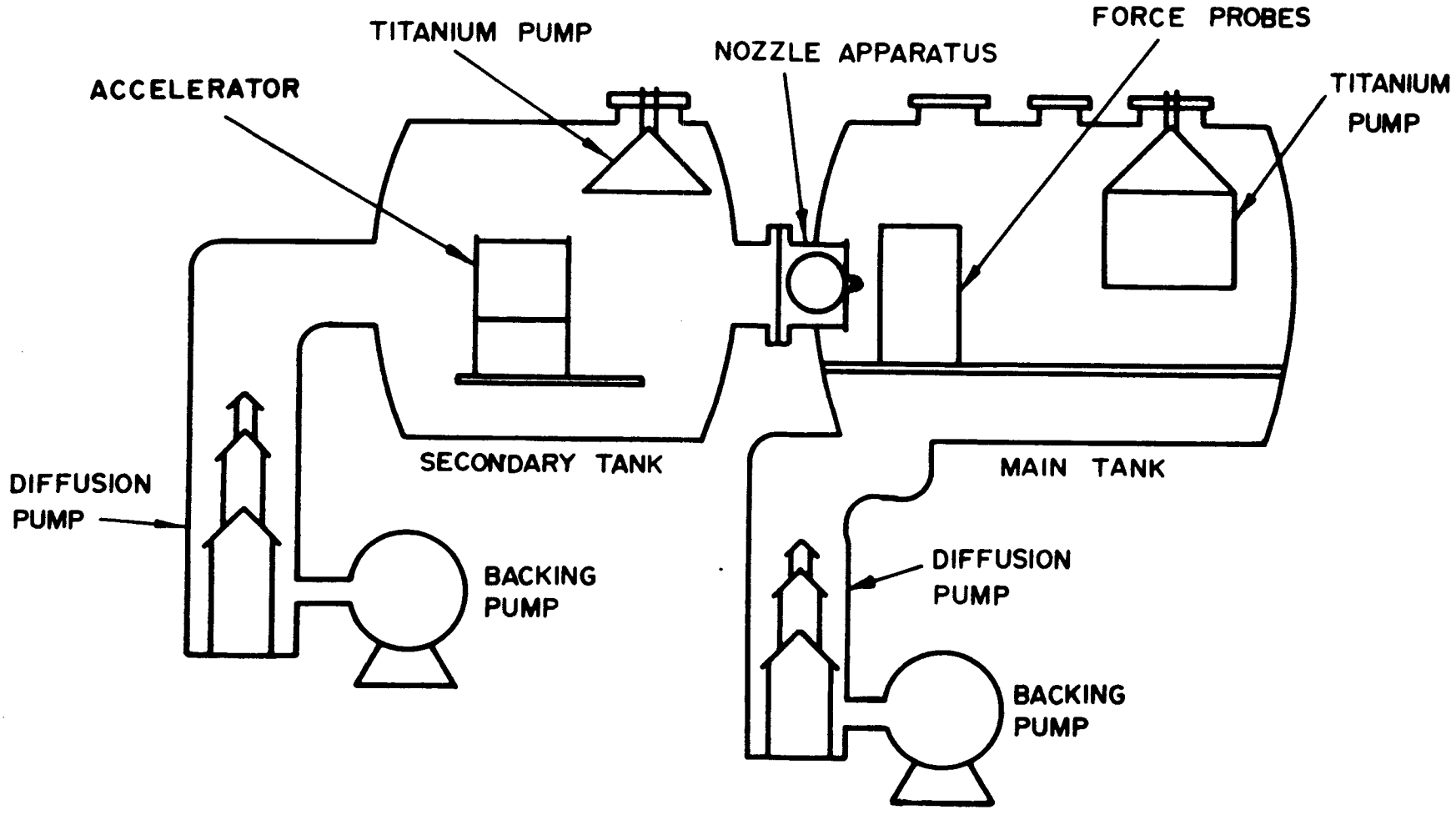

FIG. 1 OVERALL SYSTEM

The original requirements for pumping speeds are shown in Fig. 2. The pumping requirement for the secondary tank used a diffusion pumping system only, and the primary tank system was to use two ion pumps in parallel with a diffusion pumping system. Due to the high cost of the ion pumping systems, they were replaced by a titanium system, the degassing requirement lowered, and the overall pumping requirements raised over the original rates. The final goal, which was exceeded, is 25,000 liters/sec for the total of both systems. The pumping rate of the titanium system in the primary tank has been measured at over 25,000 liters N_2/sec. The pumping rate for the system in the secondary tank was not measured, but is designed for over 10,000 liters/sec. and is assumed to be operating in this range. A complete discussion of the pumping systems is given in section II.D.

The size of the tanks is determined by the required internal equipment. The primary tank size was determined by estimated probe stand size. Since the reflection of molecules from the probe will eventually be measured, the distance of a rotating, measuring tube from the surface probe will become the critical factor. The radius available for this purpose should be over one foot, so the overall tank diameter was determined as 3 ft. An overall length of 4 ft. was arbitrarily chosen to go with this diameter to provide space for the internal equipment. The secondary tank was acquired as surplus, the dimensions thereby given as 3 ft. in diameter and 3 ft. long.

The flange requirements are to provide physical, viewing, pump, gage and electrical access. Each tank has a main physical and viewing port 2 ft. in diameter, the size primarily determined by access requirements. Information after construction indicated a smaller port

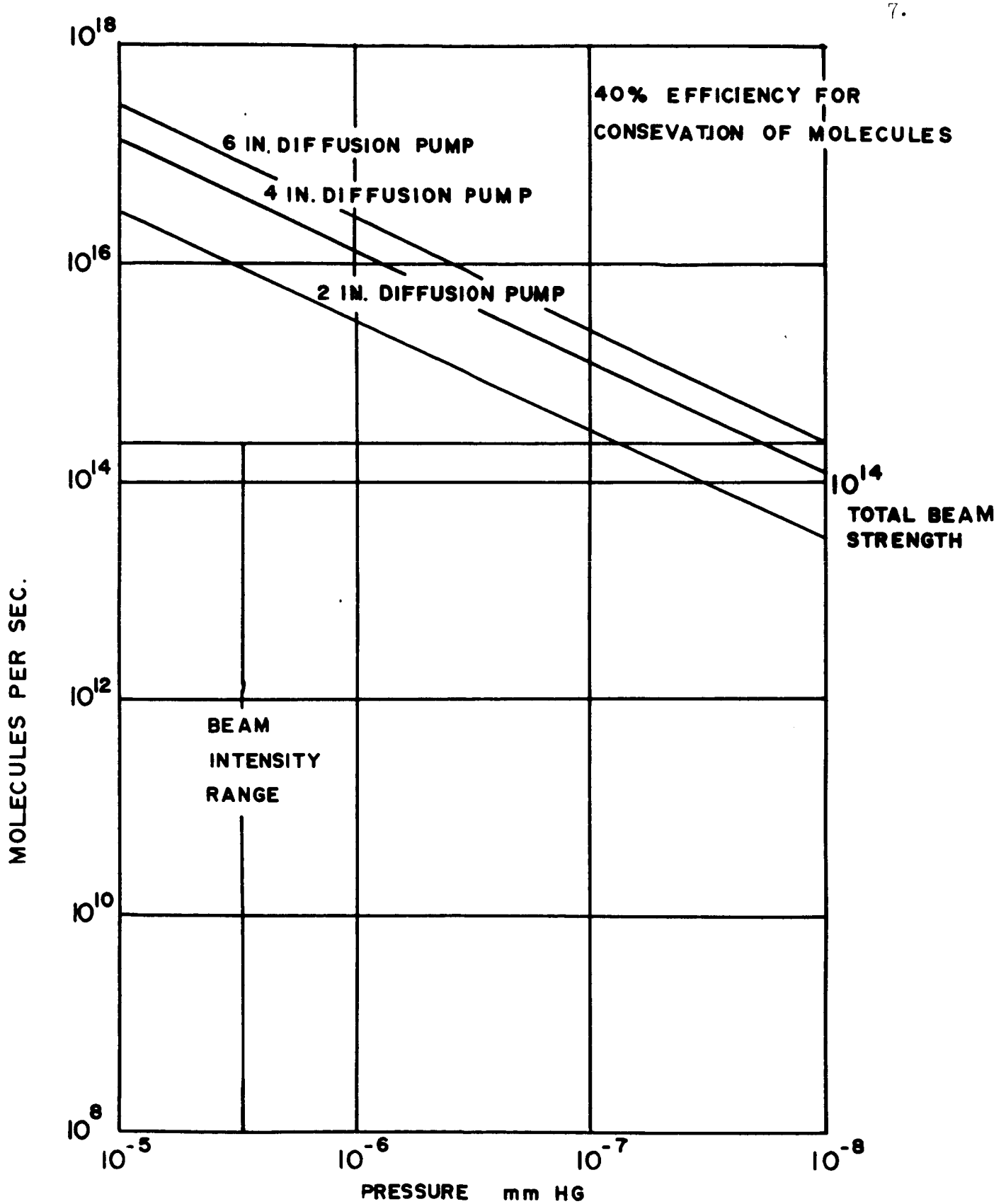

FIG. 2 PRELIMINARY PUMPING SPEEDS AND REQUIREMENTS

designed for a 2 ft, diameter window would have been better, as the windows are much easier to acquire in a 2 ft. diameter than a specially made 26 inch port. The secondary tank also has a port for connecting to the primary tank, a port for connecting to the diffusion pump system, a port for the coolant inlet for the titanium pump system, a port for gas entries, and a port for a viewing gauge. The primary tank has two ports for ion pumps, a port for diffusion pump systems, a port for electrical inlets, two special viewing ports, a port for electrical inlets, and a port for an ion gage.

All high vacuum seals were made using single rubber o-rings. These seals allow unlimited access without changing seals and hold a good vacuum with minimum care. The seals are the most inexpensive method of sealing and resealing. This allowed the use of standard o-rings for the original work and an upgrading of the system for 500°F degassing through a change to silicone rubber o-rings.

Copper seals were also given consideration, but the replacement cost after each tank opening, especially the 24 inch port, is prohibitive. A Varian electrical feed-through, being used with a titanium pump, uses copper seals and has been known to leak when the seals were not replaced after being opened.

The design of the tanks and pumping systems are made to satisfy the given requirements on pumping rates, pressure, the related temperature, physical access, and viewing access.

A. Tankage

Sketches of the final tankage are shown in Figs. 3 and 4. The primary tank (Fig. 3) is a new tank specifically constructed for the

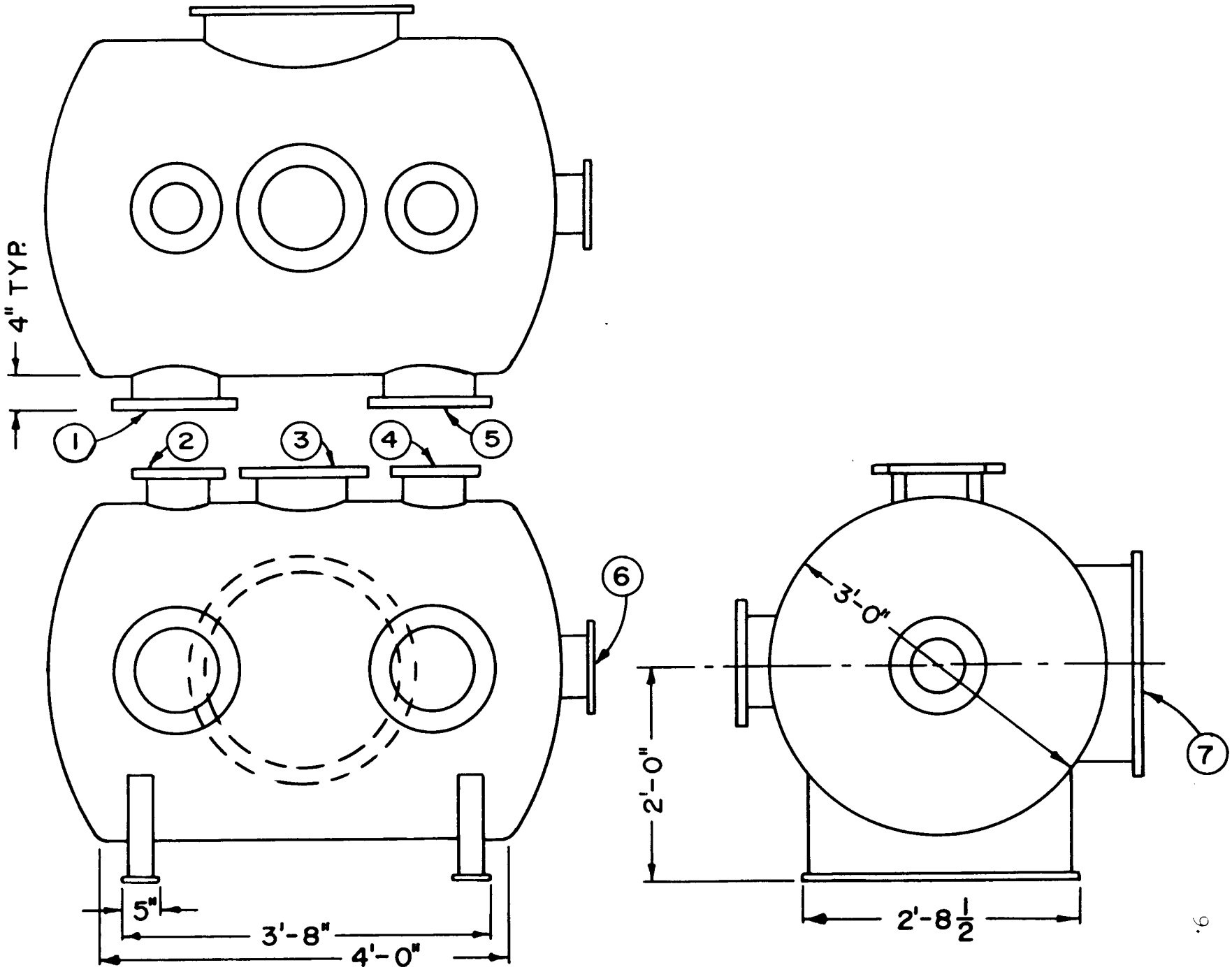

FIG. 3 PRIMARY TANK

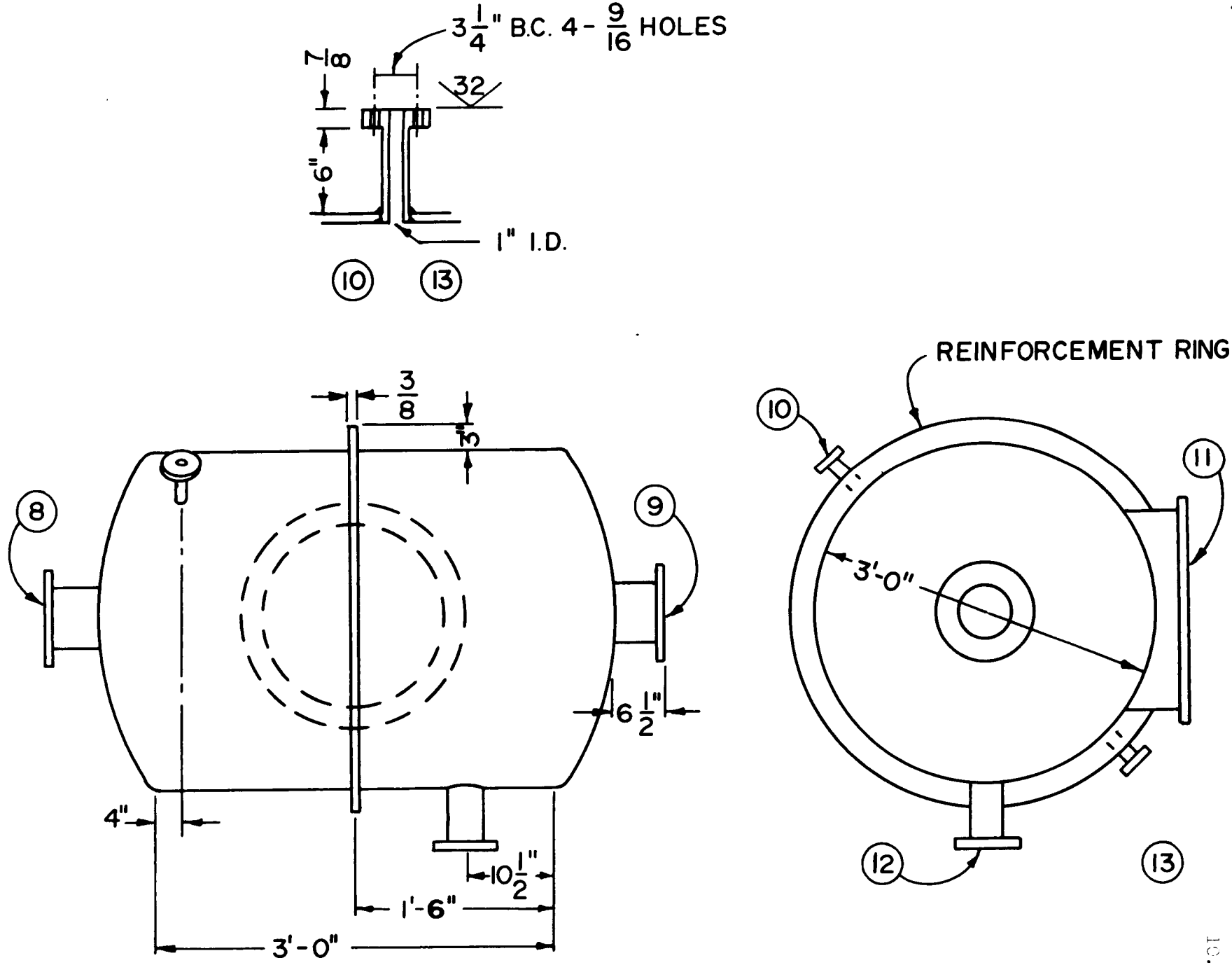

FIG. 4 SECONDARY TANK

project. It is made of 1/2 inch thick 304 low carbon content stainless steel. The secondary tank (Fig. 4) was acquired as surplus and modified. It is basically 3/16 inch stainless steel with slightly thicker elliptical ends. For additional strength it has a supporting ring around the center, but still is not designed for high temperature degassing.

Fig. 5 shows a sketch of the ports on the various tanks (related by alphabetical letters and numerical numbers to Figs. 3 and 4). They all have single o-ring seals and corresponding bolted flanges. The numerous bolt holes allow possible future use of the tanks as pressure vessels. Since both large ports are identical in size, the tanks can be joined by these ports as well as the smaller end ports. Original designs called for tank diameter end ports; however, these were eliminated for budgetary considerations and for slightly larger side ports.

1). Tank Stresses

The basic mechanism in vacuum tank failure is buckling. Neglecting the buckling, stresses in a satisfactory tank normally do not exceed 10% of the failure stress limits. After a brief survey which indicated this phenomena, stress considerations were limited to the buckling. Most basic textbooks cover the analytical phase of this subject in detail for infinite length to diameter ratio with little emphasis on the complicated end effects. The investigation follows the textbook version, with final adjustments for end effects from the ASME Boiler Construction code. The second major problem is finding sufficient data at the elevated temperatures. Stress data is available in numerous temperature ranges; however, the modulus of elasticity data is found only for limited temperature regimes.

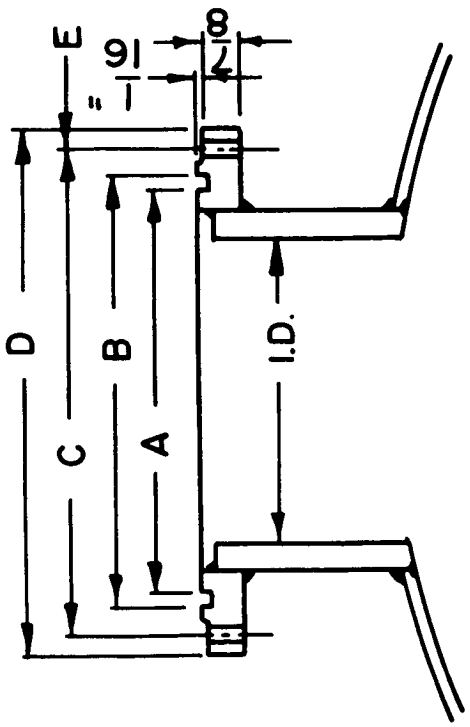

FLANGE	A	B	C	D	E	I.D.
1·3·5	11.496±.001	12.246	13 3/8 B.C.	14 1/2	16-9/16 HOLES	10"
2·4·6·8·9	7.246	7.996	9 1/8	10 1/4	12-9/16"	6"
7·11	23.995	24.745	25 7/8	27	28-9/16"	23"
12	4246	4.627	6	17 1/2	4-3/4"	3 1/4"

FIG. 5 FLANGE DIMENSIONS

The critical stress for an infinite length thin-walled cylinder under buckling (15) is given as

$$\sigma_{Crit.} = \frac{E}{1-\mu^2}\left(\frac{t}{d}\right)^2 \Delta P$$

Based on this limit for stainless steel and aluminum, the tank thickness for an infinite length tank with a safety factor of 5 is given in Fig. 6. The three-foot diameter stainless steel tank requires a skin thickness of 0.325 inches. To this figure must be added additional loads, such as pumps and other equipment attached directly to the flanges. Future use includes liquid nitrogen and even possibly liquid helium, which will provide additional thermal stress.

The ASME Code (16) for a 3 foot diameter by 4 foot-long tank gives the required thickness at 500°F as 0.288 inches. The code uses a 5 safety factor with an external minimum load of 60 psi. Using the basic form of the above theoretical equation, this would result in a overall safety factor of 40 for the primary tank with a skin thickness of 0.5 inches. However, the internal tank surface has been completely ground, sanded and polished, subtracting from the wall thickness. The exact change is not known, but a safe estimate is that less than 0.1 inches has been removed.

The ASME code for 3 ft. diameter by 3 foot long tank at 500°F requires a 0.252 inch wall thickness with required 60 psi external load. However, with an external load of only 15 psi, still including a 5 safety factor, the required skin thickness is reduced to .1285 inches. Comparing with the tank thickness of 0.1875 inch and the basic equation ratios for an infinite length to diameter tank, this gives an overall safety factor in excess of 15.5 for the basic

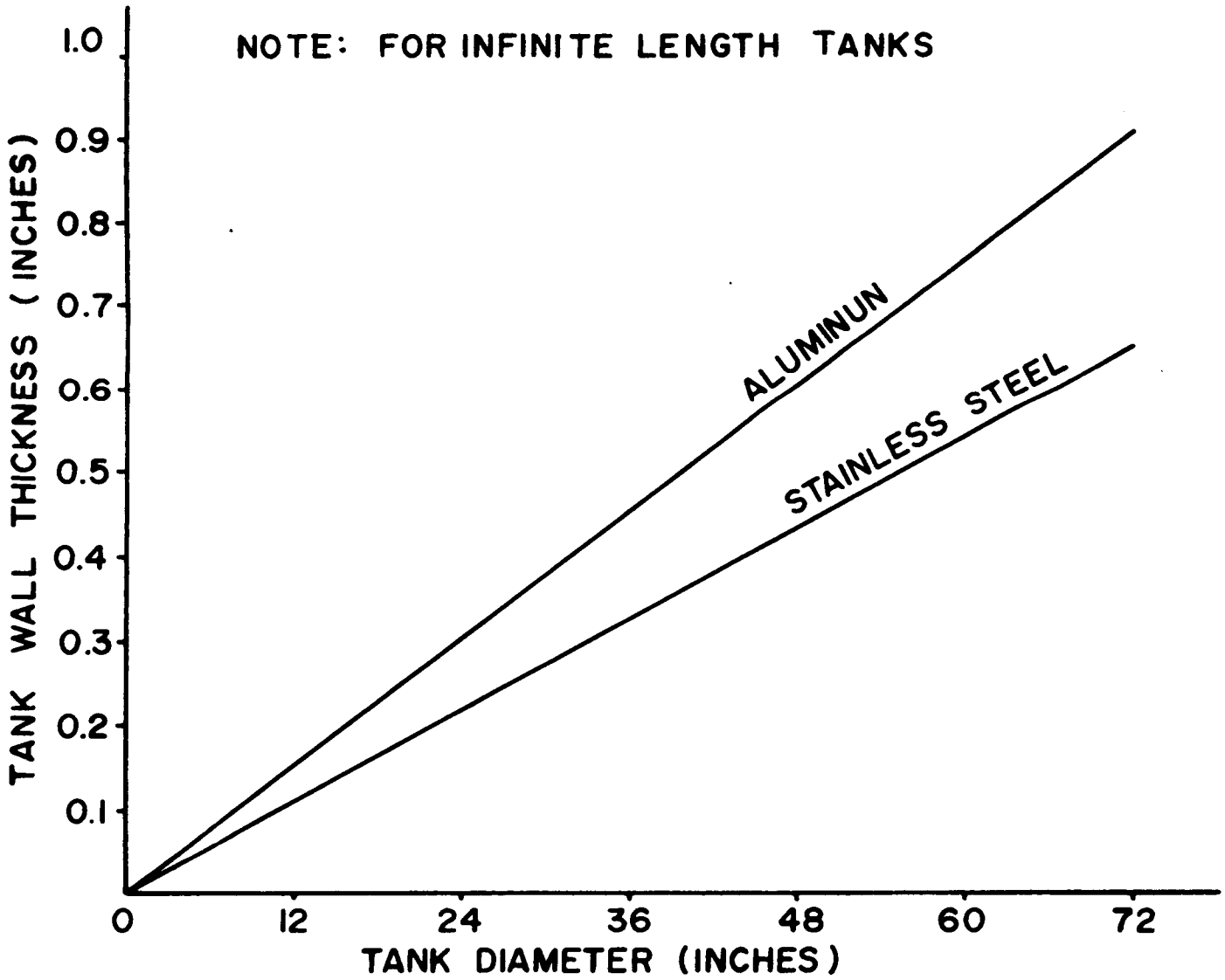

FIG. 6 TANK THICKNESS

secondary tank. However, to bring the tank within the code, an additional stress ring has been added around the center of the tank. The secondary tank is not heated for degassing purposes.

2). Plate Stresses

The plate thickness requirements (port covers) were calculated, using

$$\sigma_{Max} = \frac{3}{4}\left(\frac{r}{t}\right)^2 \Delta P$$

For a safety factor of 5 and extrapolating data to the required temperature, the radius to thickness ratio for a few materials are given in Table I.

Table I - Required Flange Radius to Thickness Ratios

Material	r/t	Temperature
Stainless Steel	18.4	500°F
Quartz	8.4	500°F
Pyrex Glass	13.3	72°F
Plastic*	8.4	200°F

*Uses extrapolated data

Original plans called for quartz windows and some stainless covers, with plans to degas at 500°F. Budgetary requirements limited original operations to plastic windows for smaller ports, and pyrex glass for the main 24 inch port. After failure of a 24 inch pyrex cover, all covers were converted to plastic. The failure is discussed in the next section.

The final thicknesses of the covers for each port are given in Table II.

Table II - Plastic Port Hole Cover Thickness

Port Diameter (Inches)	Plate Thickness (Inches)
24	3
10	1.5
6	1
3	1

3). Pyrex Plate Failure

For one of the original pump-downs a 24 inch pyrex plate one inch thick failed. The failure occurred on the fourth or fifth pump-down, with the temperature approximately 75°F. The tank had a leak and a slow trial by error technique was being used to find the leak. During the removal and replacement of some electrical lead-ins, the flange holding the pyrex glass was also tightened. Upon pump-down at a pressure between 5 and 1 mm Hg the cover failed. The implosion also damaged 4 smaller covers, an ion gage tube and possibly a backing pump. The pump required overhauling before again pumping below 10^{-1} mm Hg.

Most of the glass was pulverized into fine dust which could be rubbed through the fingers without cutting. A number of splinters also penetrated the stainless steel and had to be removed by grinding. The explosion after the implosion also implanted some splinters in a door 20 feet from the tank. Luckily no personnel were in the tank room or outside in line with the door at the time. The event took place at 12:30 A.M. The magnitude of the event can best be described by noting that two students who were on the floor above thought the building was collapsing for a few moments. Except for these students and the project director in an adjoining room, the event went unnoticed.

From an analysis of the event, it was concluded that the

tightening of the flange produced a stress concentration in the window. This concentration along with the pressure force caused failure. The flange which was straightened had been warped by approximately 1/2 inch from side to side.

The replacement of pyrex glass windows with plastic eliminated all possibilities of the stress concentrations. All safety factors are in excess of 12 for these windows.

B. Degassing

From an investigation of references 17 and 18 and a set of literature from Consolidated Vacuum Corporation, it was concluded that a maximum temperature requirement to reach 10^{-9} mm Hg would be 500°F. Original plans were to uprate the covers and o-rings to this temperature on the primary tank; however, budgetary requirements eliminated the uprating. The primary tank is being degassed between 180 and 190°F, which results in over an order of magnitude in attainable pressure.

To degas the tank, two prime systems were investigated, both of which have been shown to give satisfactory results. The first system applied resistance wire to the tank and the second used radiation lamps.

The wire is shown in part "a" of Fig. 7. In the tests the wire had been soft soldered (520°F. solder) to steel plates. Within 10 minutes the plates could be heated to 500°F with the solder melted. In attempts to silver solder and braze the braided wire to plates, the braid melted or became brittle. The explanation is that the fine braid has no heat capacity and quickly approaches the flame temperature.

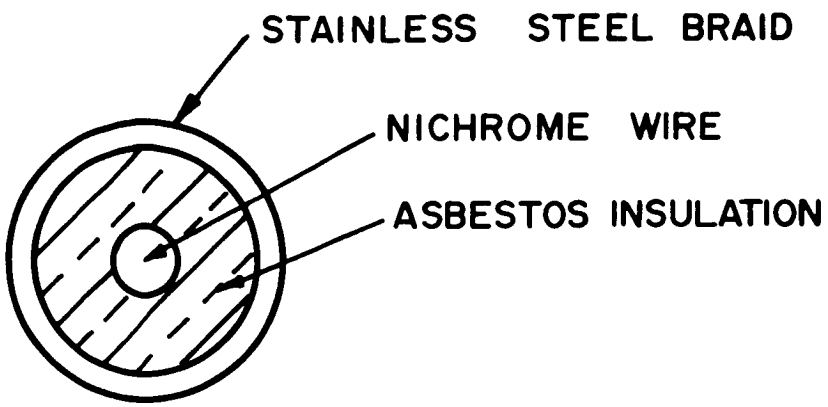

a. WIRE

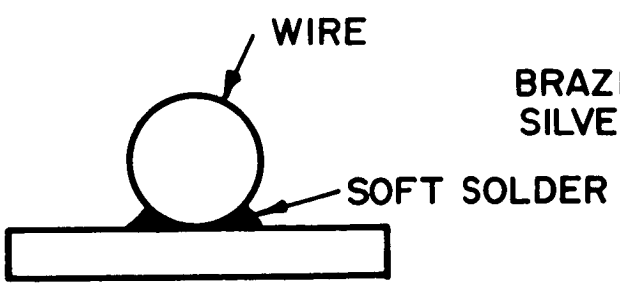

b. BASIC EXPERIMENTS

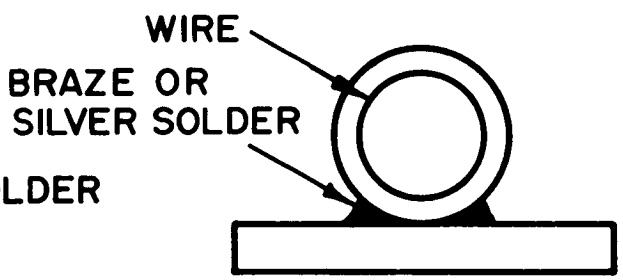

c. PROPOSED SYSTEM

FIG. 7 RESISTANCE WIRE HEATING EXPERIMENTS

This could be overcome by using a furnace, but a furnace of sufficient size for the tank is not available. A second remedy which worked in some small experiments is to place the braided wire in a tight-fitting copper tube which can be brazed to the tank. Some experimental work along this line has produced successful results.

The radiation lamps were tried on a full scale tank. A number of interesting results developed.

1). Over 60% of the heat loss at 250°F was determined to be due to radiation.

2). The overall stainless tanks are very poor conductors. On the secondary tank over 100°F differences occurred in distances under one foot under steady state condidtions.

3). Over 50 kw in lamp heating would be required to reach 500°F.

4). The time required to reach 90% of steady state was less than one hour. On these tests the lamps were 500-watt quartz bulbs from army aircraft wing deicing heaters. Since these radiation lamps were available, 16 kw are being used to degas the primary tank at 180 to 190°F.

C. Electrical Feedthroughs

The electrical feedthroughs were made of brass or aluminum, with an o-ring seal as shown in Fig. 8. The primary tank has 36 feedthroughs available and the secondary tank has 19 available. To date no known leaks have occurred at an electrical feedthrough. The units have demonstrated the capability of carrying up to 30 amperes.

D. Pumping Systems

The pumping system is centered around two titanium pumping units

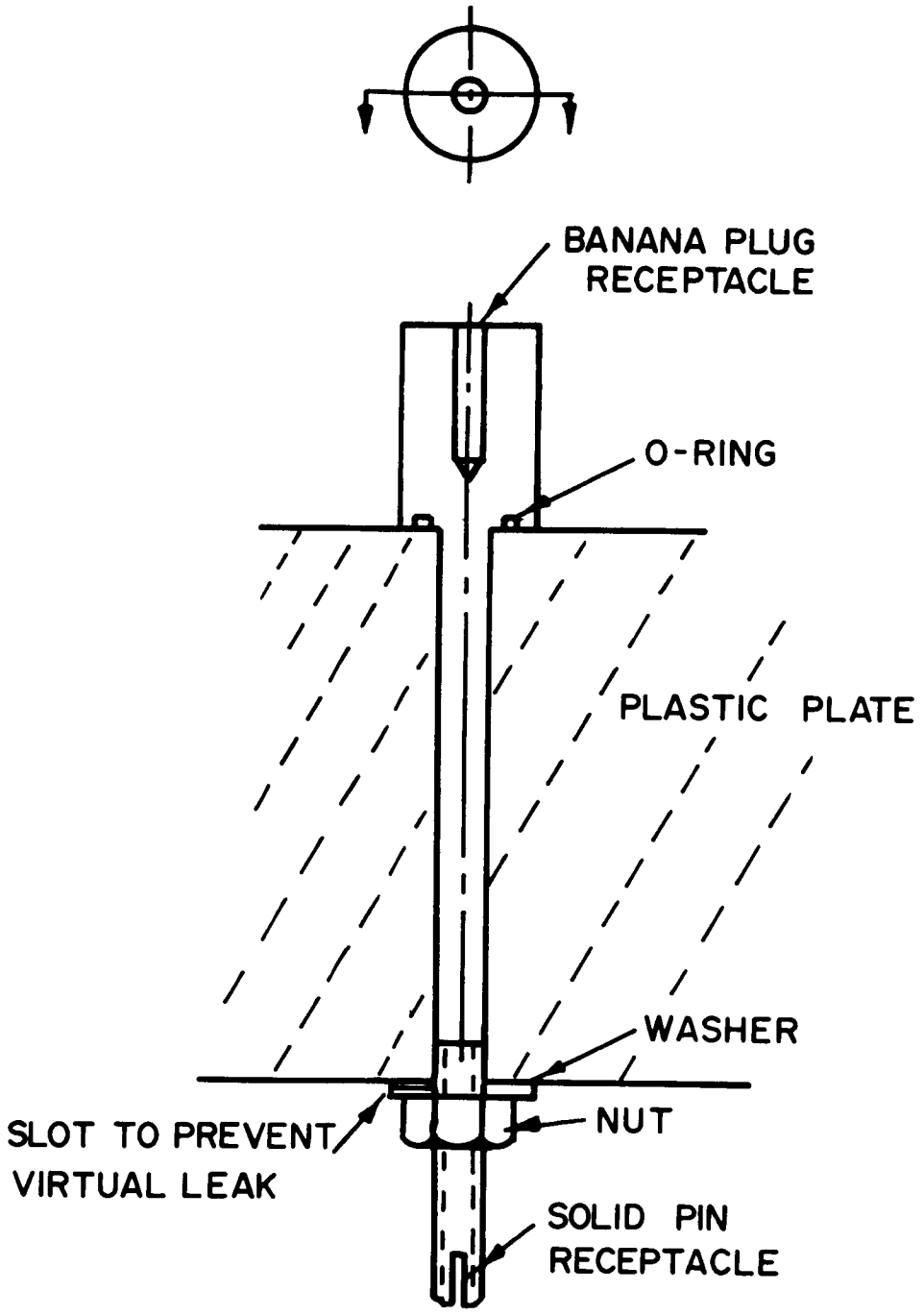

FIG. 8 ELECTRICAL FEEDTHROUGH

with diffusion pumping systems in parallel. Maximum pumping rates are over 25,000 liters/sec. in the primary tank and over 10,000 liters/sec. in the secondary tank.

The original pumping systems were to consist of the diffusion pumps with two 600 liter/sec. ion pumps added in the primary tanks. After an investigation of titanium sublimation pumps, it was determined higher pumping rates could be achieved at an appreciably lower cost. This also gave a possibility of achieving the required pressure levels with plastic windows and without the high degassing temperatures.

1). Diffusion Pumping Systems

The primary tank has a 4 inch Veeco diffusion pumping system with a cold trap and supporting valves. In the basic configuration, there is a water-cooled baffle, a cold trap, a 6 inch valve and a 6 inch right angle elbow between the diffusion pump and the tank. To increase conductance, the 6 inch valve and elbow have been eliminated, and the cold trap is directly flanged to the tank.

The secondary tank has a 10 inch diffusion pumping system by Consolidated Vacuum Corporation with a 10 inch valve, cold trap, and a 12 inch x 18 inch long connecting tube to the tank.

2). Titanium Sublimation Pumping Systems

The initial investigation of titanium pumping systems showed very little data was available with the equipment companies noting pumping rates of 15 - 40 liters/sec. $inch^2$, depending on the deposit surface temperatures. The best specific data is by Clausing (19), and the test results on the system pumping speeds are in general agreement with his work.

Schematics of the internal components of the titanium sublimation pumping systems are shown in Figs. 9 and 10. A titanium element is suspended inside a stainless steel panel surrounded by cooling coils. The coils will normally be cooled with water; however, liquid nitrogen is used for the included results. The panel is in the shape of a cylinder with a cone at one end. The cone cylinder shape is chosen to protect the surrounding equipment from sublimed titanium vapors. The titanium solidifies on the panels with a small percentage escaping the open end. This fraction forms on the plain stainless steel surface at the bottom of the tank. The stainless steel cooling tubes are one continuous coil and exit through an 8 inch diameter flange on the tank. The tubing exit and entrance ends are heli-arc-welded onto a small, machined 2 inch diameter flange, and an o-ring is used as a seal between the tubing flange and the tank port-hole flange (Fig. 11). The o-ring will be replaced with a copper seal in the near future. The tubing is heli-arc-welded to the cooling panels. The electric feedthroughs are part of the basic titanium sublimation pump unit produced by Varian Corporation for their titanium sublimation pump.

The internal parts of the unit have been modified to extend the titanium element further into the tank. The titanium elements extend from the top level of the cone down to 18 inches into the center of the panel in the primary tank and down to 12 inches in the secondary tank. Titanium elements consist of the basic filaments sold by Varian, and are a titanium wire core over-wrapped with tungsten. The modified unit accepts three groups of two filaments in series in the primary tank, and the three groups of one element in the secondary tank.

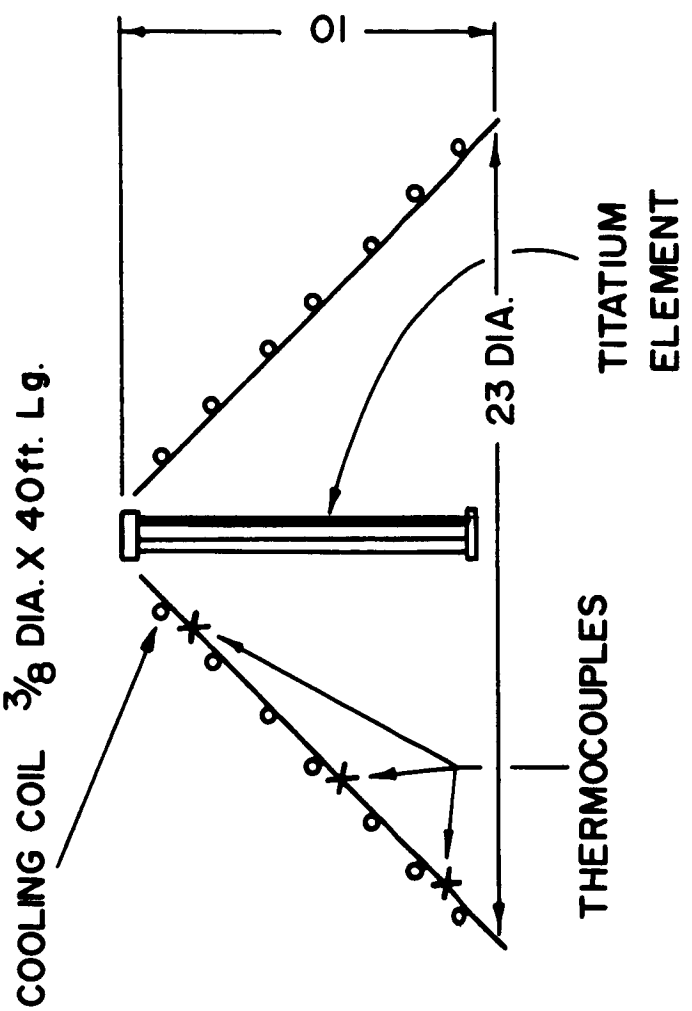

FIG.9 CROSS-SECTION OF TITANIUM SUBILIMATION PUMP COOLING PANEL SECONDARY TANK

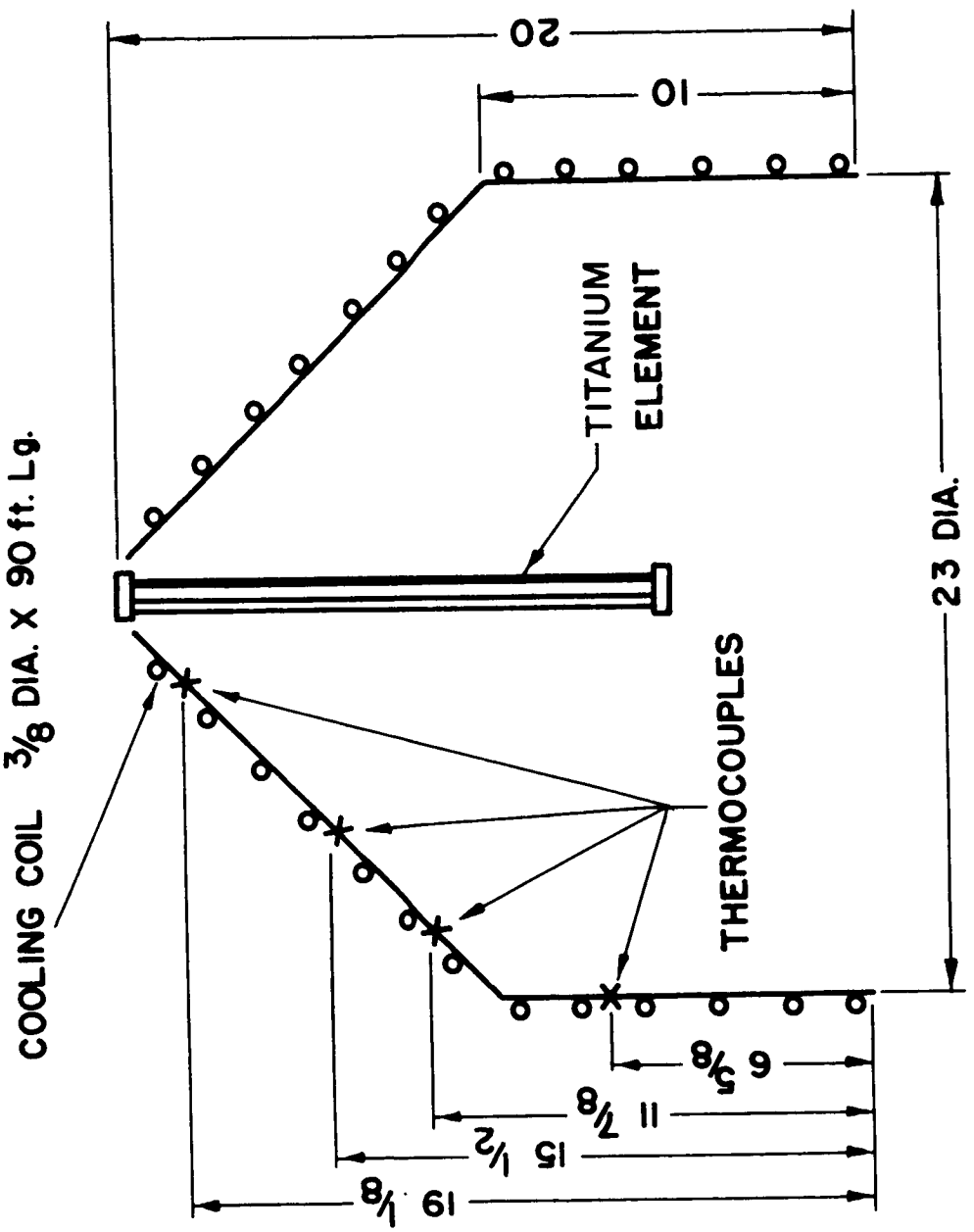

FIG. 10 CROSS-SECTION OF TITANIUM SUBILIMATION PUMP COOLING PANEL PRIMARY TANK

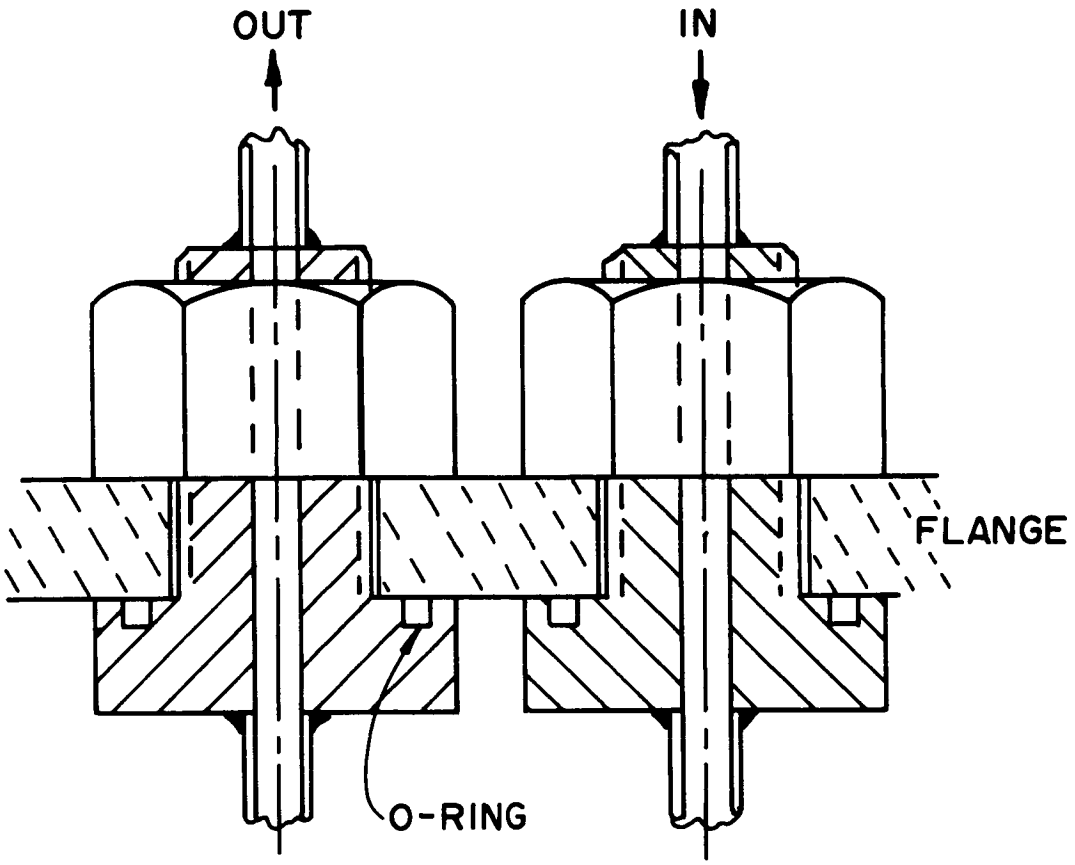

FIG.II LIQUID FEED THROUGHS FOR TITANIUM SUBLIMATION PUMPING SYSTEMS

A schematic of the electrical system is shown in Fig. 12. The 110 volt variac system goes with the secondary tank and was purchased as a power supply from Varian. The 220 volt system was purchased in parts.

The overall cost of equipment was less than $1,200 versus $12,000 for the ion systems at lower pumping speeds. However, the sublimation systems in turn does not pump the inactive gases.

A number of test runs were made on the sublimation pumping system in the primary tank. A metering device (Fig. 13) was placed between the two tanks. The flow is metered through a 1/2 inch diameter orifice leading from the sphere in the metering system into the main tank. Gases flow into the sphere primarily from openings near the front of the sphere and a small opening in the rear of the sphere. The pressure in the sphere is measured with an ionization gage.

The pressure in the secondary tank and the metering device is controlled by variable leaks from Varian. The leaks are either open to the atmosphere or to a gas bottle. The leak rate diffusion pump combination in the secondary tank (near diffusion pumping stalling pressures) results in an unstable pressure system and causes the major measuring problems. Due to this instability the data taken is very limited.

The pressure in the primary tank or downstream side of the metering device is measured with an ionization gage on the side of the tank. The largest probable errors are in the measurement of this pressure. However, the pressure measurements are assumed to be correct but could very easily be off by a factor of 2 to 3. Supporting the mentioned

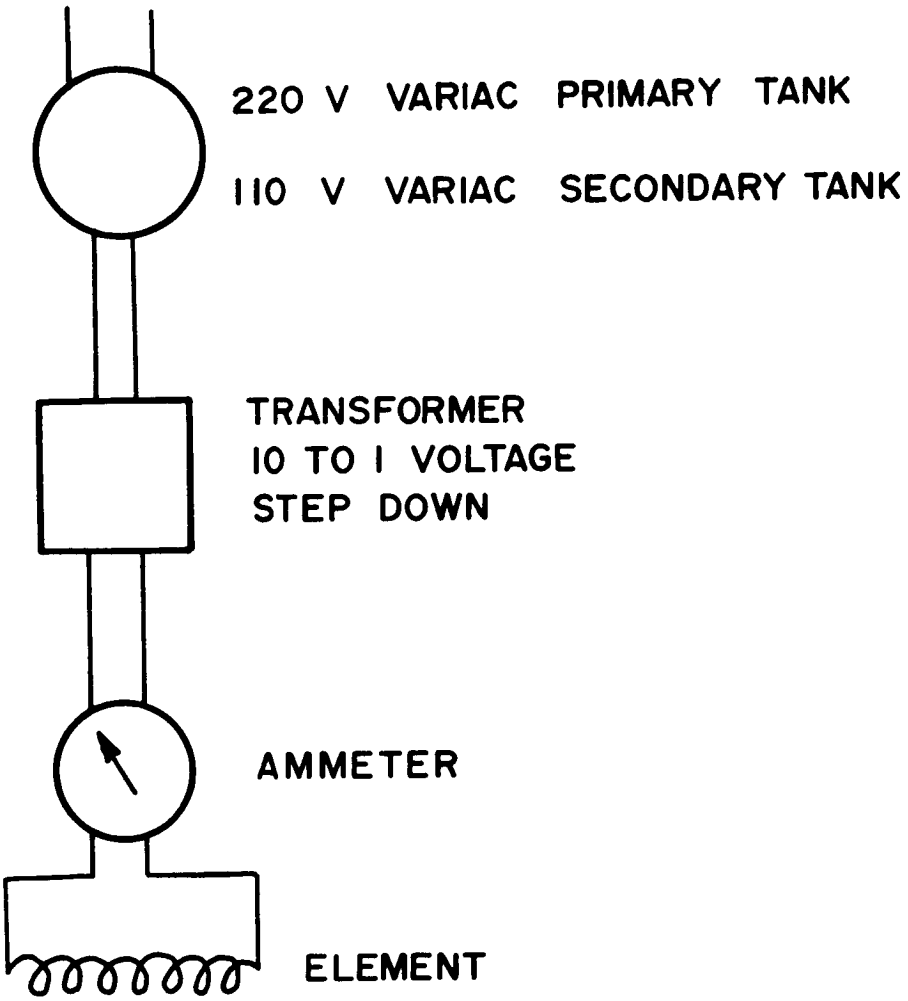

FIG. 12 SCHEMATIC OF TITANIUM SUBLIMATION SYSTEM WIRING DIAGRAMS

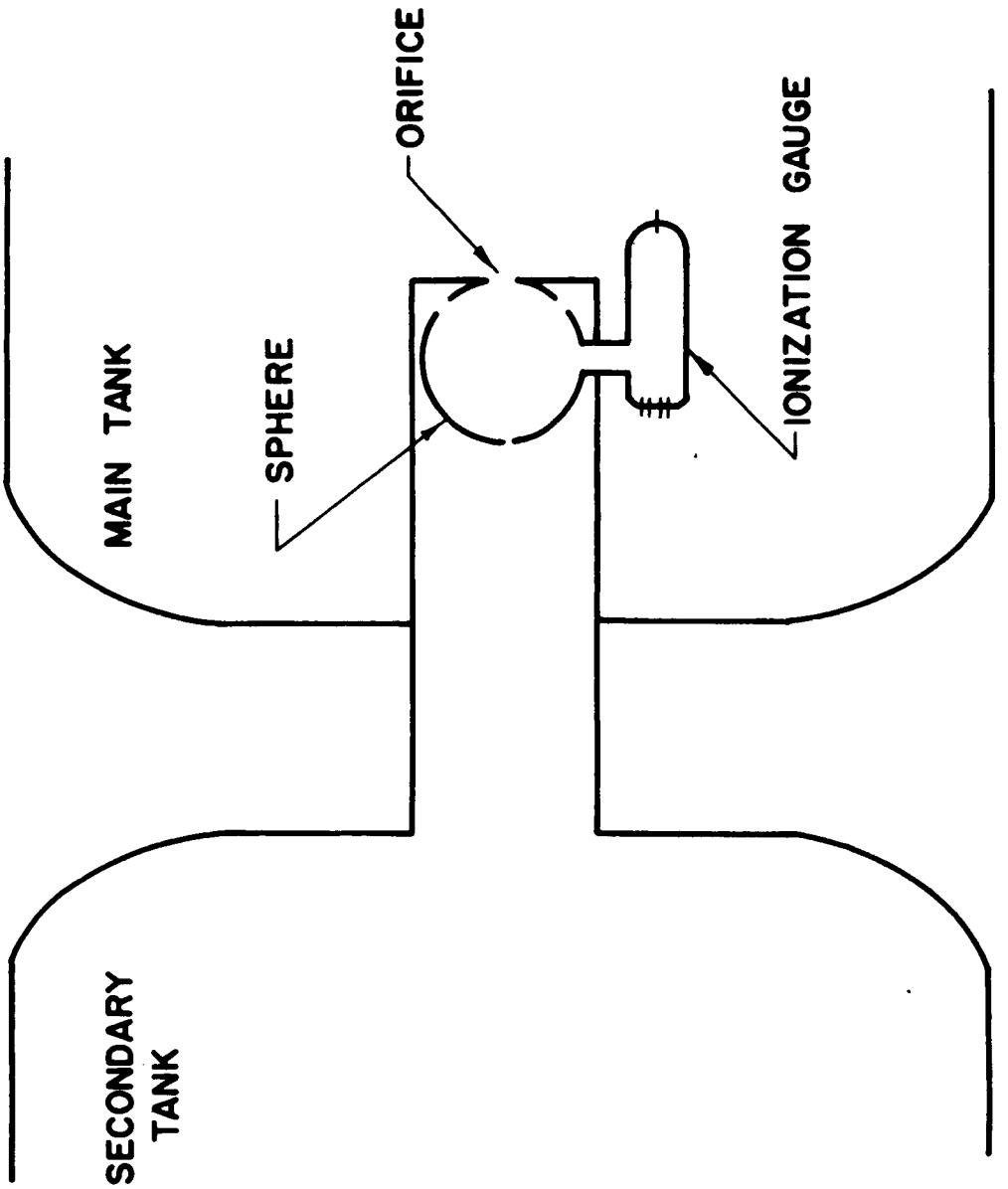

FIG. 13 METERING CROSS-SECTION

pressure instrumentation are ionization gages on each of the diffusion pumps and on the secondary tank. Backing these at higher pressures are three thermocouple gages.

The temperature of the cooling panels are measured by coper-constantan thermocouples at the locations shown in Fig. 10.

All the data is simultaneously recorded on three channels of an oscillograph. The two prime pressures are recorded continuously, and the temperatures are alternated on one channel. Actual recording errors are negligible compared with other errors.

The test runs were made at various pressures, various panel temperatures, and with different size titanium elements. Of the data recorded, a great deal was found to be inaccurate due to tank pressure instabilities and slow response times of the pressure instrument. This data was discarded and only data near equilibrium conditions has been included.

For the data the titanium deposit is from different length titanium wires. However, all deposit rates are above the theoretical limits which were calculated and plotted in Fig. 14. The curves are based on a one gas molecule combination, or basically TiN and TiO. However, it might be noted TiO_2 is found in the natural state. The titanium rates are based on a sample weight variation of elements over a period of time. These calculations are supported by shutting off Titanium deposit during runs for short periods of time without subsequent change in pressure.

The pumping speeds are calculated from the leak rate through the sphere orifice and from an unwanted leak rate calibrated by shutting off the pumping systems to the tank and measuring the variation of

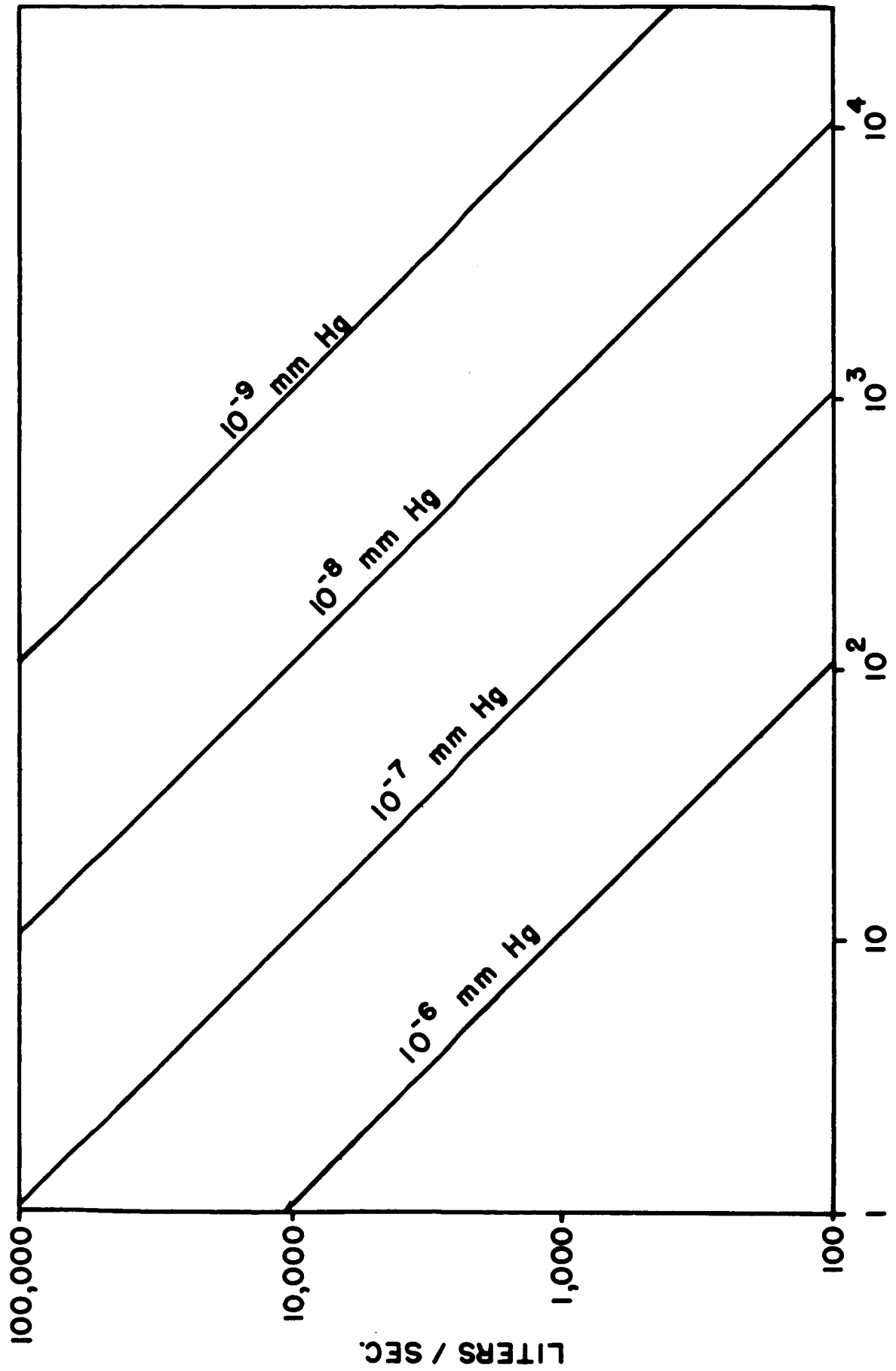

FIG. 14 THEORTICAL PUMPING CAPABILITY FOR 0.1 GRAM TITANIUM

pressure with time. This value could be in error by a considerable amount due to pressure gage response, but the leak accounts for less than 10% of the pumping rates so the error from this source is at most a few percent.

The data in Fig. 15 is taken near minimum available pressures in the tank system. The data is for nitrogen bleed at a pressure of 4.0×10^{-8} mm Hg. The minimum available tank pressure for the runs is just under 3×10^{-8} mm Hg. It should be noted that the primary tank is baked to only 150°F and the secondary tank is not baked. Since the values are near the minimum pressure available, near equilibrium exist, minimizing the transient error. However residual pressures from inactive gases are a possible error source. The limits placed on the values noted are due to transient errors from recording variations. Points "b" and "e" are single values with little variation, so no limits were placed on these values. The groups of points are taken at different times with a transient pressure variation between the points. To confirm the order of magnitude on the pumping rates, a run was made on pressure fluxuation in the main tank after the titanium system is shut off for a reasonable amount of time. The pumping speed of the diffusion pump with the cold trap, lines, etc. is evaluated at 40/liters/sec. from the transient data. The pressure ratio from titanium shutoff to equalibrium is above 500, indicating a rate in excess of 20,000 liters/sec. or supporting the general magnitude of the data.

For the runs a sticking factor is defined as the ratio of the observed pumping rate divided by the theoretical possible pumping rate. The maximum theoretical rate results from the limitation of molecules

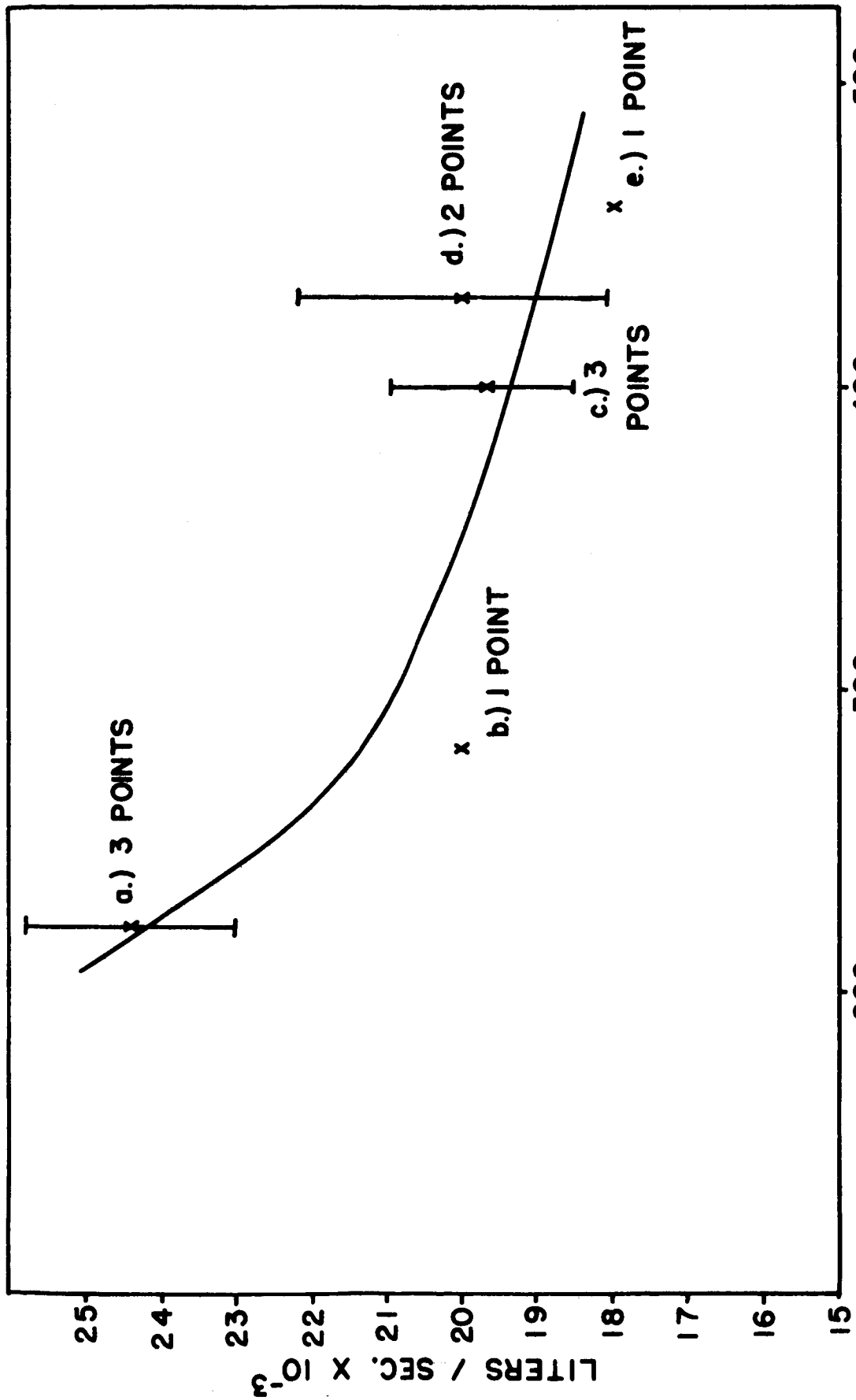

FIG. 15 PUMPING RATE VERSUS TEMPERATURE

entering at the cylindrical end. As a result, an absorbed gas molecule could have more than one collision before being absorbed. This differs slightly from the classical definition used for cryo-pumping. An error also occurs since some sublimed titanium escapes through the open end of the cylinder to the tank surface increasing actual pumping rate.

The values of sticking factor for nitrogen corresponding to the curve in Fig. 15 at 200, 300, 400, and 500°R are respectively 0.79, 0.66, 0.61, and 0.58. A similar sticking factor for air at 200°R and 4×10^{-8} mm Hg is 0.76. It should be noted that the tank is slightly longer in length than in diameter, resulting in a higher molecule flow rate parallel to the tank length than across its diameter or somewhat reducing the above values. They are, however, still similar to the values found by Clausing (19).

An unusual phenomena was observed near the ultimate pressure point. For example, on one run with air and zero bleed into the secondary tank a pressure of around 5.7×10^{-8} mm Hg was acquired in the main tank with a pressure of 5.0×10^{-5} mm Hg in the secondary tank. Raising this pressure to 5.2×10^{-5} mm Hg, the pressure in the primary tank dropped to under 4×10^{-8} mm Hg. The same phenomena occurred with nitrogen bleed in similar proportions. A possible explanation is the trapping of some inactive gases by TiO, TiN, etc., compounds.

A final set of pumping speeds are given in Fig. 16 with a short titanium element located in the top of the cone. The standard Varian element was kept at a constant current of 42 amps. The pumping speeds are much lower than the ultimate pumping speeds but do show trends of temperature and pressure. The temperatures at the various points on the curve are designated. It might be noted at temperatures above

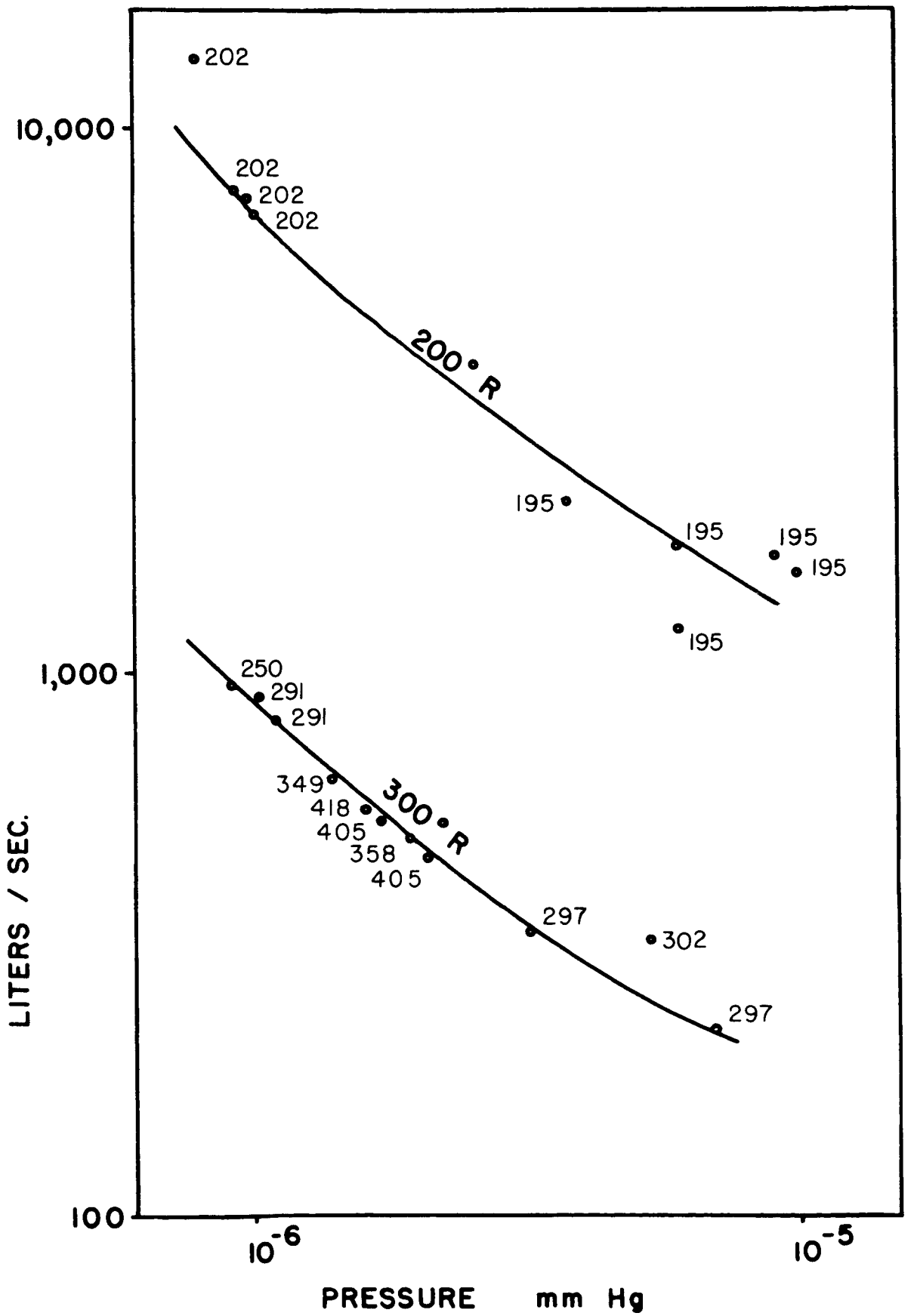

FIG. 16 PUMPING RATE VERSUS PRESSURE

$300^{\circ}R$ the pumping rate is independent of temperature.

These tests on the titanium pump configuration indicate a high pumping rate is available with an inexpensive system. In order to eliminate inactive gases, a parallel system such as a diffusion pump or an ion pump must still be utilized. The pumping speeds recorded approached about 50% of the advertised value of vendors; however, the variation can be in this system. The only unusual data strongly indicated some trapping of inactive gases.

E. Calibrated Leaks

To supply the required gas flows, two calibrated leaks are attached to the secondary tanks. The flow is determined by the pressure in a chamber between the leaks and a flow orifice. Two thermocouple gages are used to measure the pressures. When the accelerator (Section 5) is running, one leak provides gas to the accelerator and one leak provides gas to the charge exchange section.

III. FORCE PROBES

The prime invocation of the project was the design of probes which could measure the normal and tangential forces independently. Two types of probes were developed to measure these forces. The first type is the swinging pendulum and the second type is the torsional pendulum. The probes are attached in the tank to a stand which can be controlled by remote control from outside the tank. Movement is available in four dimensions, the three dimensions in cartesian coordinate plus rotation.

The swinging type pendulums which are suspended on micron size quartz fibers are shown in Fig. 17. That the normal force probe can measure only a normal force and the tangential probe can measure only a tangential force can be deduced from the figures. The minimum mass of the probes is of the order of magnitude of 10^{-2} grams. The pendulums were 10 inches long and the accuracy of measurement is ± 0.001 inches. This results in an accuracy of $\pm 10^{-5}$ dynes.

The method of distance measurement is shown in Fig. 18. The probe is centered in the cross-hairs of a scope by reflection off a mirror mounted on a milling machine table. The movements of the table can be measured to within 0.001 inches. Keeping the probe in the scope cross-hairs, results with the table movement equal to probe movement. All horizontal measurements were made with this technique, allowing accurate external measurements of internal movements.

The rotating torsional type probes are also suspended on quartz fibers. Again it can be deduced from Fig. 19 that the normal probe can measure only normal forces and the tangential probes can measure

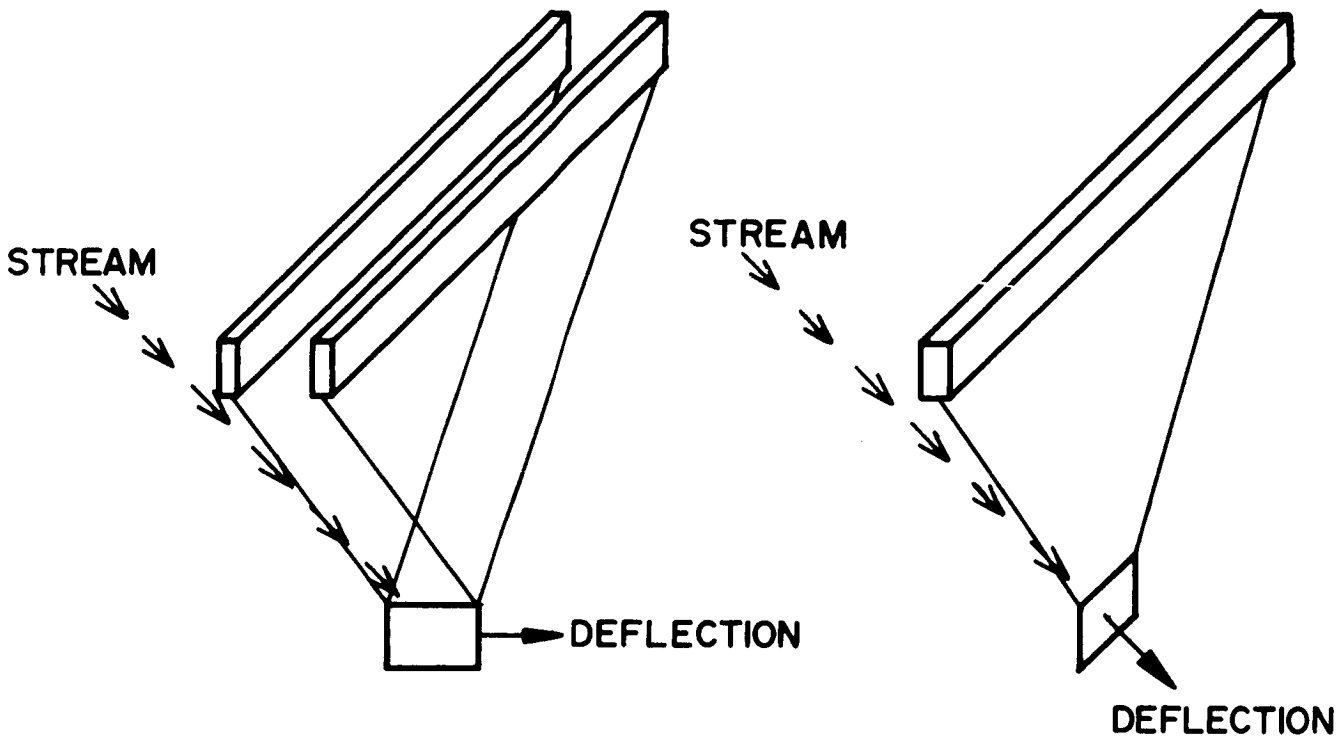

TANGENTIAL FORCE PROBE

NORMAL FORCE PROBE

FIG. 17 SWINGING PENDULUM PROBES

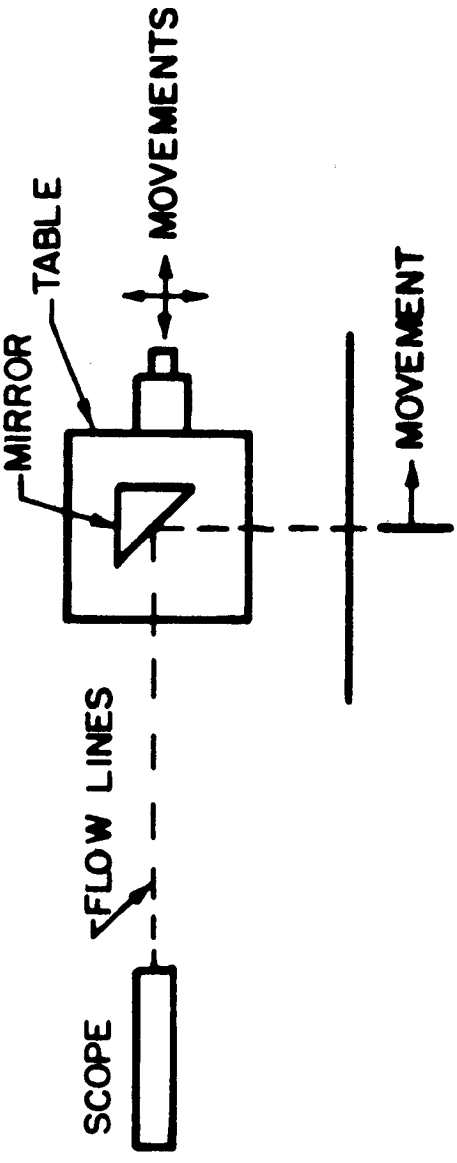

FIG. 18 MEASUREMENT OF FORCE PROBE DEFLECTIONS

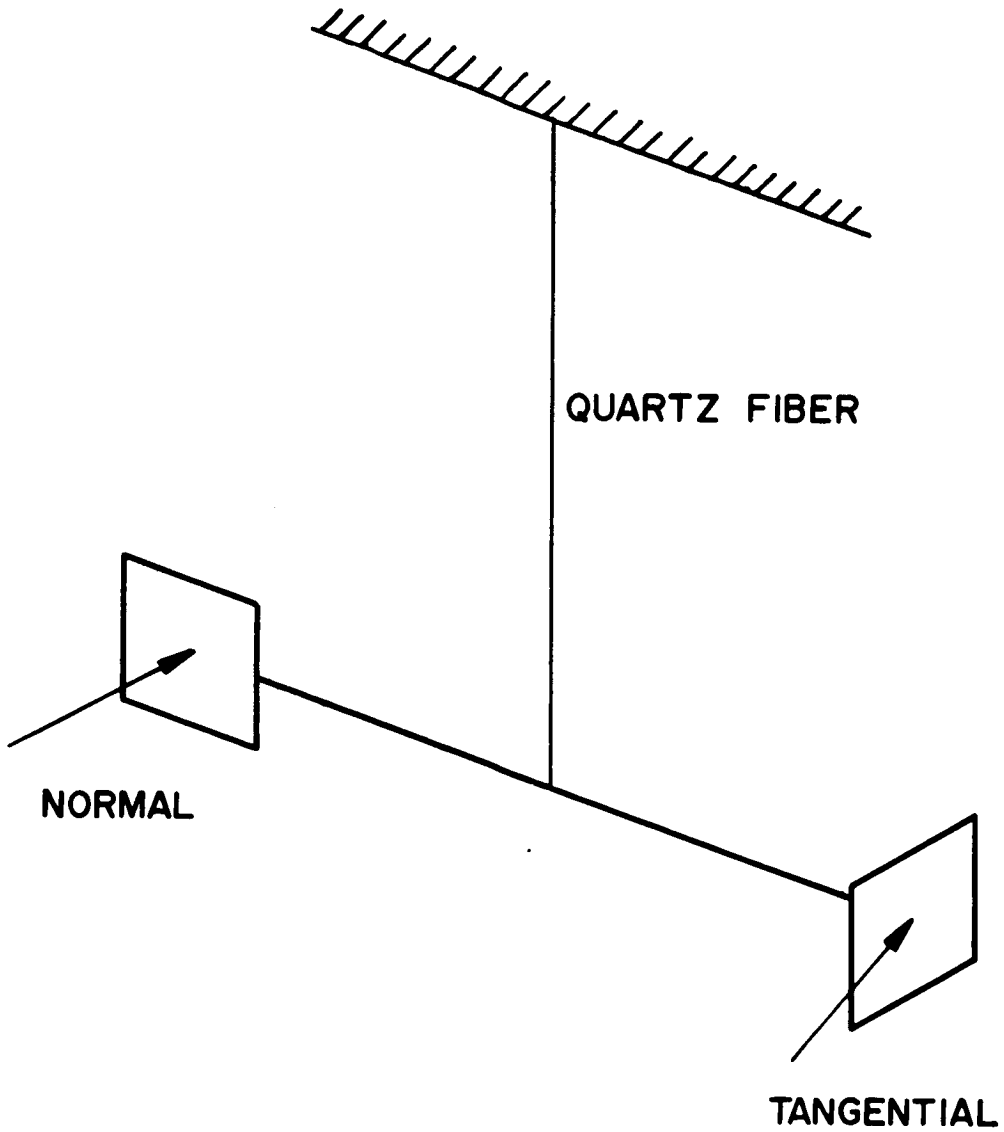

FIG. 19 TORSIONAL PROBE

only tangential forces. The torsional constants vary as a function of fiber diameter, and with fibers as small as 3 microns in diameter and 20 cm long, forces down to 10^{-8} dynes can be measured. The spring constants of the probes are determined by the period of rotation and probe moment of inertia during free oscillations in a vacuum. The major problem with the probes is the damping of the free oscillations. Spring constants are chosen by trial and error to give measured deflections large enough to keep recording errors below 1%.

A technique to measure the rotation was devised using a photo electric cell. A semi-circle was blocked on a thin circular disk photo cell. A second semi-circle was attached to the bottom of the probe and a light was inserted above the probe. The interaction of the two semi-circles was amplified and recorded on an oscillograph. Repetition of the data was within one degree.

An isometric view of the force probe holder is shown in Fig. 20. Small electric motors are used to move in the various directions noted. They are 28 volt D.C. geared down motors put out by Gemini Corporation. Vacuum tests were made at 10^{-6} mm Hg and no appreciable degassing from the motors could be detected. A number of motors originally burned out; however, the cause was traced to a power supply which was not floating. As a result there was a 110 AC voltage between the ground and power output.

The variation on normal and tangential probe forces for a constant flow rate and diffuse reflections is given in Figs. 21 and 22 as a function of probe angle. The flow colliding with the probe is constant per unit area thereby including the effect of solid angle.

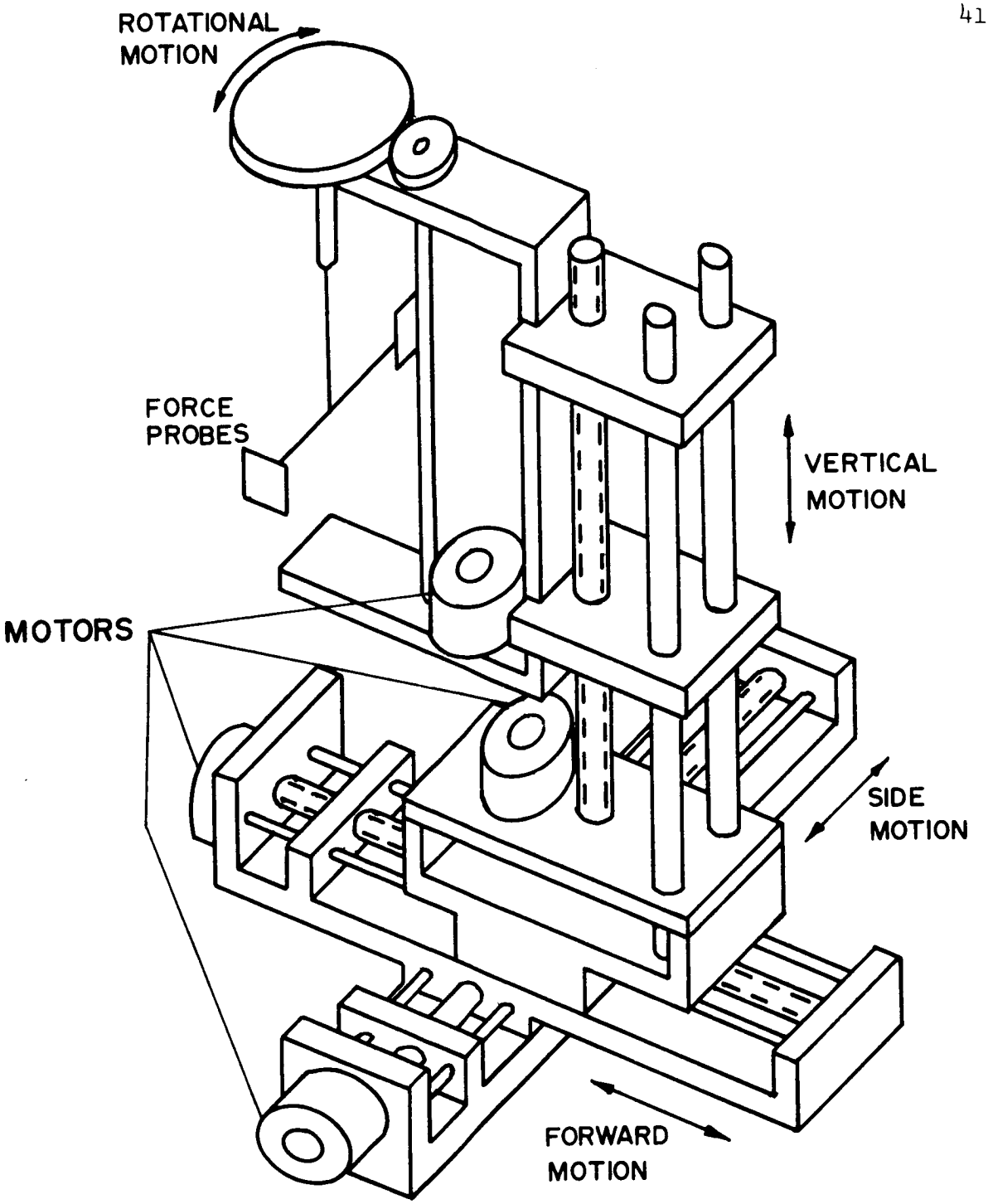

FIG. 20 FORCE PROBE POSITIONING APPARATUS

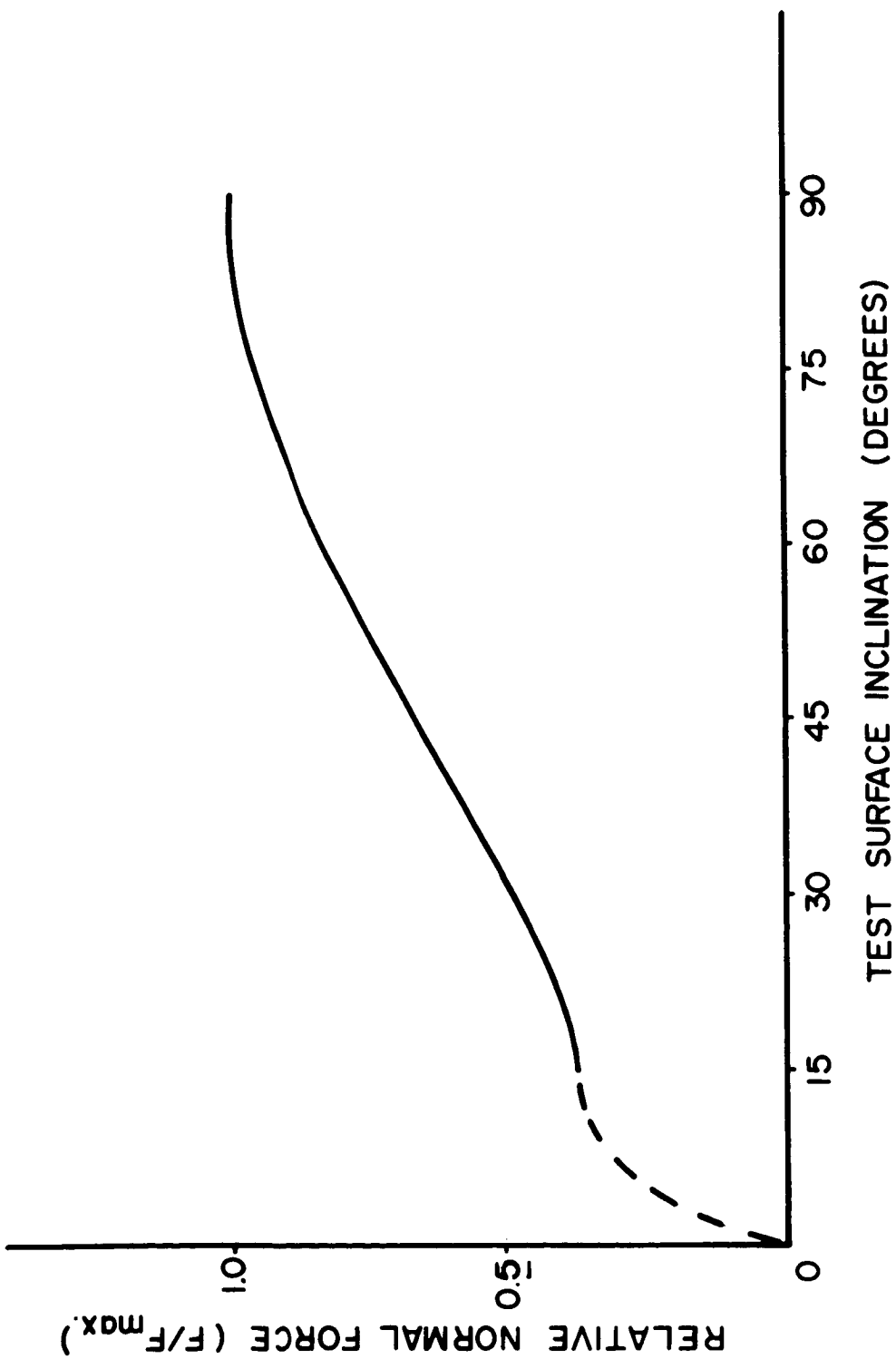

FIG. 21 RELATIVE NORMAL FORCE vs TEST SURFACE INCLINATION

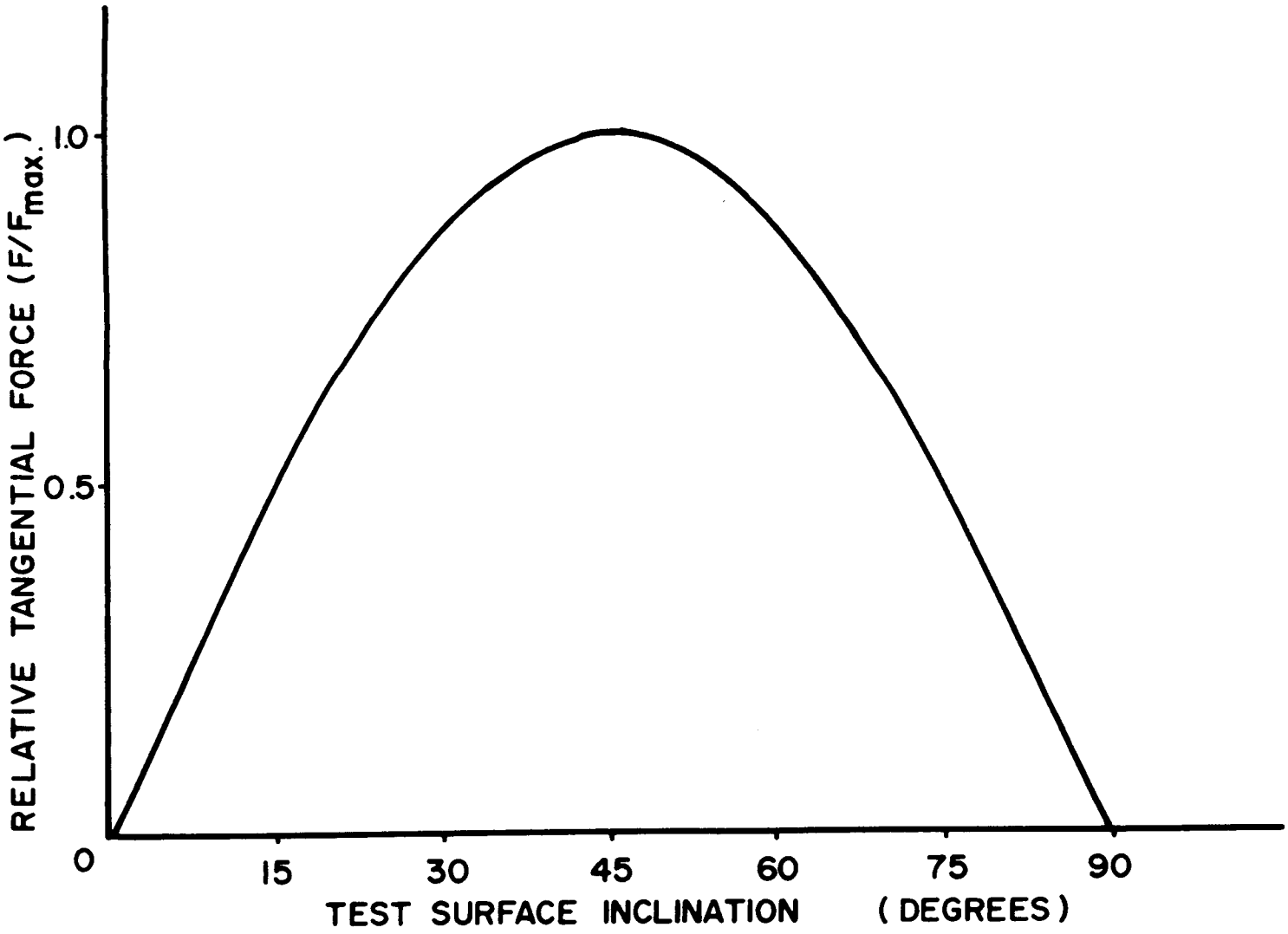

FIG. 22 RELATIVE TANGENTIAL FORCE vs TEST SURFACE INCLINATION

IV. FREE MOLECULAR FLOW NOZZLE SYSTEM

In order to calibrate and perfect the force probe system, a low velocity molecular beam was developed to impinge on the probes. The beam was formed through the use of a free molecular flow nozzle system. The system used relatively high pressures, 10^{-4} mm Hg range, on the back side of an orifice and cylindrical tubes of various length to radius ratios to form the beam. The original experimental results showed large variations from the theoretical work of Dayton (20) but were similar to experimental results by Cook, et al (21). Since the exit distributions affect the calibration procedure critically, an intensive investigation developed, which showed a sensitive dependence of the nozzle exit distributions on the inlet equilibrium distributions of molecules. This situation was corrected by placing an integrating sphere at the entrance of the nozzles to create the equalibrium. This addition also shows a marked improvement in the flow rate calibrations for the nozzles. The nozzle results are given before and after the addition of the integrating sphere.

A. The Nozzle System

The nozzle system is set up to allow a number of combinations of nozzles to be used without requiring access inside the vacuum chamber. This is accomplished by placing a 4 inch tube between the primary and secondary tank. The end of the tube is covered with a flat plate with a fairly large orifice in the center. On the outside of the plate, a rotating gear is mounted so that as the gear rotates individual nozzles will be centered over the large orifice. An electrical motor operated from outside the tank rotates the gear.

The original set of nozzles, mounting, and equilibrium chamber are shown schematically in Fig. 23 with the sizes and diameter to radius ratios given in Fig. 24. A baffel in the entrance section is used to try and set up an equilibrium condition among the molecules. It is located one entrance tube diameter behind the nozzle openings to approximate an integrating sphere. Analysis of the data from this system and comparison with theoretical results showed large deviations from equilibrium as will be noted in the next section.

To correct the deviations and improve the tolerances on the nozzles, a second system was installed as noted in Fig. 25. The nozzle sizes and length to radius ratios are given in Fig. 26. The installation of an actual sphere improved the correlation with theory and thereby has been accepted as a suitable combination. The nozzles are made of brass and silver soldered to a brass gear. The silver soldering was done in an electric furnace to achieve a perfect fit. The machining was done after the soldering. The sphere tolerance is a few thousandths of an inch and is silver soldered into the brass entrance tube. The entrances to the sphere are on the nozzle side so that a molecule must have a minimum of one collision before passing through a nozzle. A soft solder seal is used between the sphere and nozzles. Spring pressure of approximately 10 pounds is applied between the gear and seal on an area under 1/2 sq. inch. To measure pressure directly in the sphere, an ion gage is connected to the side of the sphere.

B. Nozzle Exit Distributions

In order to use the free molecular flow nozzle, the exit distributions were measured. The remotely controlled system shown in Fig. 27 was constructed to measure the distributions. The system is made so the

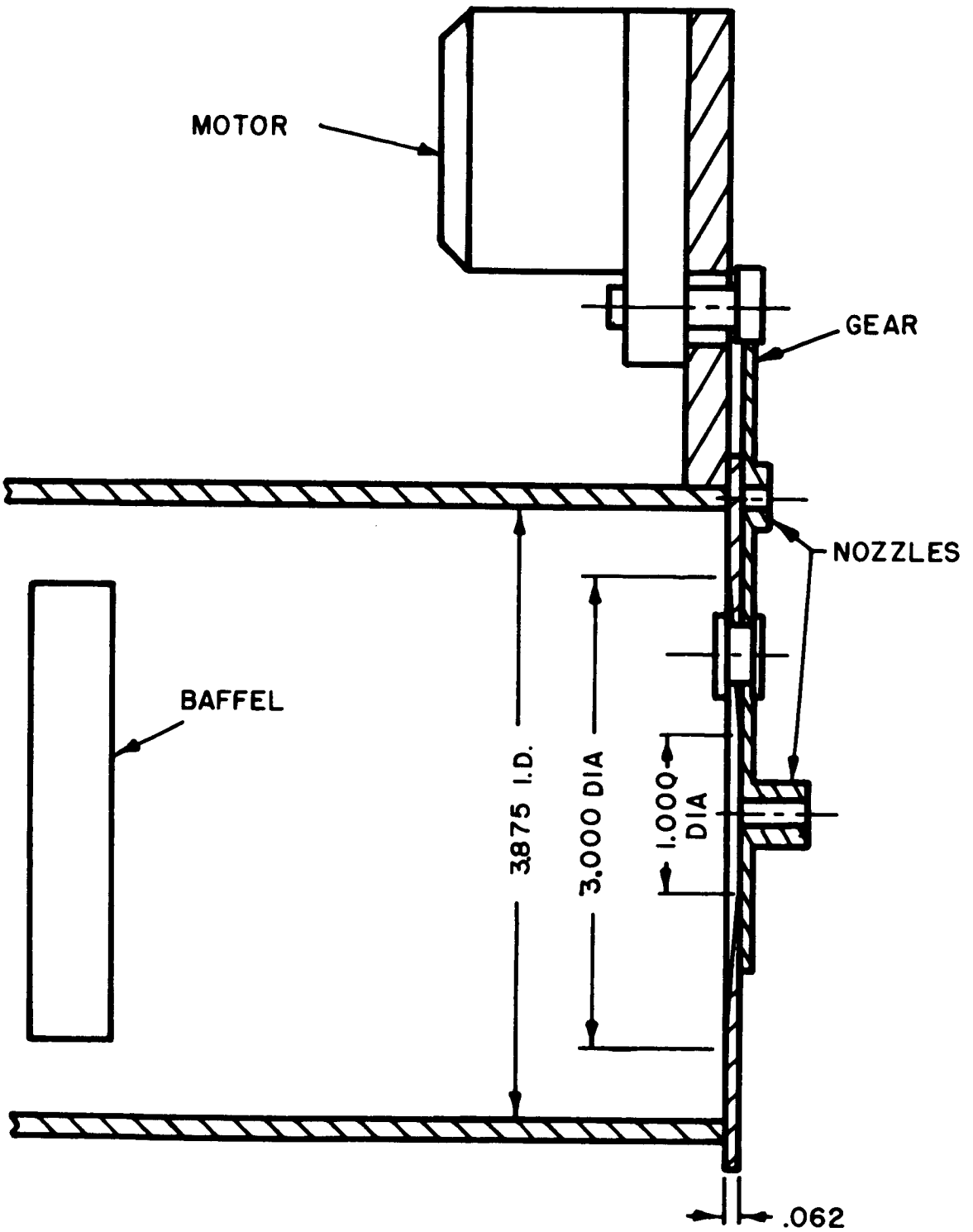

FIG. 23 OVERALL NOZZLE APPARATUS
(ALL DIMENSIONS IN INCHES)

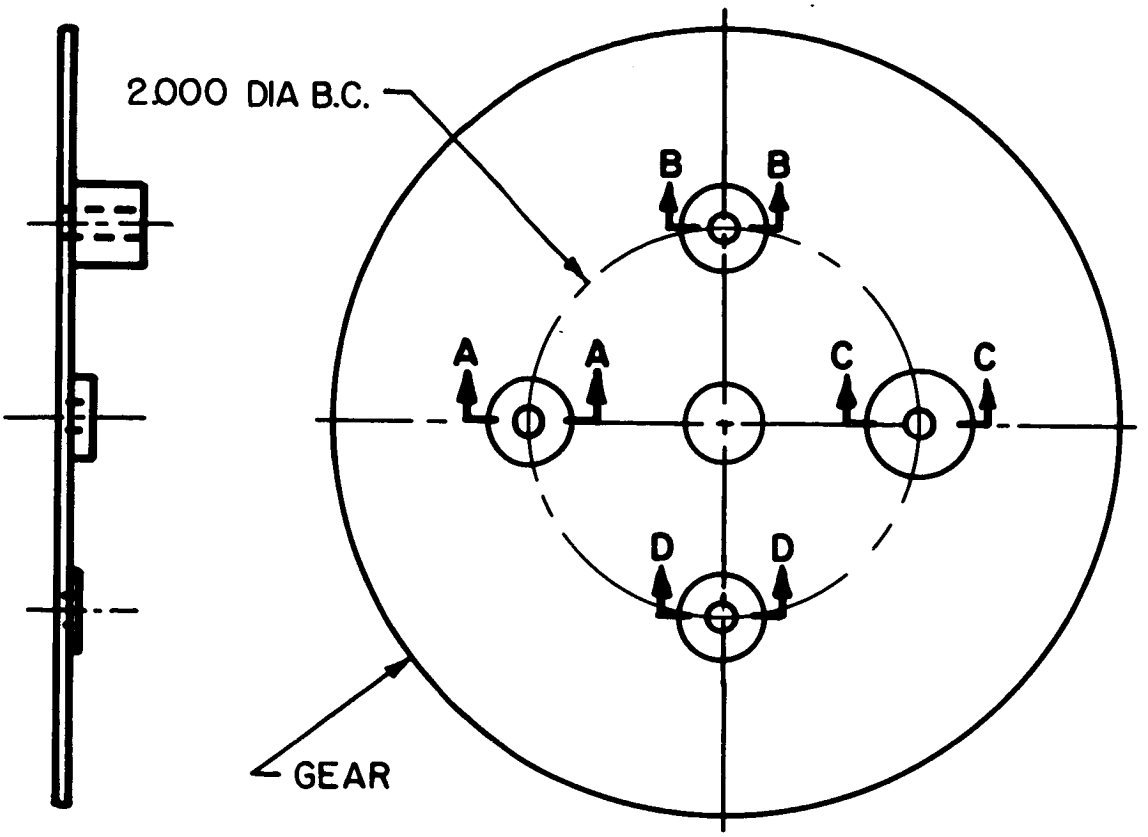

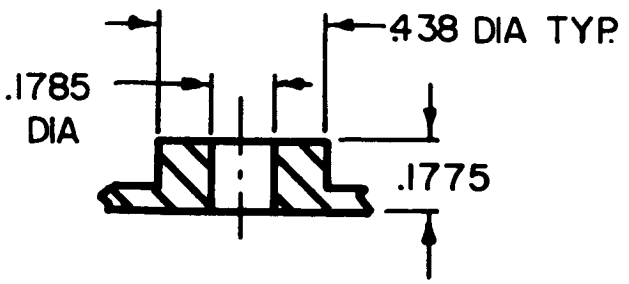

SECTION A-A

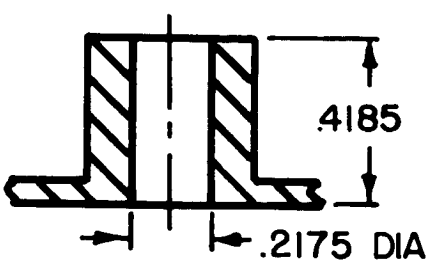

SECTION B-B

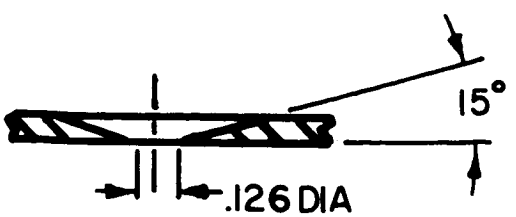

SECTION C-C

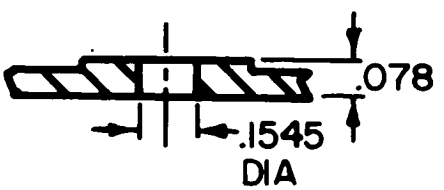

SECTION D-D

FIG. 24 NOZZLE DETAIL
(ALL DIMENSIONS IN INCHES)

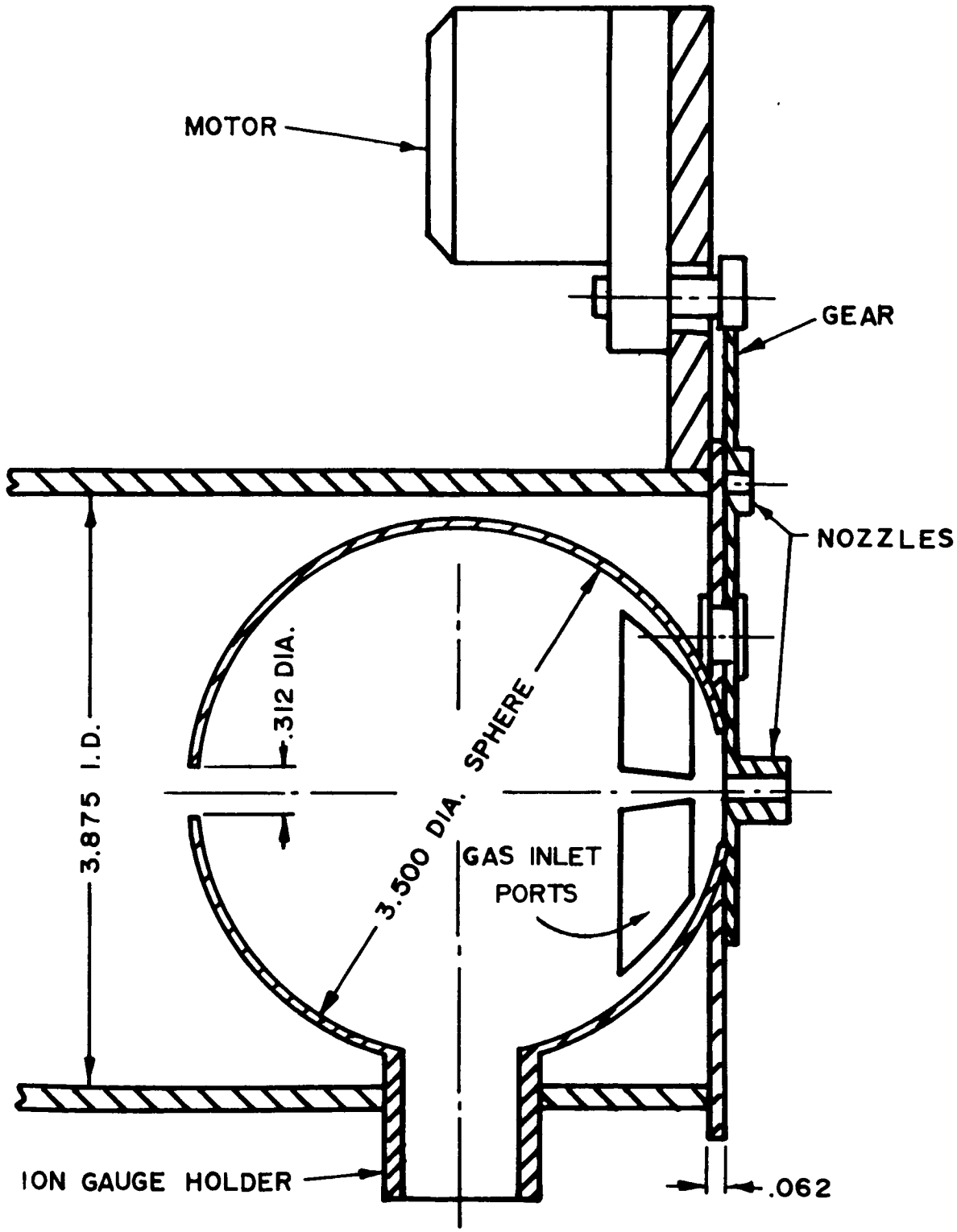

FIG. 25 FREE MOLECULAR FLOW NOZZLES

(ALL DIMENSIONS IN INCHES)

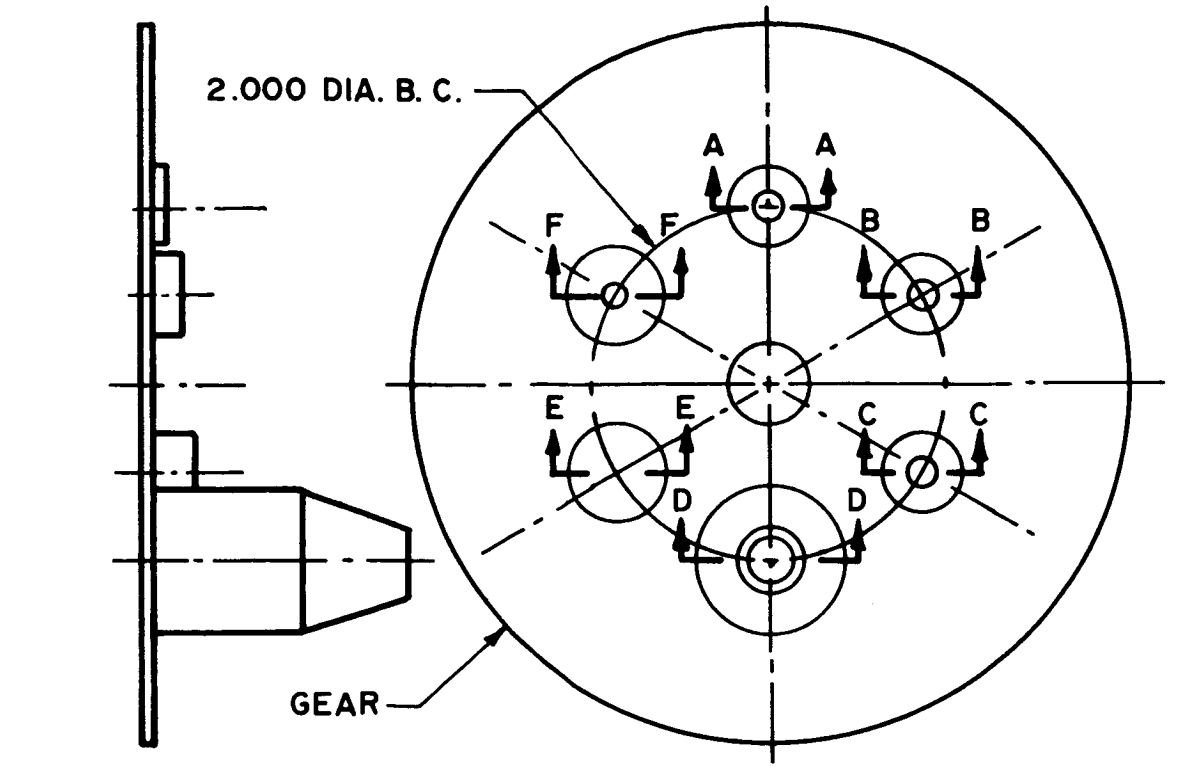

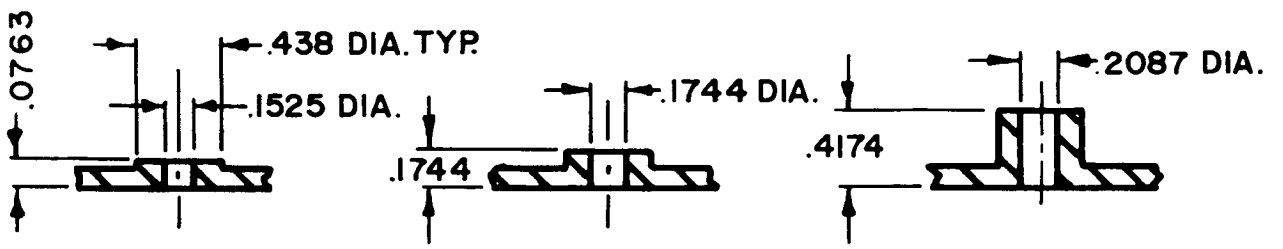

SECTION A—A SECTION B—B SECTION C—C

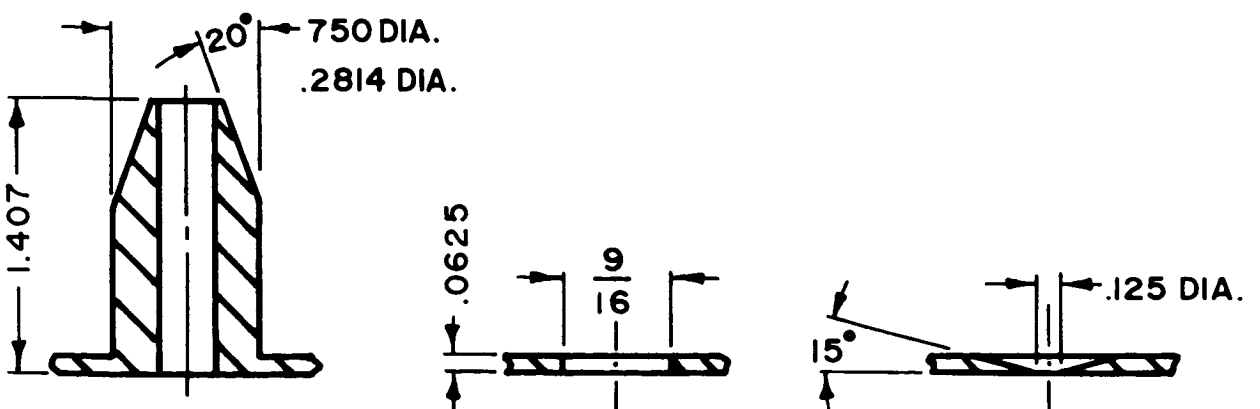

SECTION D—D SECTION E—E SECTION F—F

FIG. 26 NOZZLE DETAIL

(ALL DIMENSIONS IN INCHES)

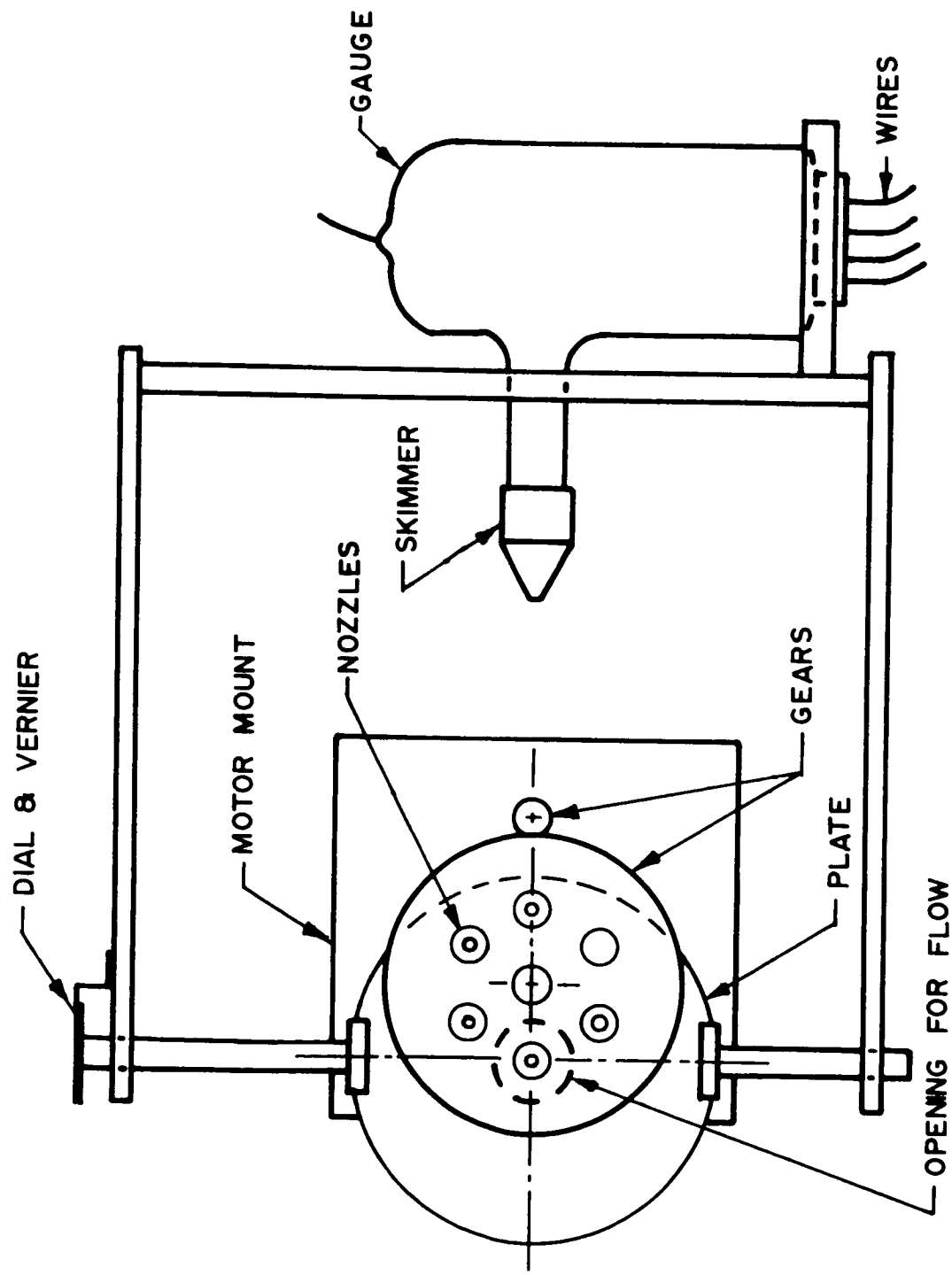

FIG. 27 APPARATUS FOR MEASURING EXIT DISTRIBUTIONS

ion gage can be rotated around the nozzle exit at the centerline height. The skimmer details are given in Fig. 28. The distance from the nozzle to the skimmer was over 10 nozzle diameters for all data to give a point source effect. This gives an error of less than 2% according to the theory by Cook, et al (21).

Figs. 29 through 37 give the exit distributions for the old system of nozzles with the cylindrical "equilibrium" chamber. In general, the data falls outside the theoretical values for all figures. However, as the inlet pressure is increased, collisions begin to form in the cylindrical chamber, moving the distribution towards equilibrium. The experimental data as a result moves towards the theoretical results. It should be noted that, as the pressure is further increased, a second effect enters--the increased pressure in the nozzles also produces collisions, and a deviation from free molecular flow begins. This tends to spread the distributions. However, in this pressure range, the larger size of the joining cylinder behind the nozzle dominates, and the curves do begin to approach the theoretical results.

In the second nozzle system the integrating sphere is directly incorporated and the results should be near equilibrium. The experimental exit distributions are given in Figs. 38 through 50. For this configuration, the correlation between the experimental data and theory is excellent at the low pressures (High Knudsen Numbers). For the higher pressures, the deviation from free molecular flow can be detected.

The only other experimental data known, by other than the author, is by Cook, et al (21). In their data the distributions came from a cylindrical chamber, similar to the author's first configuration, with similar results as the data falls outside the theoretical curve. On this

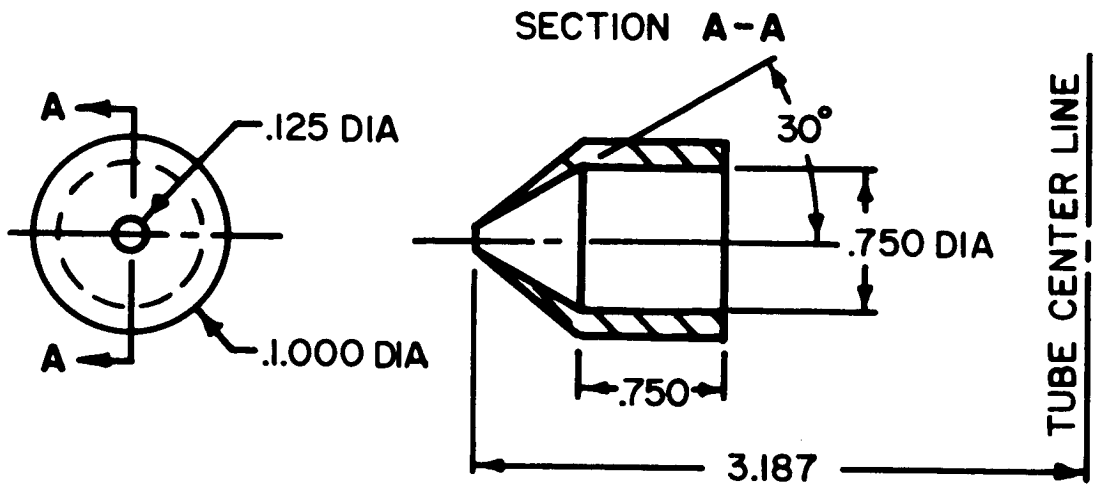

FIG. 28 SKIMMER DETAILS
(ALL DIMENSIONS IN INCHES)

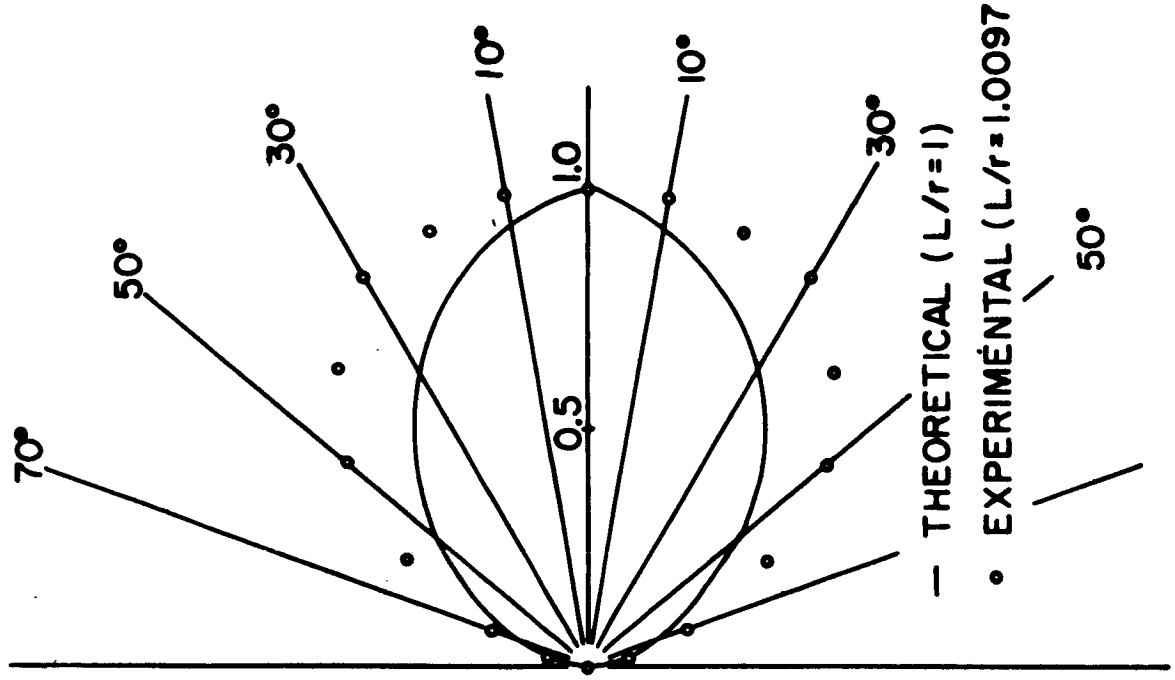

Knudsen Numbers

$\frac{\lambda}{L}$ = 110 $\frac{\lambda}{D}$ = 53

INLET PRESSURE 4×10^{-4} mm Hg

WITHOUT INTEGRATING SPHERE

FIG.29 NOZZLE EXIT DISTRIBUTION

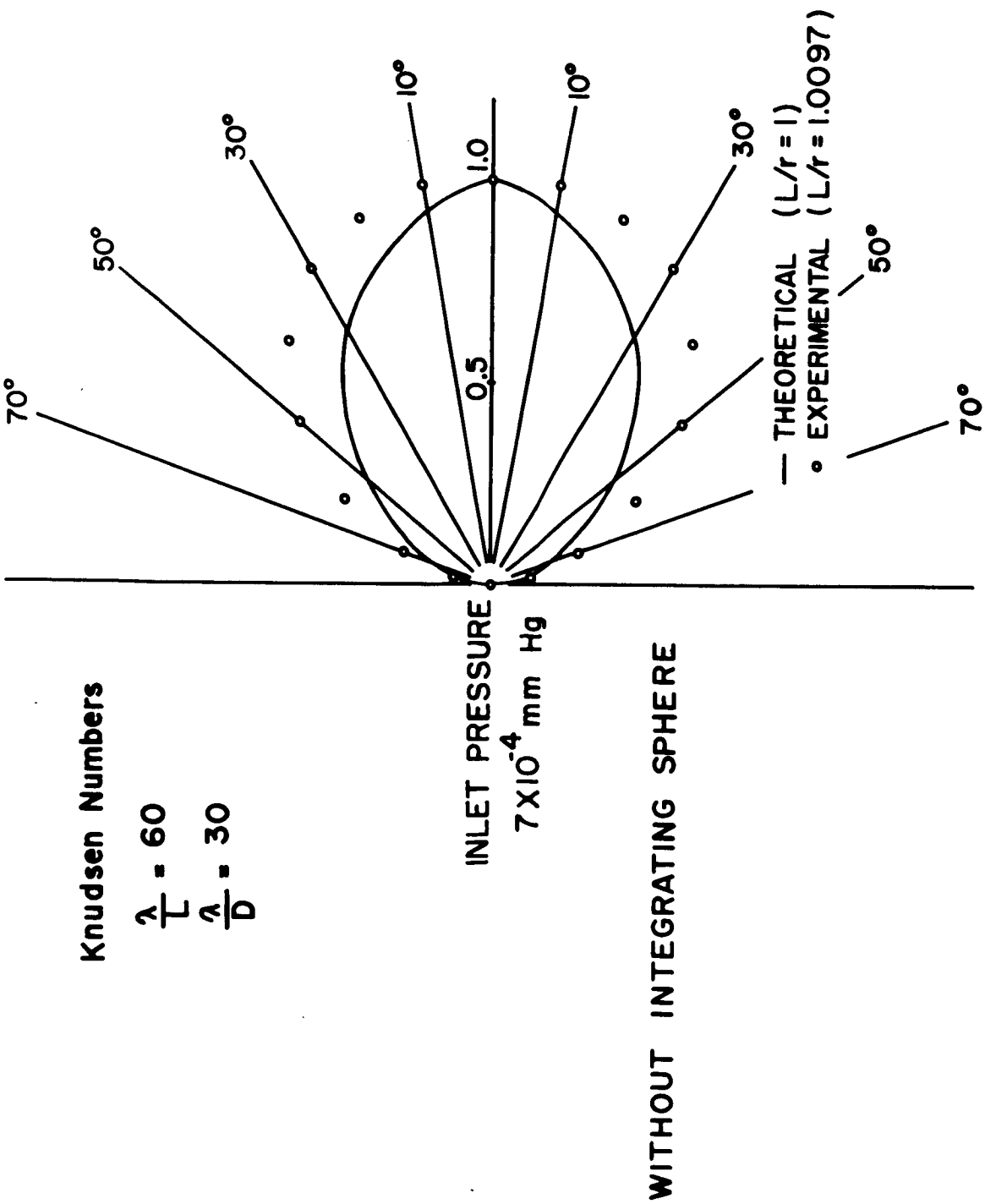

FIG. 30 NOZZLE EXIT DISTRIBUTION

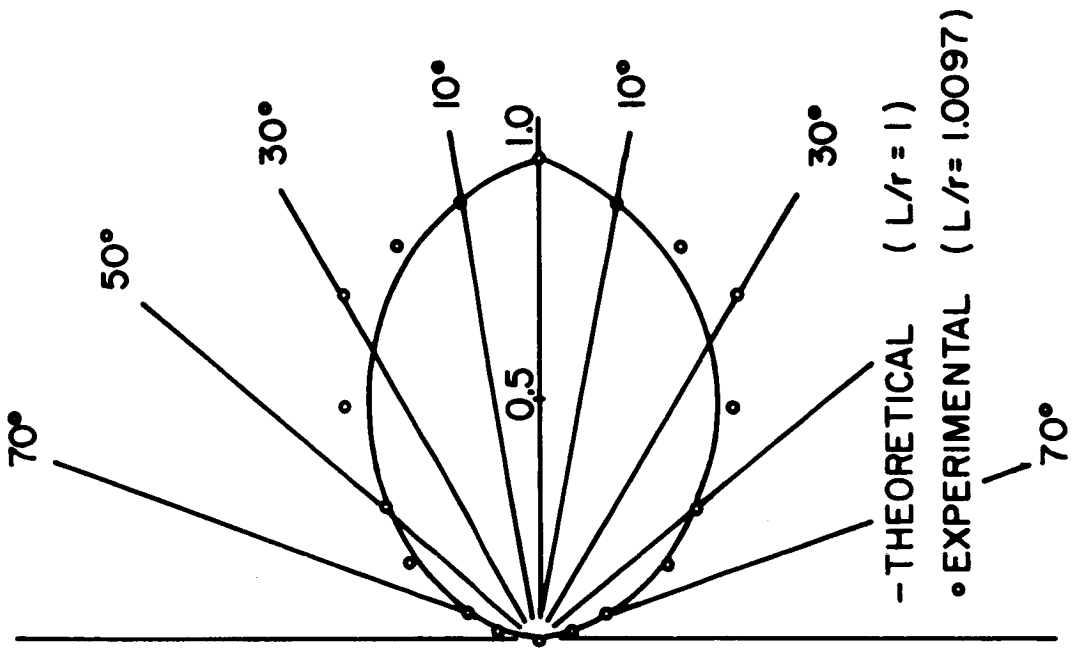

FIG 31 NOZZLE EXIT DISTRIBUTION

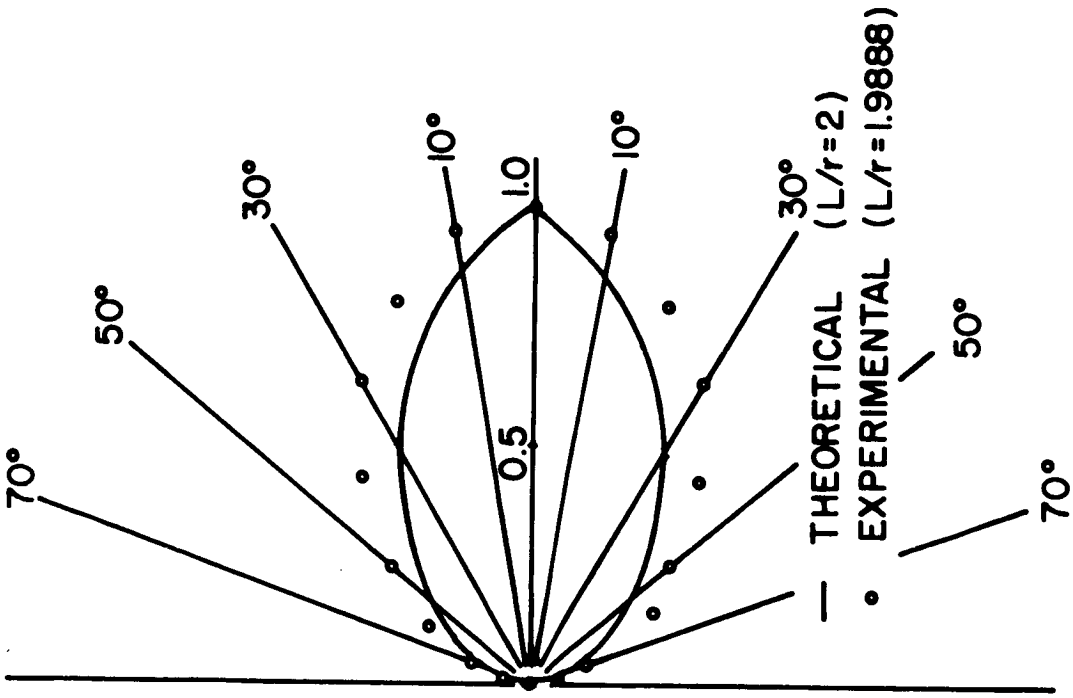

FIG. 32 NOZZLE EXIT DISTRIBUTION

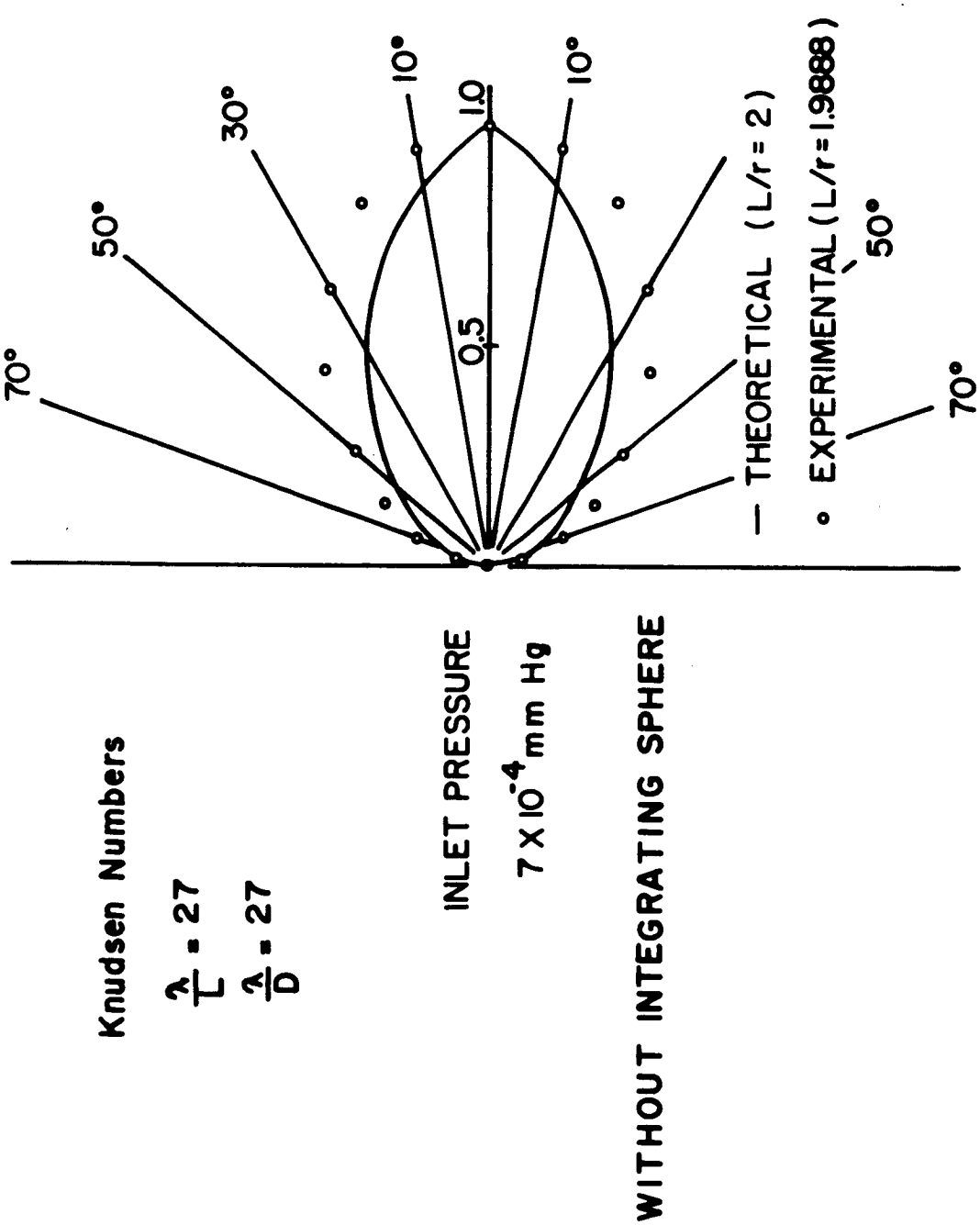

FIG. 33 NOZZLE EXIT DISTRIBUTION

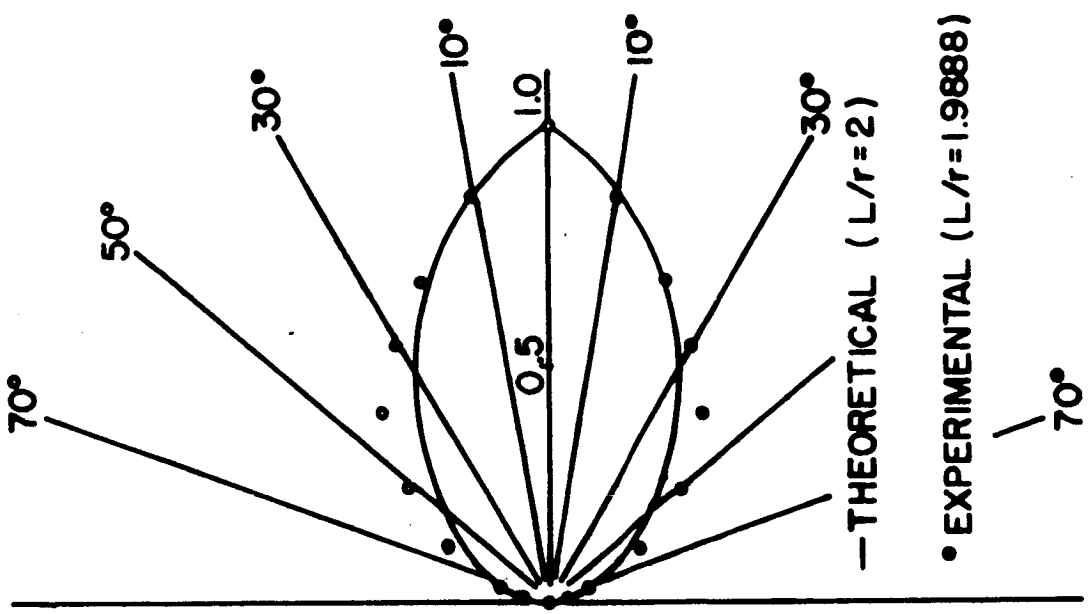

FIG. 34 NOZZLE EXIT DISTRIBUTION

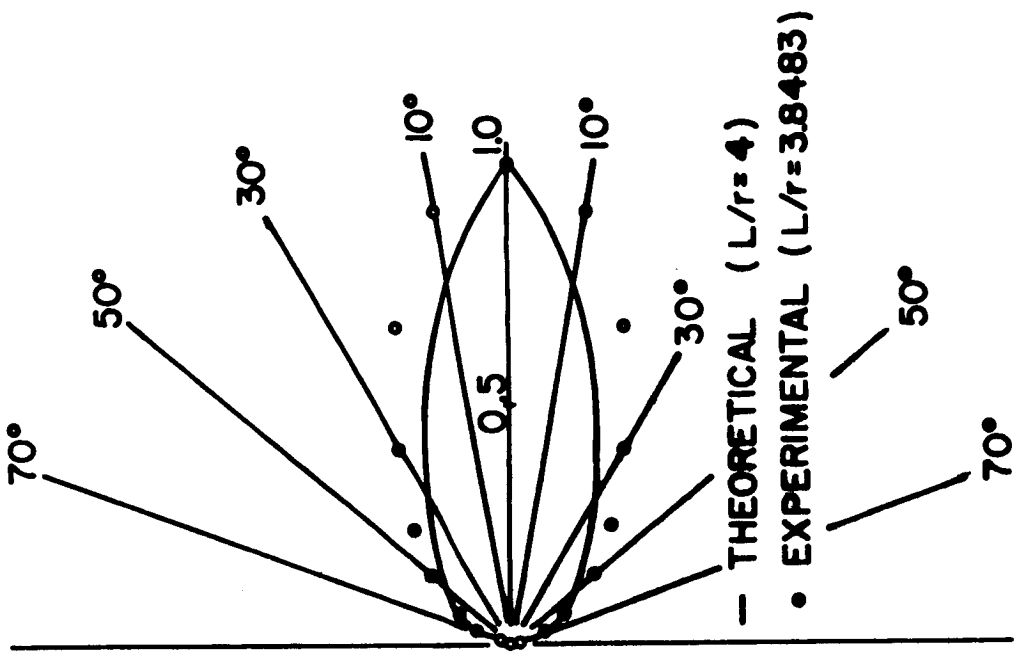

FIG. 35 NOZZLE EXIT DISTRIBUTION

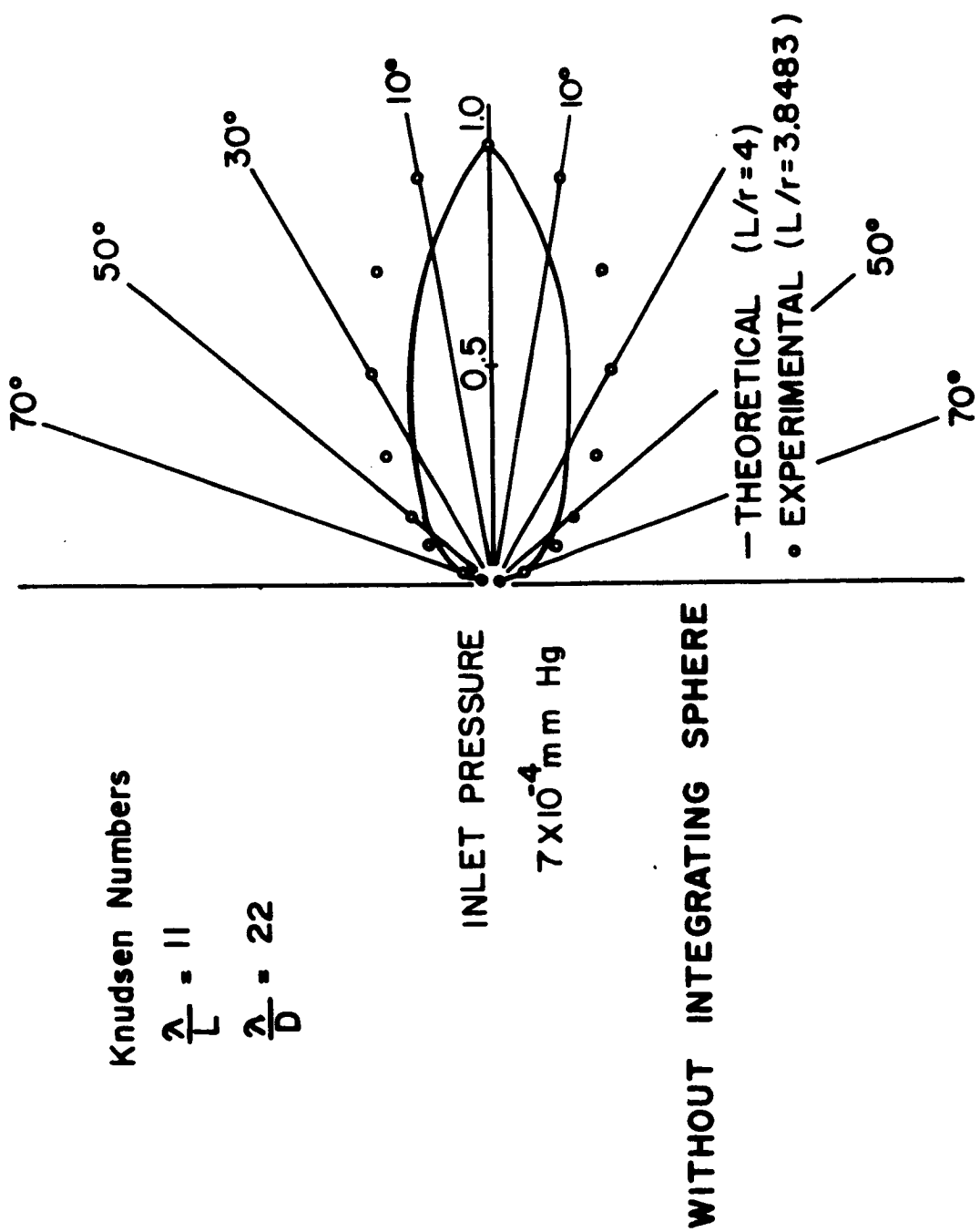

FIG.36 NOZZLE EXIT DISTRIBUTION

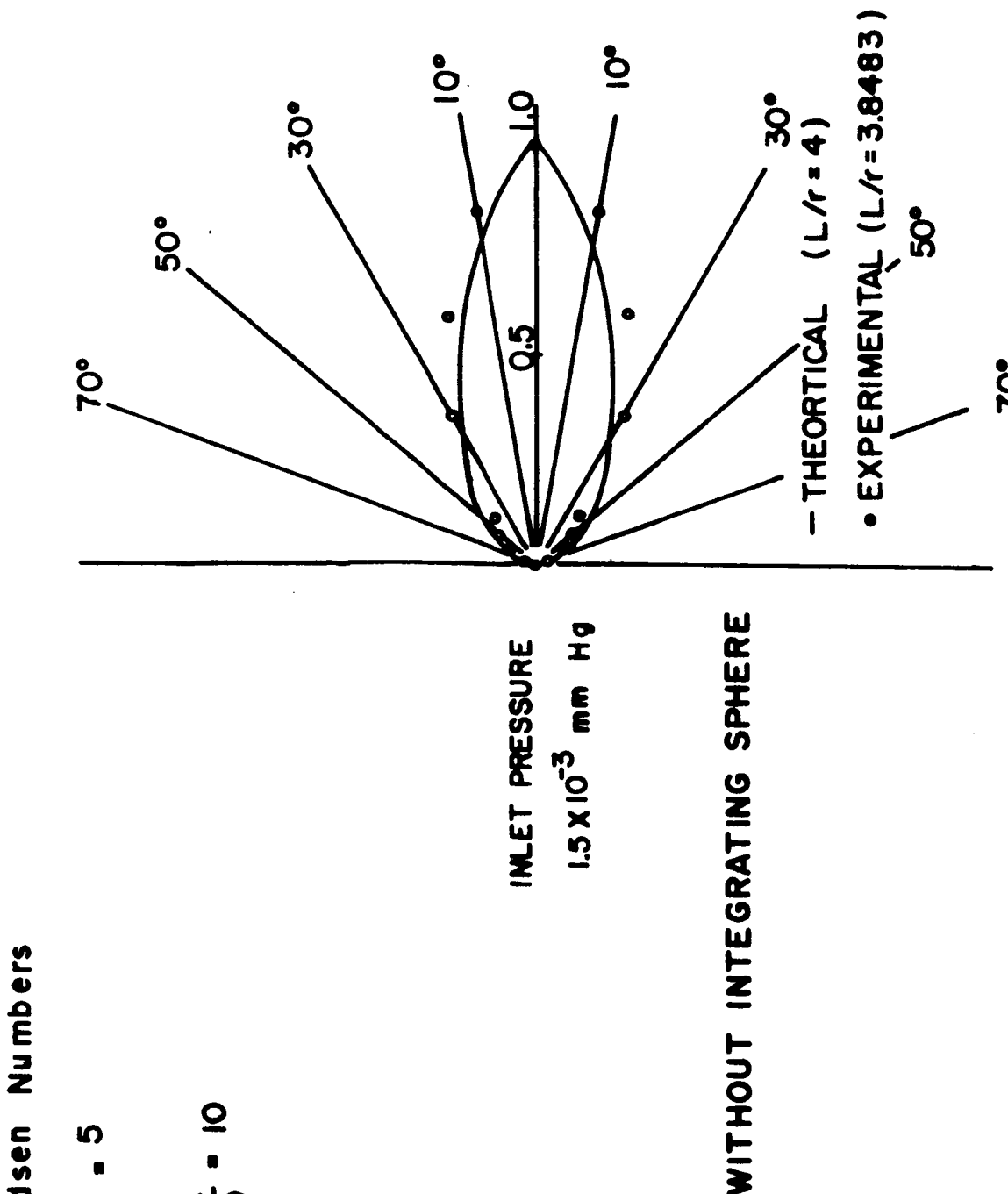

FIG.37 NOZZLE EXIT DISTRIBUTION

Knudsen Numbers

$\frac{\lambda}{L} = \infty$

$\frac{\lambda}{D} = 2600$

INLET PRESSURE
1×10^5 mm Hg

WITH INTEGRATING SPHERE

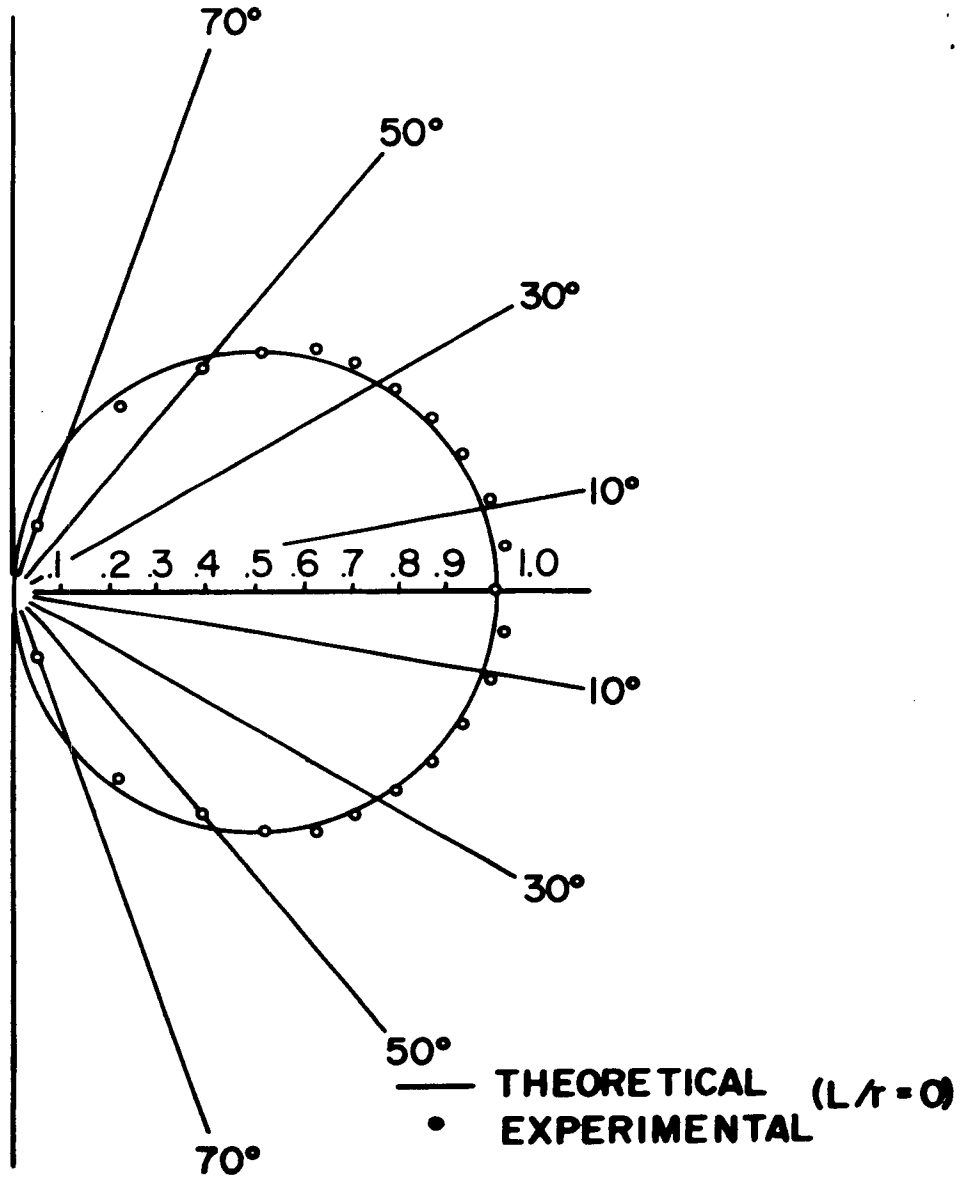

FIG.38 NOZZLE EXIT DISTRIBUTION

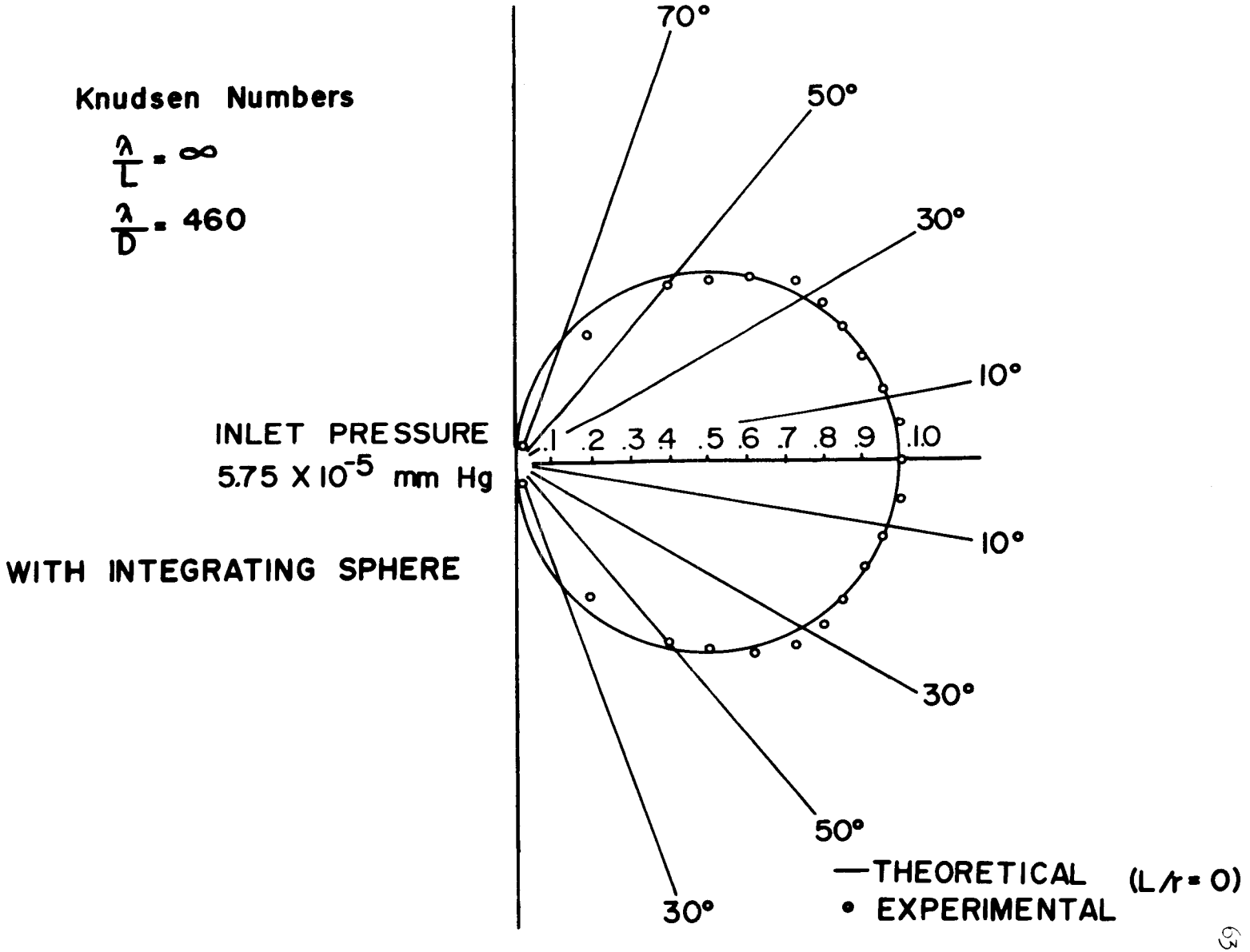

FIG. 39 NOZZLE EXIT DISTRIBUTION

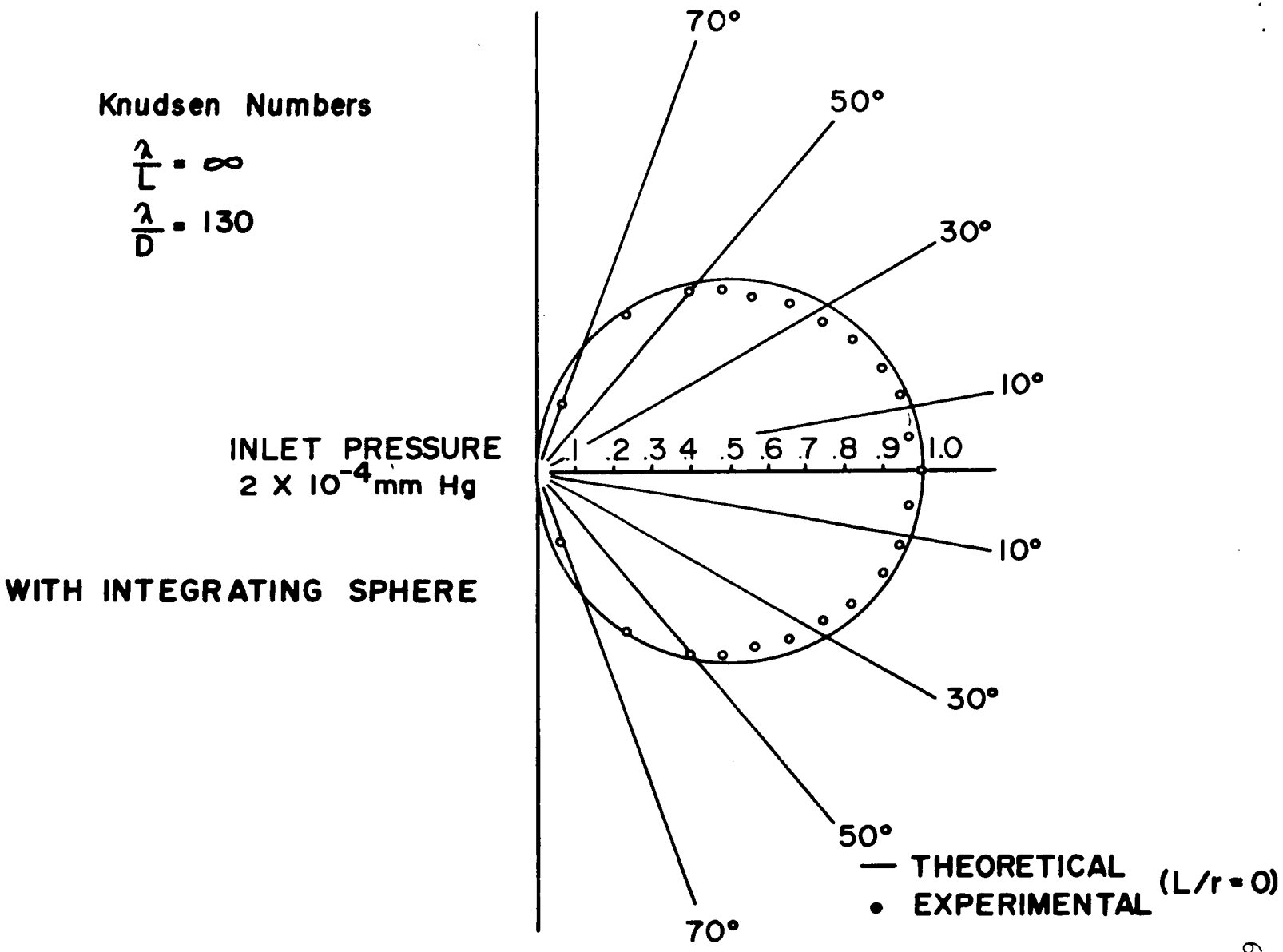

FIG. 40 NOZZLE EXIT DISTRIBUTION

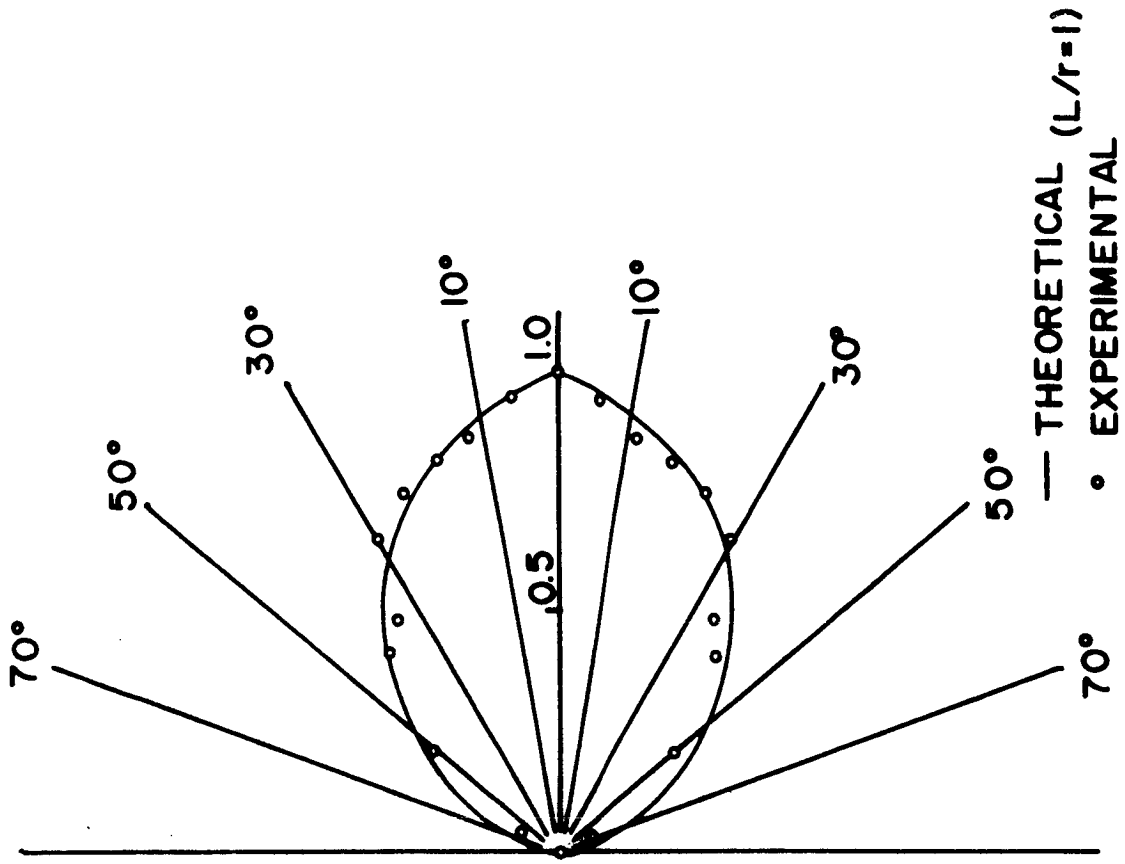

FIG. 41 NOZZLE EXIT DISTRIBUTION

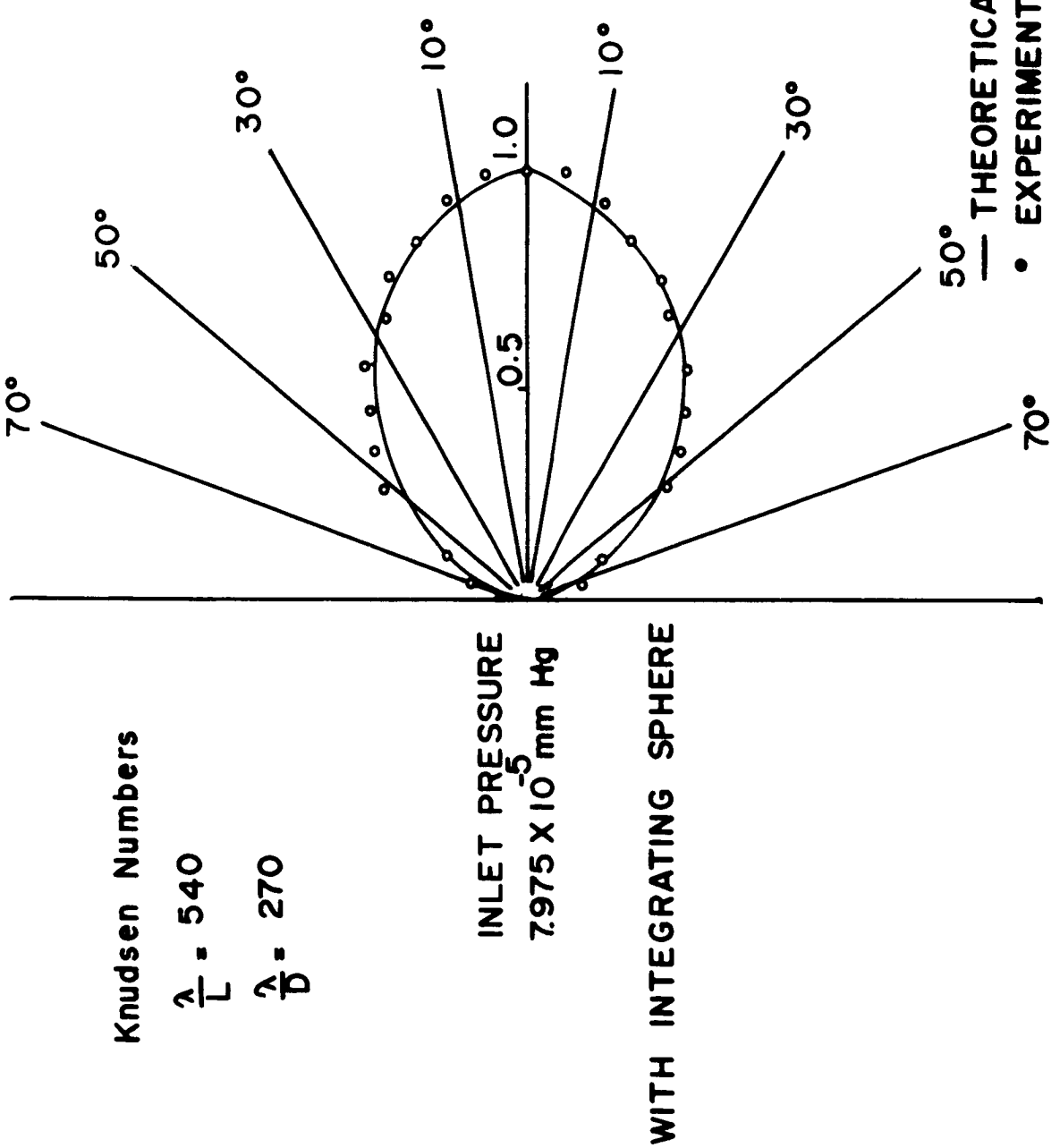

FIG. 42 NOZZLE EXIT DISTRIBUTION

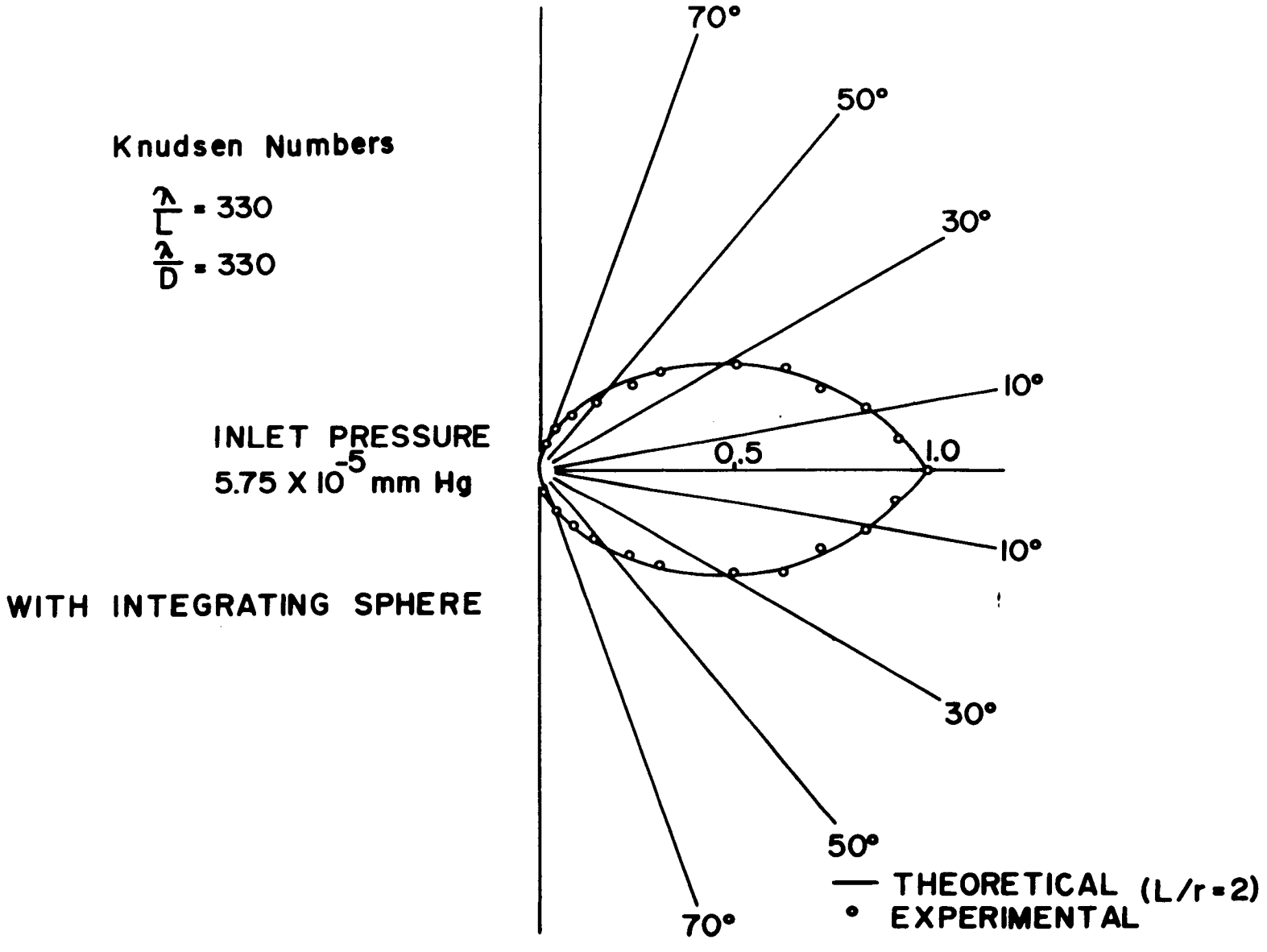

FIG. 43 NOZZLE EXIT DISTRIBUTION

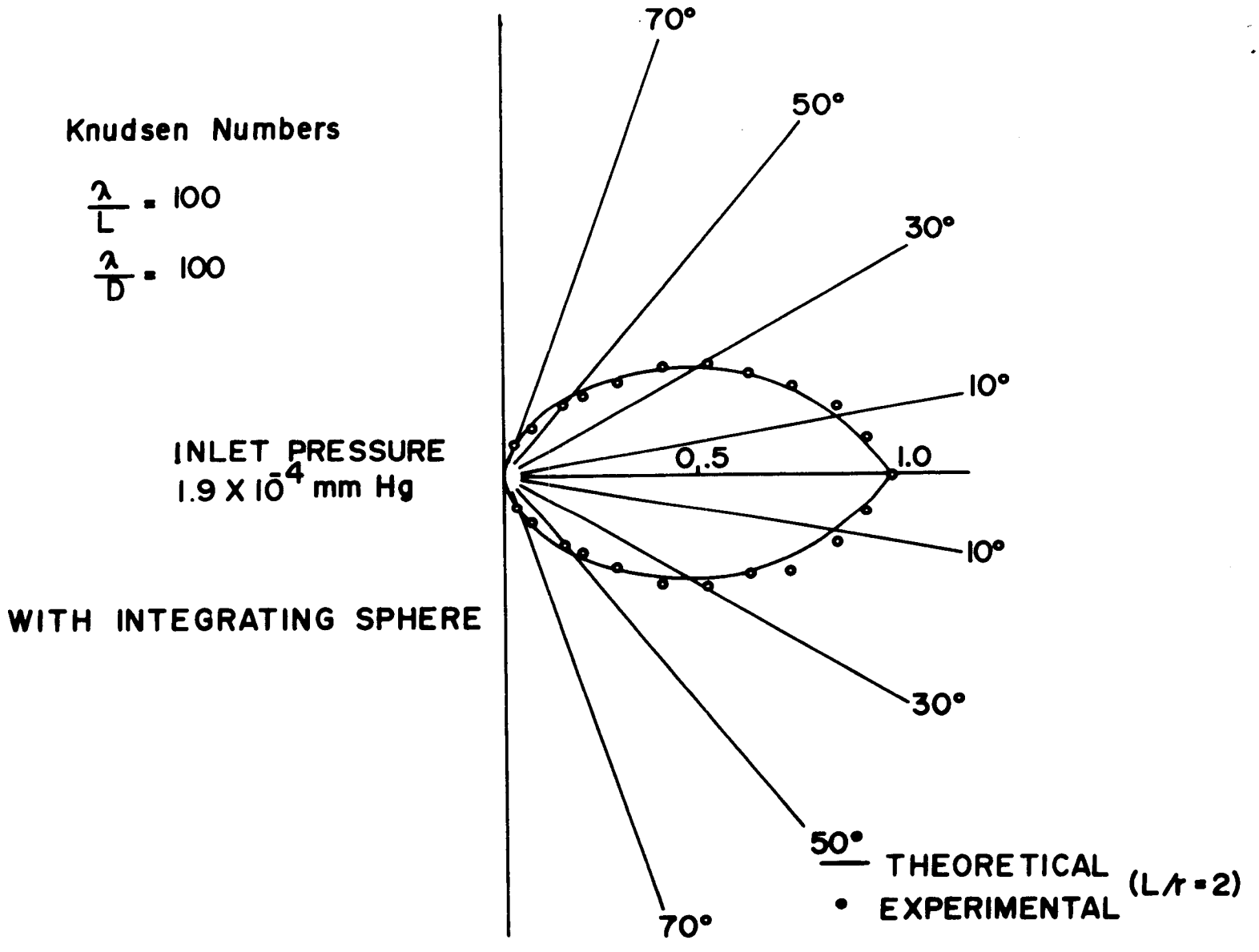

FIG. 44 NOZZLE EXIT DISTRIBUTION

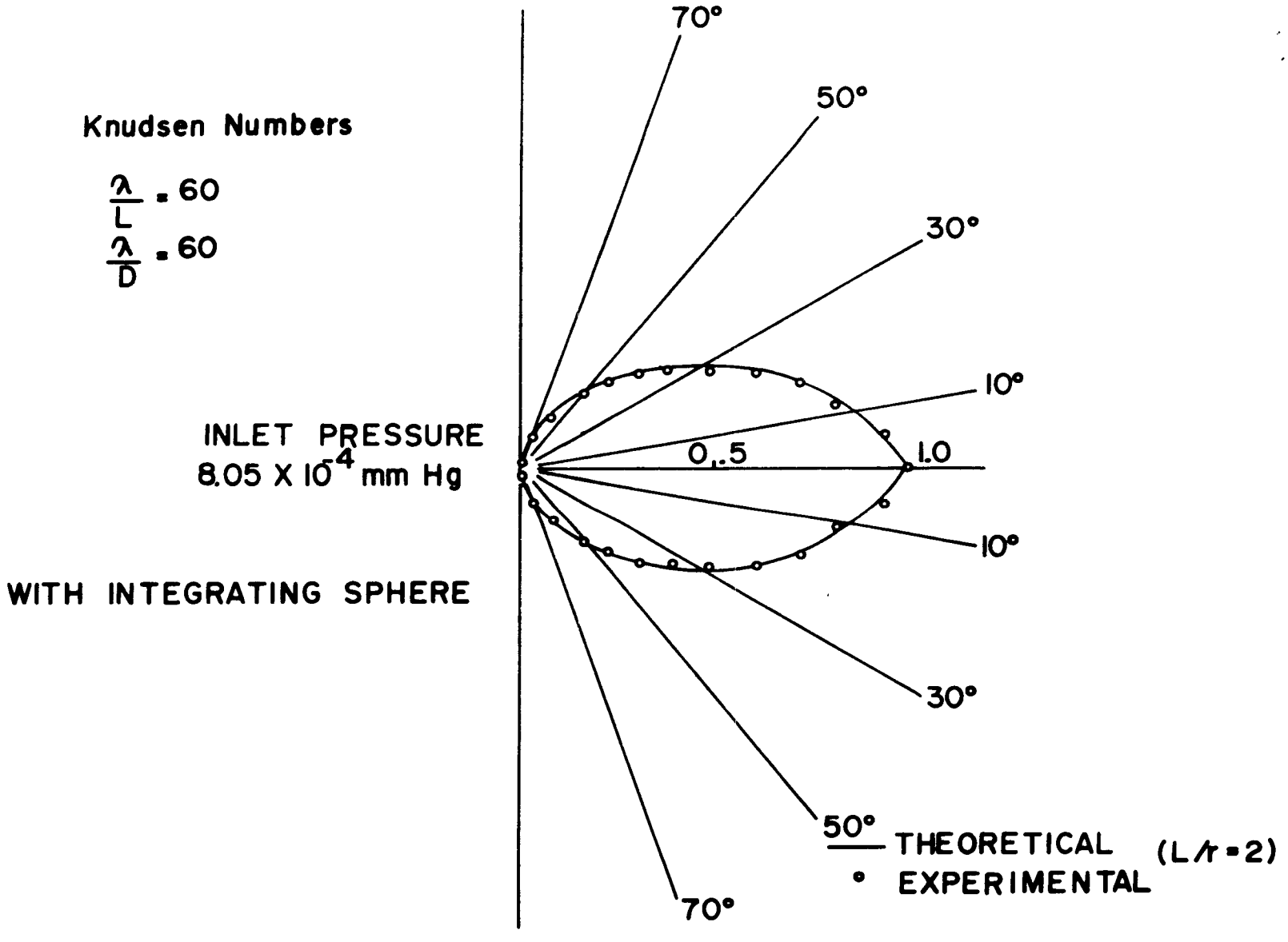

FIG. 45 NOZZLE EXIT DISTRIBUTION

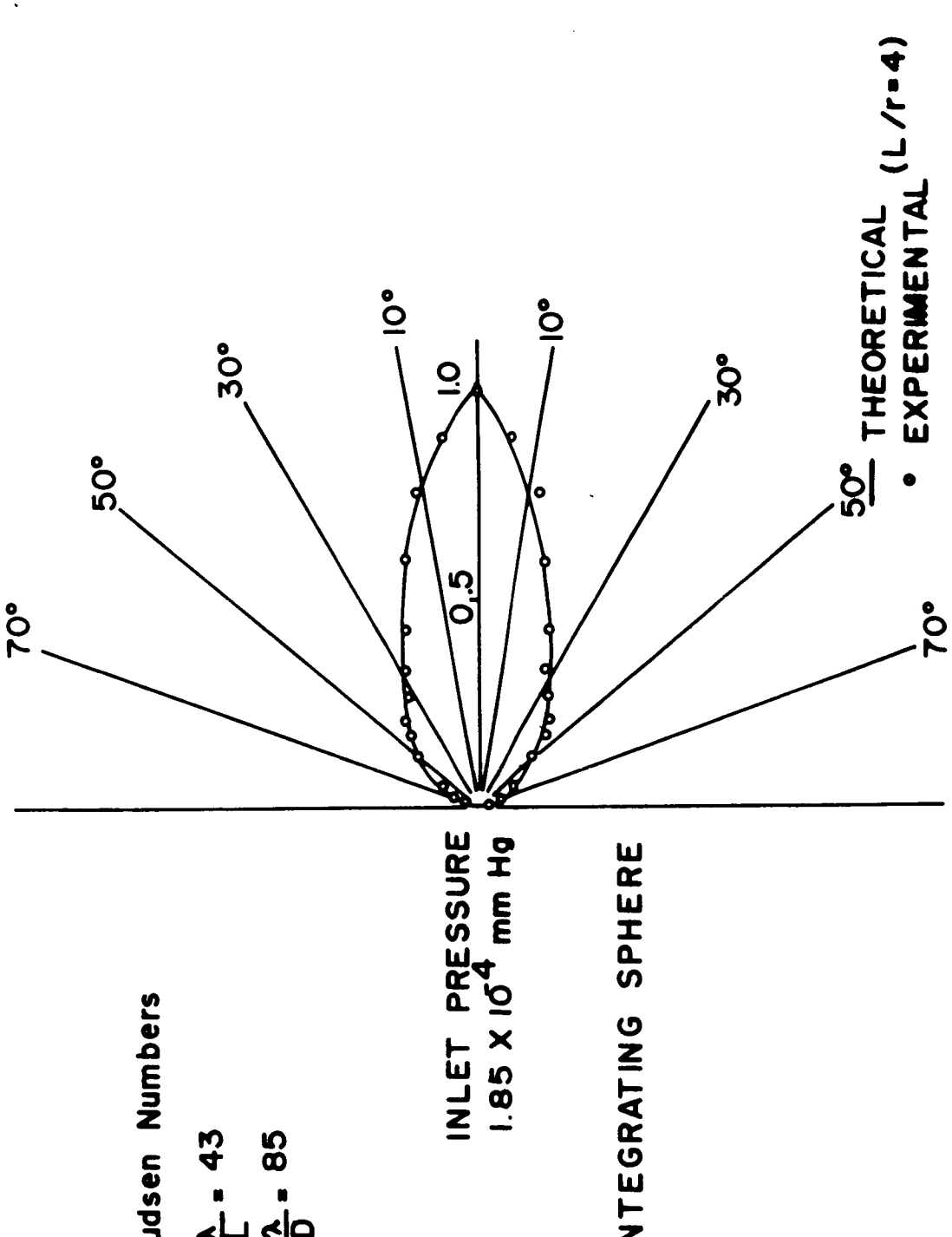

FIG. 46 NOZZLE EXIT DISTRIBUTION

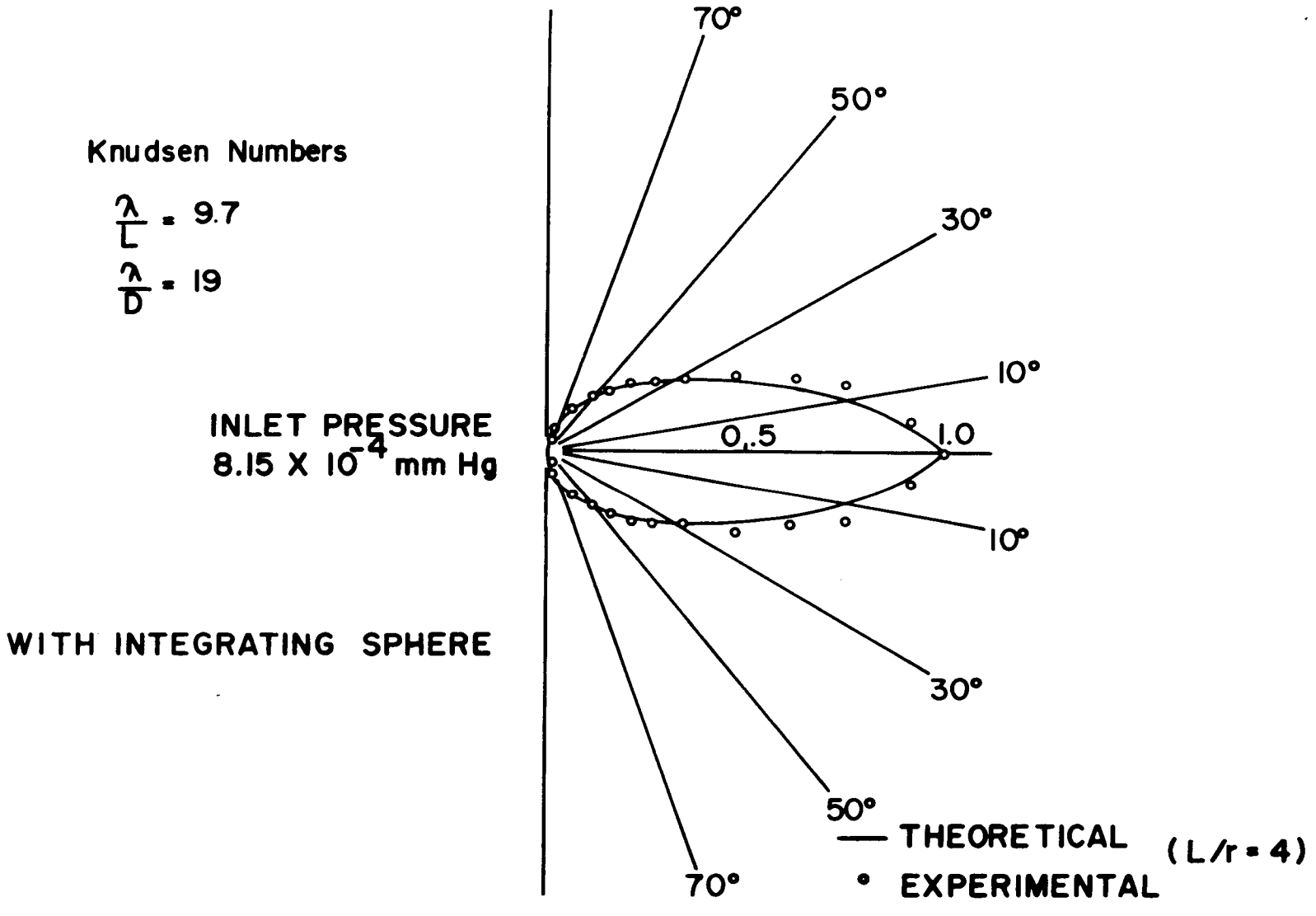

FIG. 47 NOZZLE EXIT DISTRIBUTION

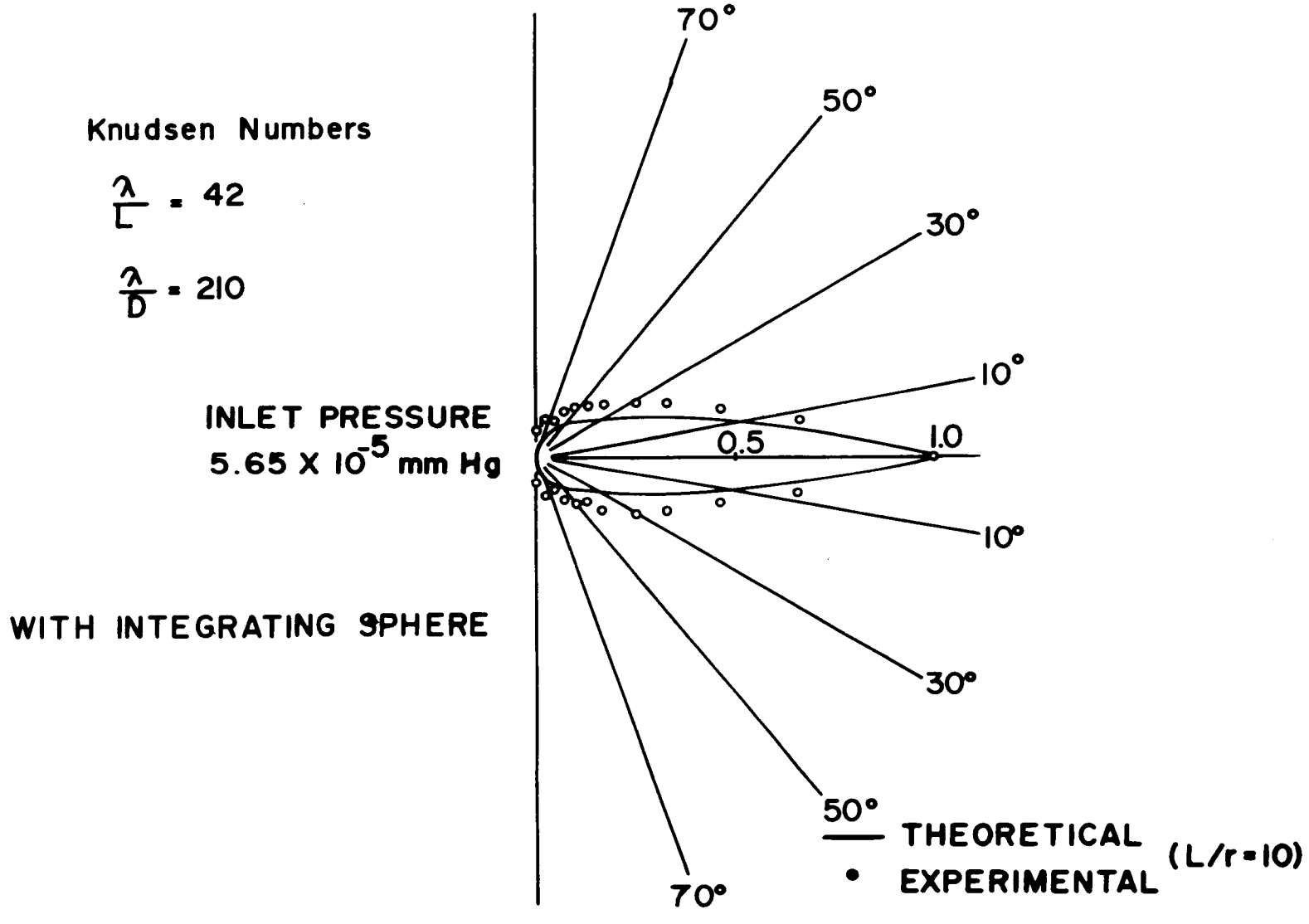

FIG. 48 NOZZLE EXIT DISTRIBUTION

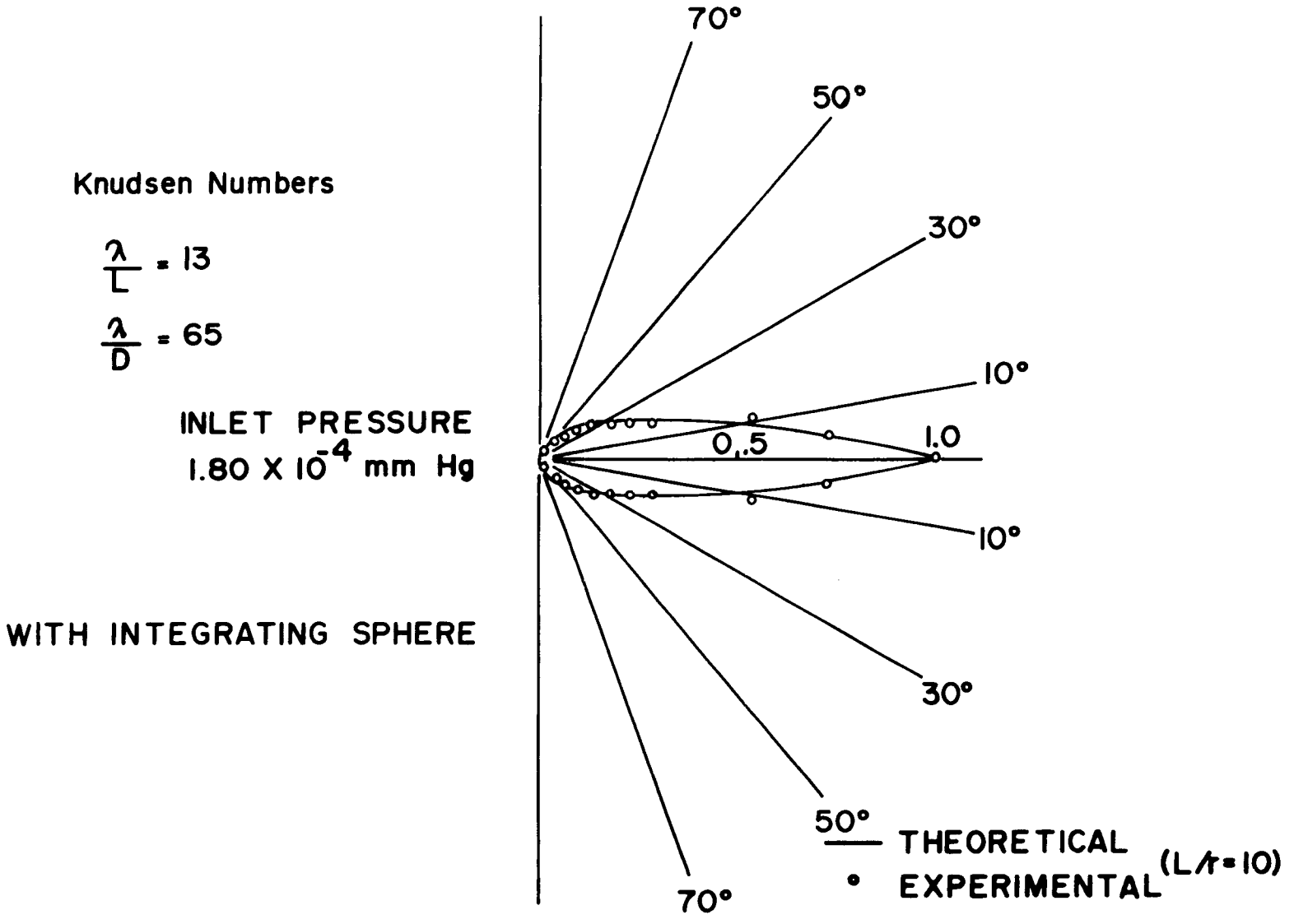

FIG. 49 NOZZLE EXIT DISTRIBUTION

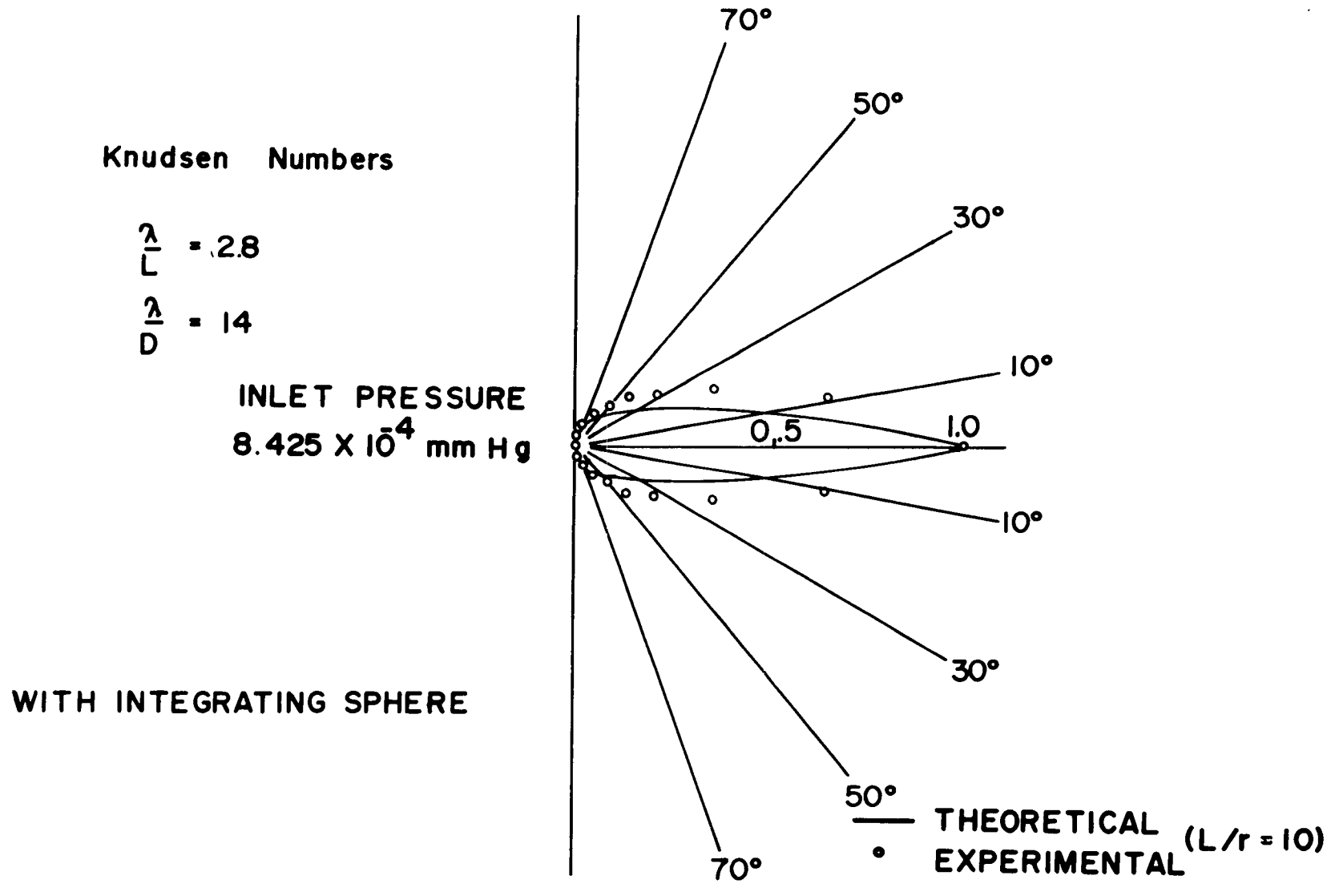

FIG. 50 NOZZLE EXIT DISTRIBUTION

basis the primary disagreement with theory can be traced to equilibrium considerations.

C. Nozzle Flow Rates

The nozzle flow rates were also determined experimentally. The flow rate is determined by calibrating the primary tank equilibrium pressure as a function of flow rate into the tank through the orifice. The orifice flow is assumed to agree with the theoretical free molecular flow as a function of upstream pressure. The nozzle flow rates are then determined relative to the orifice flow. It should be noted this eliminates any displacement errors in the pressure gages and only assumes the gages are repetitive. However, the Knudsen Numbers were determined directly from gage pressure readings.

Fig. 51 gives the flow rates versus pressure for the cylindrical configuration and Fig. 52 gives the same results for the spherical configuration. It should be noted, based on theoretical considerations, the cross-sections of the nozzles are made to give identical flow for the orifice and all nozzles at the same inlet pressure. The spherical chamber gives excellent agreement with theory and strongly supports the previous equilibrium conclusions. The change in probabilities can again be detected at the higher pressure where the flow begins to deviate from free molecular flow. A comparison with Monte Carlo theory by Ballance (22) shows similar deviations as collisions in the nozzles begin to take effect.

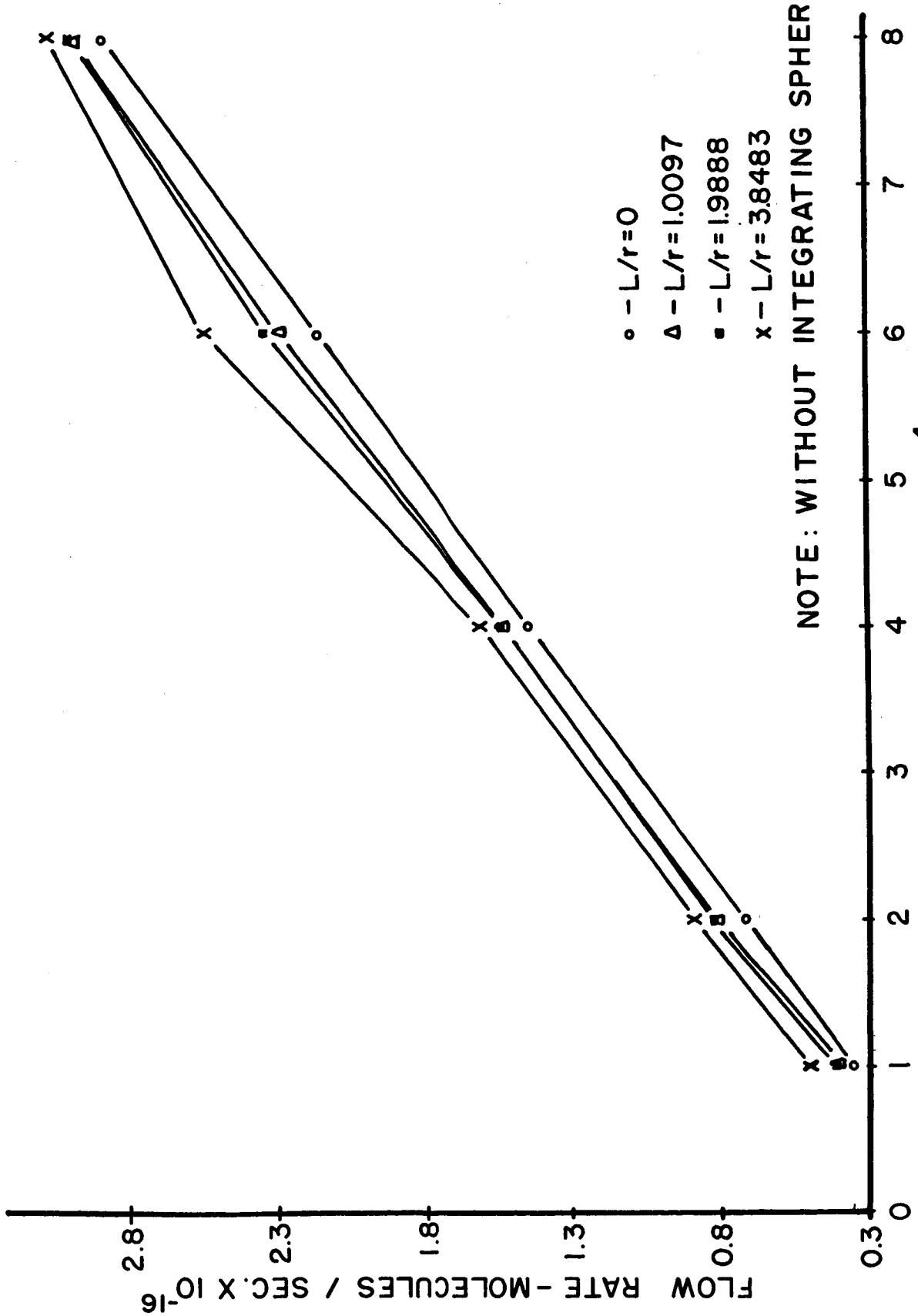

FIG. 51 NOZZLE PRESSURE VERSUS MOLECULE FLOW

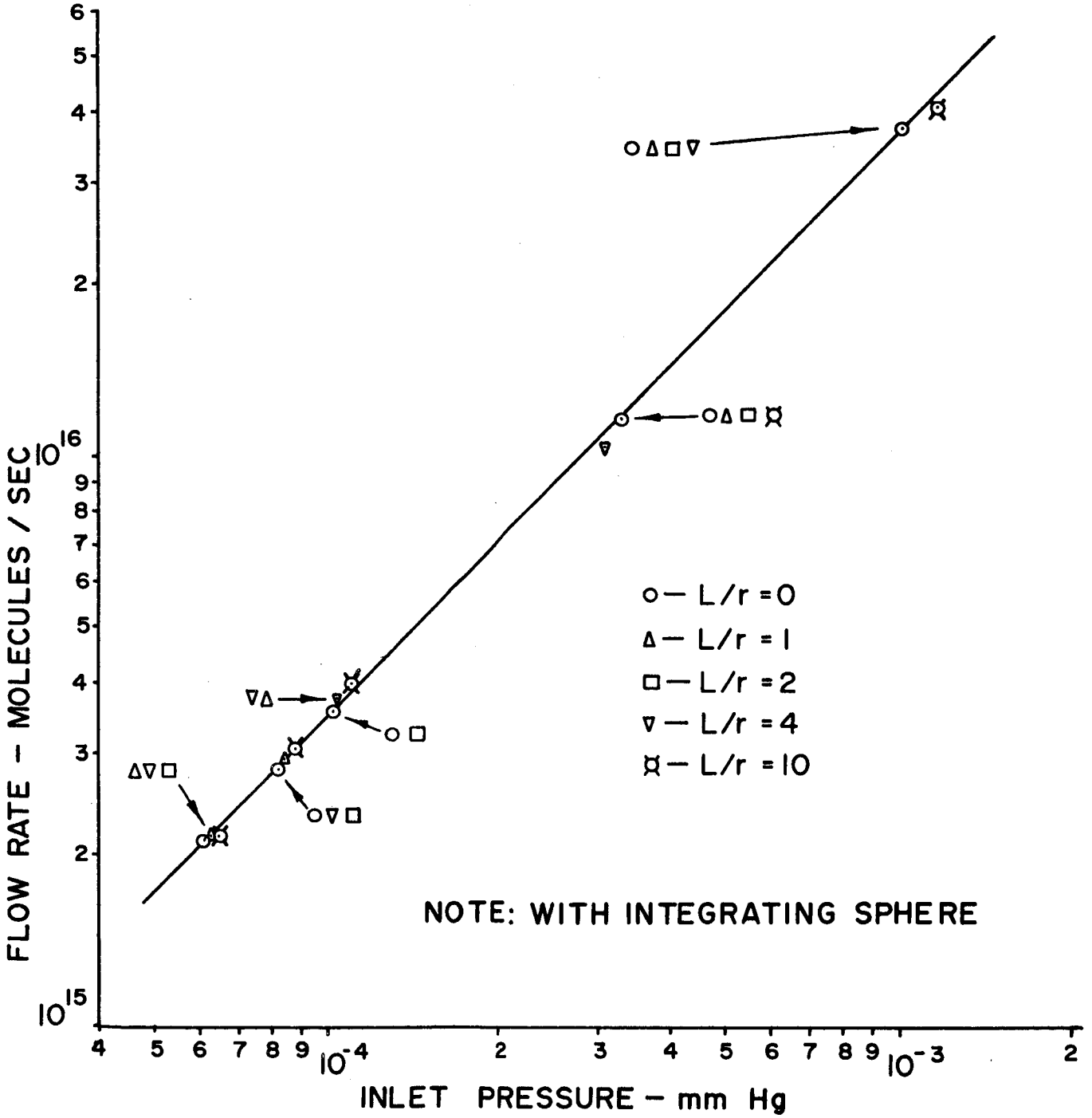

FIG. 52 NOZZLE PRESSURE VERSUS MOLECULE FLOW

V. MOLECULAR ACCELERATOR

The molecular accelerator (Fig.53) consists of an ion accelerator, the focusing mechanism, the charge exchange section, the ion remover, and orifice. The ion accelerator or ion engine is a close copy of the Kaufmann Source developed at the Lewis Research Laboratories. It consists of a gas distribution system, an electron source, accelerating plate and decelerating plate. The ion beam discharges into a focusing tube at a positive potential relative to the decelerating plate and is compressed. The ideal beam would come to a point approximately 3 feet from the end of the focusing tube. The beam is neutralized immediately after leaving the focusing tube with a charge exchange section. This consists of crossing the ion beam with a neutral beam of 5 to 10 times the ion beam intensity. Any remaining ions are eliminated with an electric field across the beam downstream of the neutralizer. To guarantee a small diameter, the beam is skimmed by passing it through a 0.3 inch orifice.

The diameter of the beam leaving the accelerator is 4 inches. A maximum of 4,000 volts is used to accelerate the beam, the potential is reduced to 1,000 volts or less with the decelerator, and finally reduced to the desired potentials. The system is designed for flow over an order of magnitude above the desired flow of 10^{16} molecules per sec. This requires less than 10% of the molecules to pass through the skimmer, and allows large allowances for the focusing. The upper limit on the accelerator also keeps the flow of molecules fairly constant over a large velocity range. All power supplies are regulated to guarantee steady state condition. The downstream end of the focusing tube is screened to

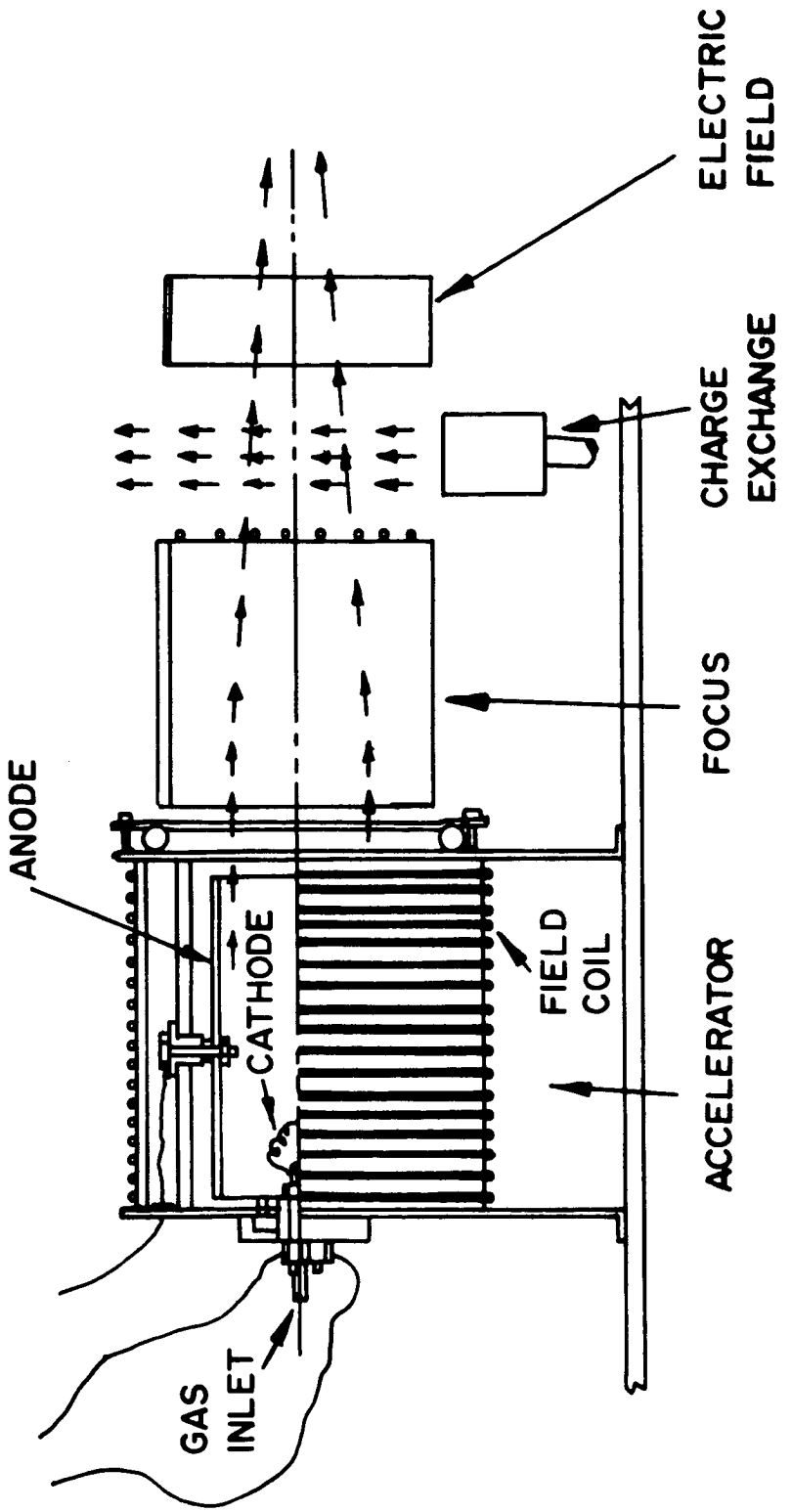

FIG. 53 MOLECULAR ACCELERATOR

guarantee the same potential on the molecules across the beam at the exit.

The molecule directed energy range varies from a maximum of 1,000 electron volts down to a minimum of a few volts. To date, runs on the unit have been from 1,000 electron volts down slightly below 100 electron volts. Voltages below 100 volts are difficult to operate.

A. Ion Accelerator

The basic requirement for the accelerator is a steady state reliable system. A literature survey (23 to 26) of various systems was made and the Kaufmann type source was chosen. Units of this type had been run continuously for many months at Lewis Research Laboratories with excellent reliability. The beam also has a constant potential across the face compared to the type systems using o-ring accelerators. The current densities in previous runs were over 2 orders of magnitude above the required values for the molecular beam.

An experimental study was made to provide tungston elements for the electron emitter. A number of different types of elements donated by Westinghouse have given good experimental results. Current versus usage time curves were recorded and found that a difference of approximately 1 amp (running at approximately 12 amps) would change the element life from in excess of 10 hours to less than 30 minutes.

B. Focusing

The two types of focusing investigated were magnetic and electric fields. Both systems should give satisfactory results from a physical analysis, as demonstrated in Fig. 54. A theoretical analysis shows good prospects with the magnetic focusing. The main disadvantage is the

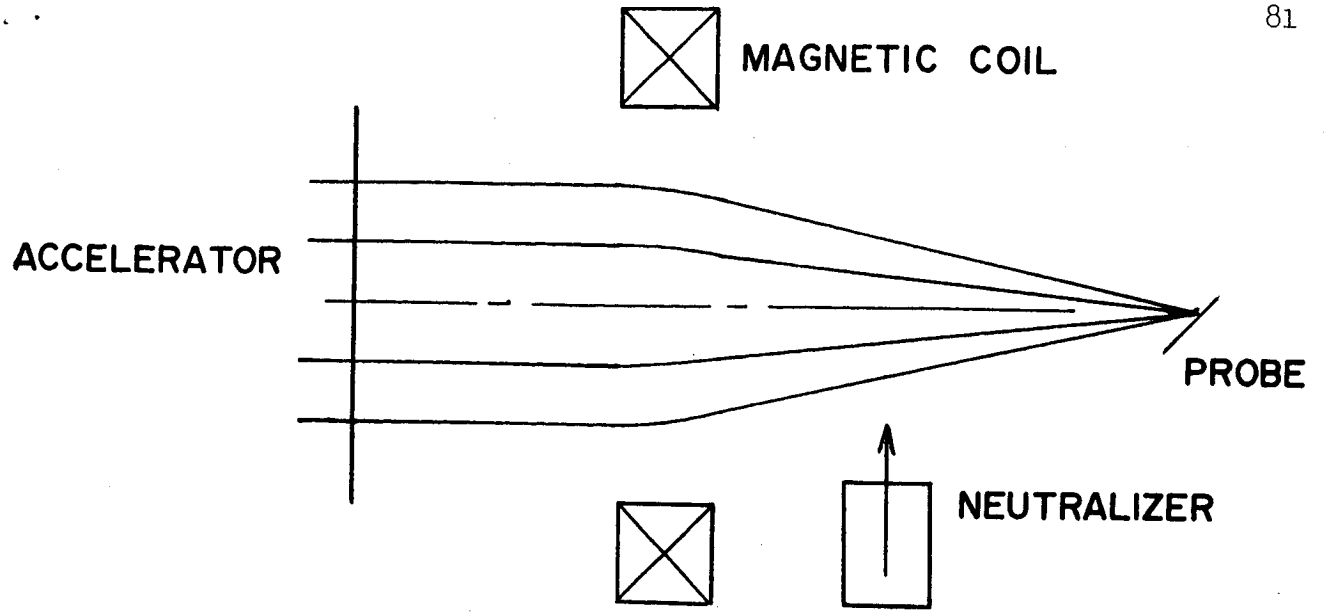

MAGNETIC FOCUSING

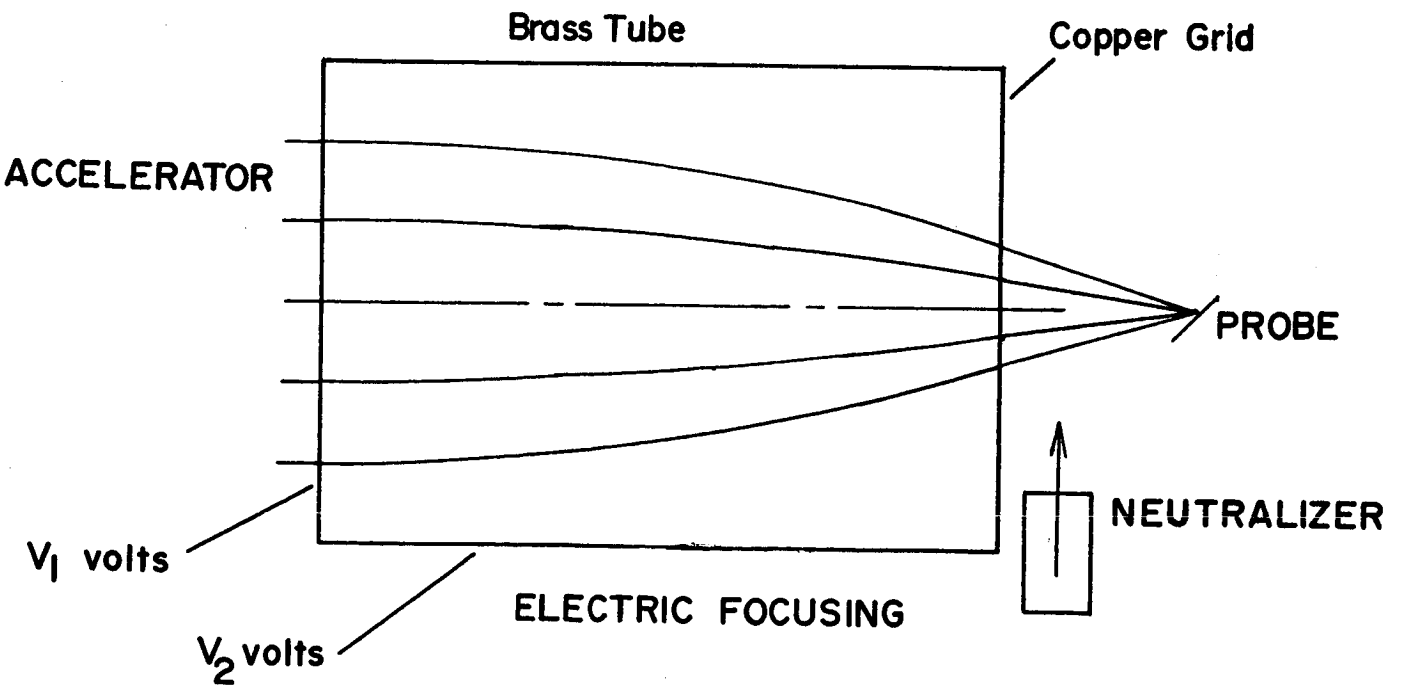

Fig. 54 MAGNETIC and ELECTRIC FOCUSING

equipment (large coils and core) required inside the vacuum system. A straight theoretical approach to the electric field approach failed to give satisfactory conclusions. An appreciable amount of work has been done with electron focusing but the simplifications of the equations do not hold for the higher mass ions. As a result a partial experimental type of analysis was used.

A simulated analog of the focusing using the full scale apparatus was set up. The system is represented by the Laplace Equation. The actual size system was emerged in a tank of water (Fig.55), voltages applied to the accelerator screen and focusing tubes, and the internal area was probed with a point electrode. The only major problem encountered was disturbances from the bubbles formed by the hydrolysis of the water. This was corrected by reducing the surface tension through the additon of soap powder. The resulting potential fields are given in Fig. 56 and 57. The constant voltage lines in Fig. 56 show the variation between the flat exit screen and one focusing tube. Fig. 57 shows the constant voltage between two focusing tubes at different potentials. Numerical calculations were made to follow ions through these fields. Newton's Second Law was integrated over small movements of the ions through the field. Final results indicated the focusing should be no problem.

An analysis was also made to determine the effect of charge concentrations in the focusing tubes. The results showed that the force due to charge is at least 2 orders of magnitude below the force of the electric field, with beams one order of magnitude intensity higher than the required beam. Due to these calculations, the effects of charge forces have been otherwise neglected.

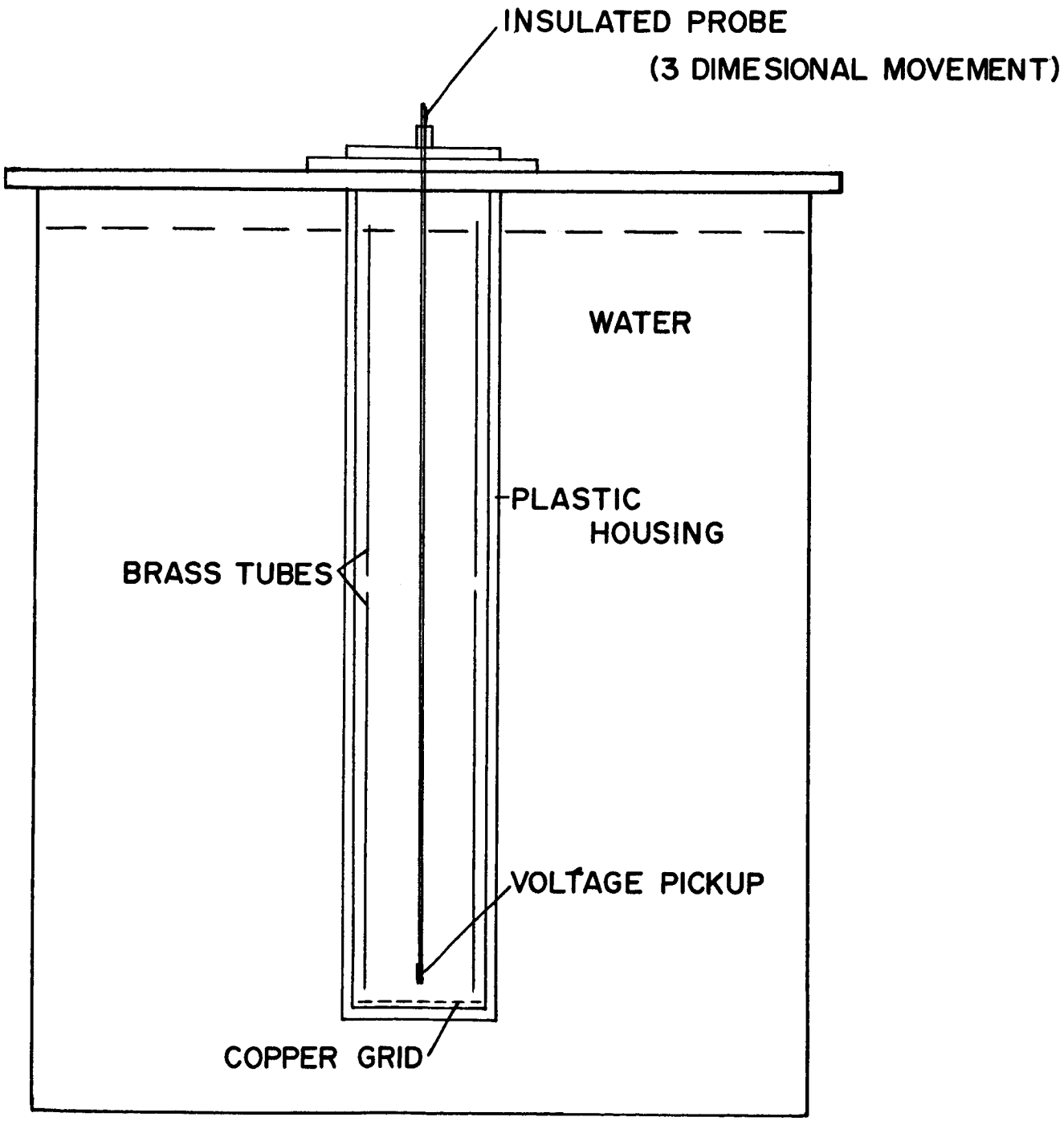

FIG. 55 SIMULATED VOLTAGE ANALOG

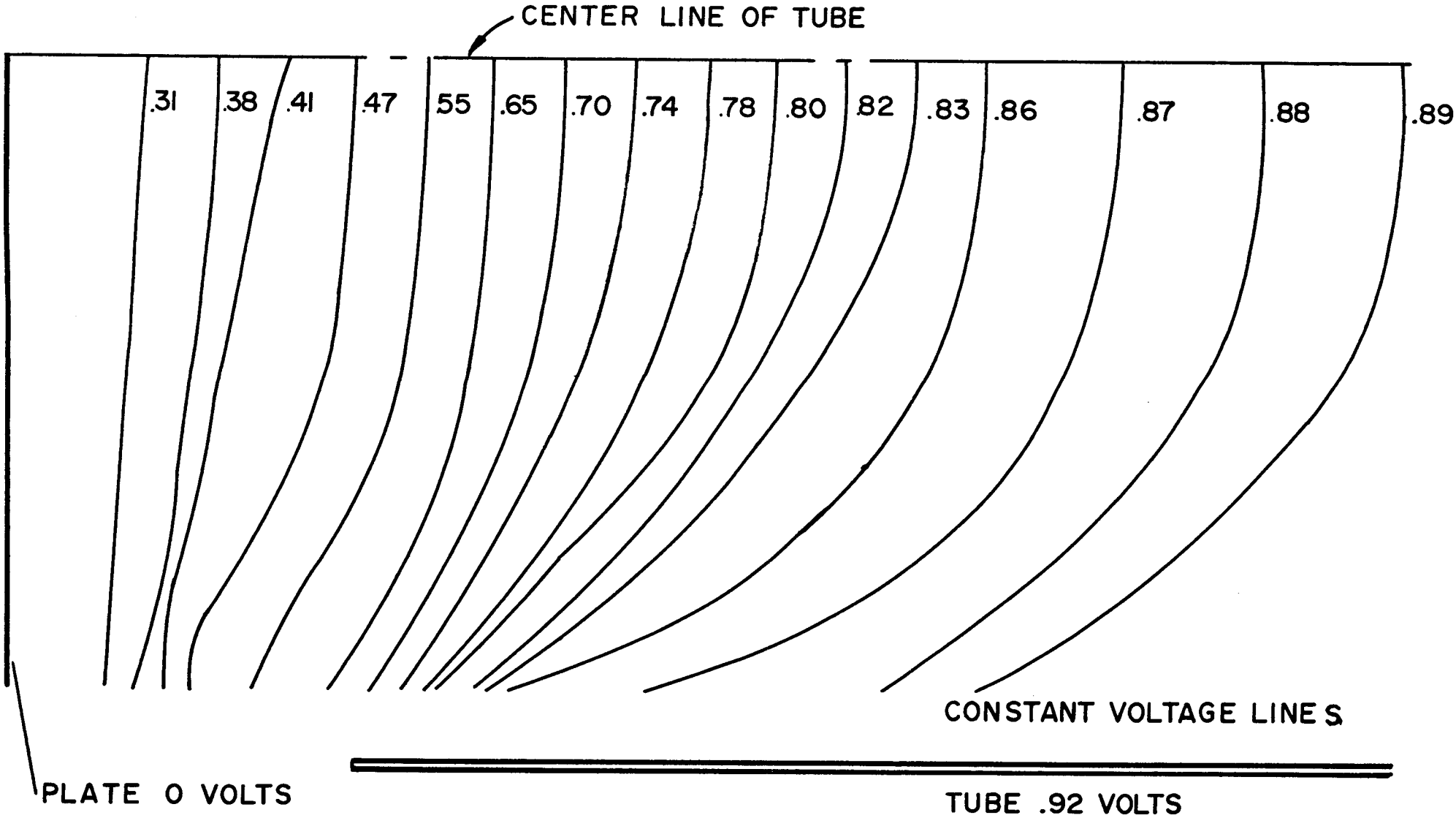

FIG 56 POTENTIAL FIELDS (1 TUBE INLET)

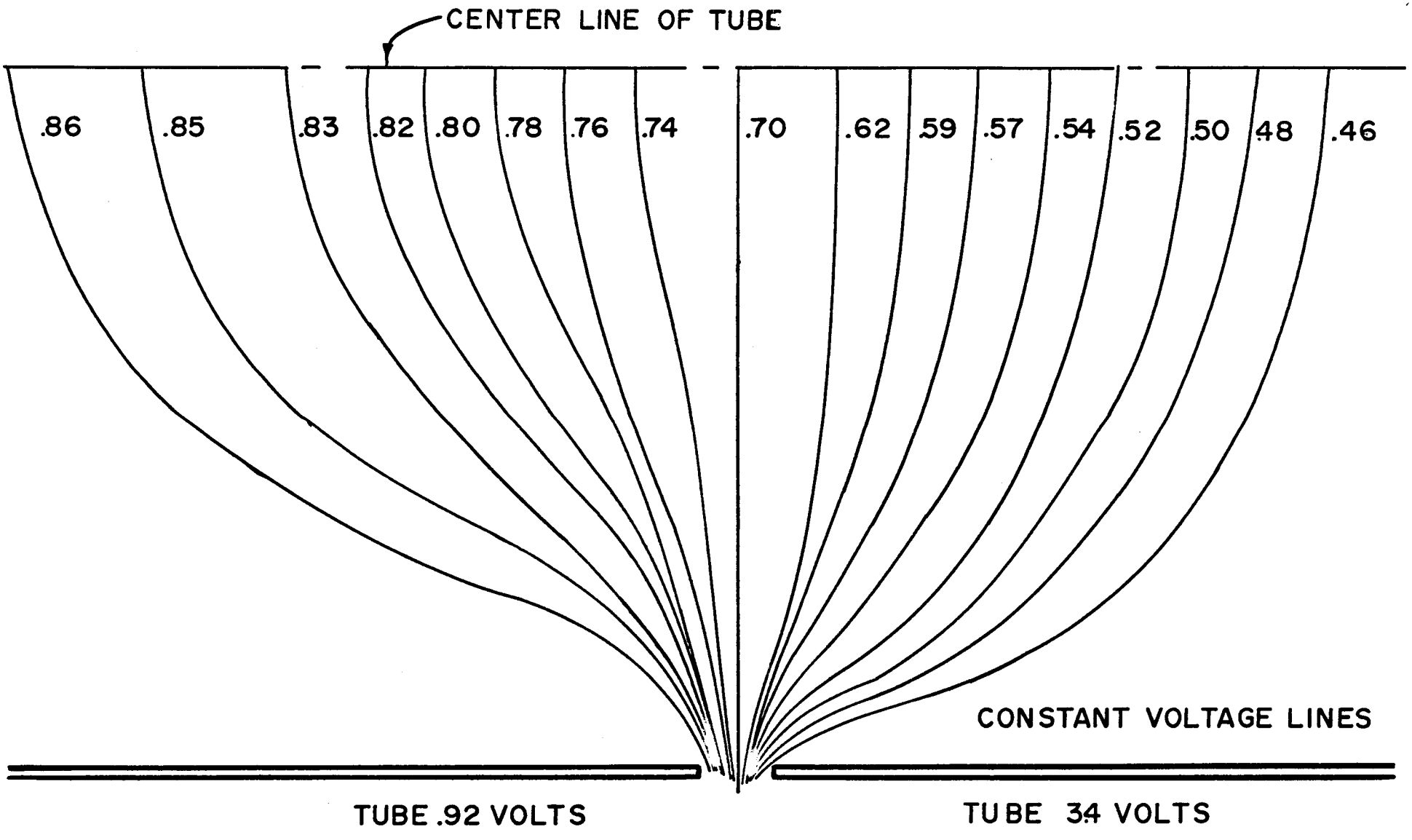

FIG 57 POTENTIAL FIELDS (ADJACENT TUBES)

C. Neutralization

The ion beam cannot be neutralized by injecting electrons because at the operating pressures recombination would require a few hundred feet. Thereby a charge exchange system was incorporated. A stream of neutral molecules is directed across the ion beam and the electrons are shared by the nuclei in each beam. The cross-sectional area for this interaction is sufficiently large that the electrons can be assumed to be shared by the two beams. Using a neutral beam 10 times as intense as the ion beam results in a high speed beam 90% neutralized after passing the charge exchange section. The ionized particles remaining in the beam are removed with an electric field.

The charge exchange stream of molecules is produced with a group of parallel free molecular flow nozzles (Fig. 58). The length to radius ratio is 10 to 1 to form a directed beam. The angular distribution can be taken from Fig. 49. A concentration of nozzles is produced in the center to match the ion beam.

D. Accelerator Status

The accelerator has been developed to the point where starting and continuous operation have become routine. Operation has been in the 100 ev to 1000 ev range with operation below 100 ev intermittent. The main problem is to measure exact flow rates (within one or two percent) and the exact beam location. Focusing is obvious in the operation; however, exact extent of beam focusing has not been determined.

The flow rates will be determined by pressure (as noted in the measurement of flow rates) in the instrument tank during steady state conditions with calibrations before each run. Runs to date give

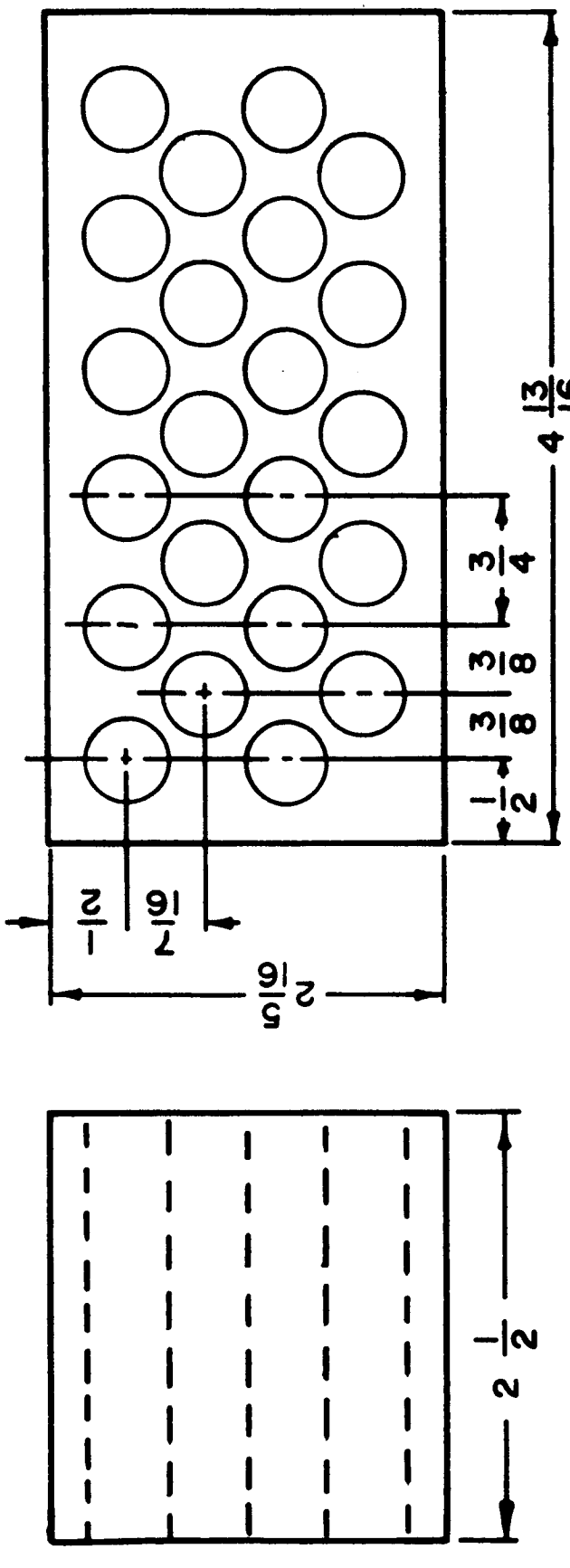

FIG. 58 NEUTRALIZING NOZZLES

accuracies of $\pm$ 10% over an hour period, but this is completely inadequate for accommodation coefficients. The variation is being hopefully corrected by placing constant voltage supplies to the pumping systems. Presently, input voltage varies by as much as 8 volts in a 110 volt system over a period of one hour. Running at night failed to solve the variation. Pressure variations have shown flow rates to be in the design ranges.

Reliable operation is expected in the near future.

VI. ACCOMMODATION COEFFICIENTS

A number of runs were made to determine accommodation coefficients. The first runs (1965) assumed diffuse reflection to compare calculated values with experimental values. The ballpark comparison is included in Schaetzle (1965) and is shown in Figs. 59 and 60. The cylindrical nozzle backup was used for this data. More precise work has been done with the final nozzle configurations.

A. Analysis for Accommodation Coefficients

The reflection of molecules is assumed to be made up of two components, one diffusely reflected with a consine distribution and one specularly reflected as represented in Fig. 61. The force, due to the incoming molecule vector plus the components of force due to the reflected molecule vectors, represents the total force on the surface.

The number of molecules colliding with the surface is equal to the integral of the number of molecules entering the orifice or nozzle, times the probability of passage through the orifice, times the solid angle from exit of nozzle to the surface, times the distribution of molecules as a function of angle between nozzle centerline and the line from nozzle exit to surface. This can be represented mathematically as

$$N_{Coll} = \int_{\substack{\text{Nozzle}\\\text{Area}}} P_t dN_{In} \int_{\substack{\text{Nozzle}\\\text{Surface}}} d\Omega_f \quad (\gamma) \int_{\substack{\text{Probe}\\\text{Surface}}} dA$$

The molecule distributions utilized are experimental data in Section IV. To find the rate of momentum transfer the velocity C and molecule weight must be included in the integral resulting in

$$M = N_{Coll} \frac{\overline{C^2}}{\overline{C}} m$$

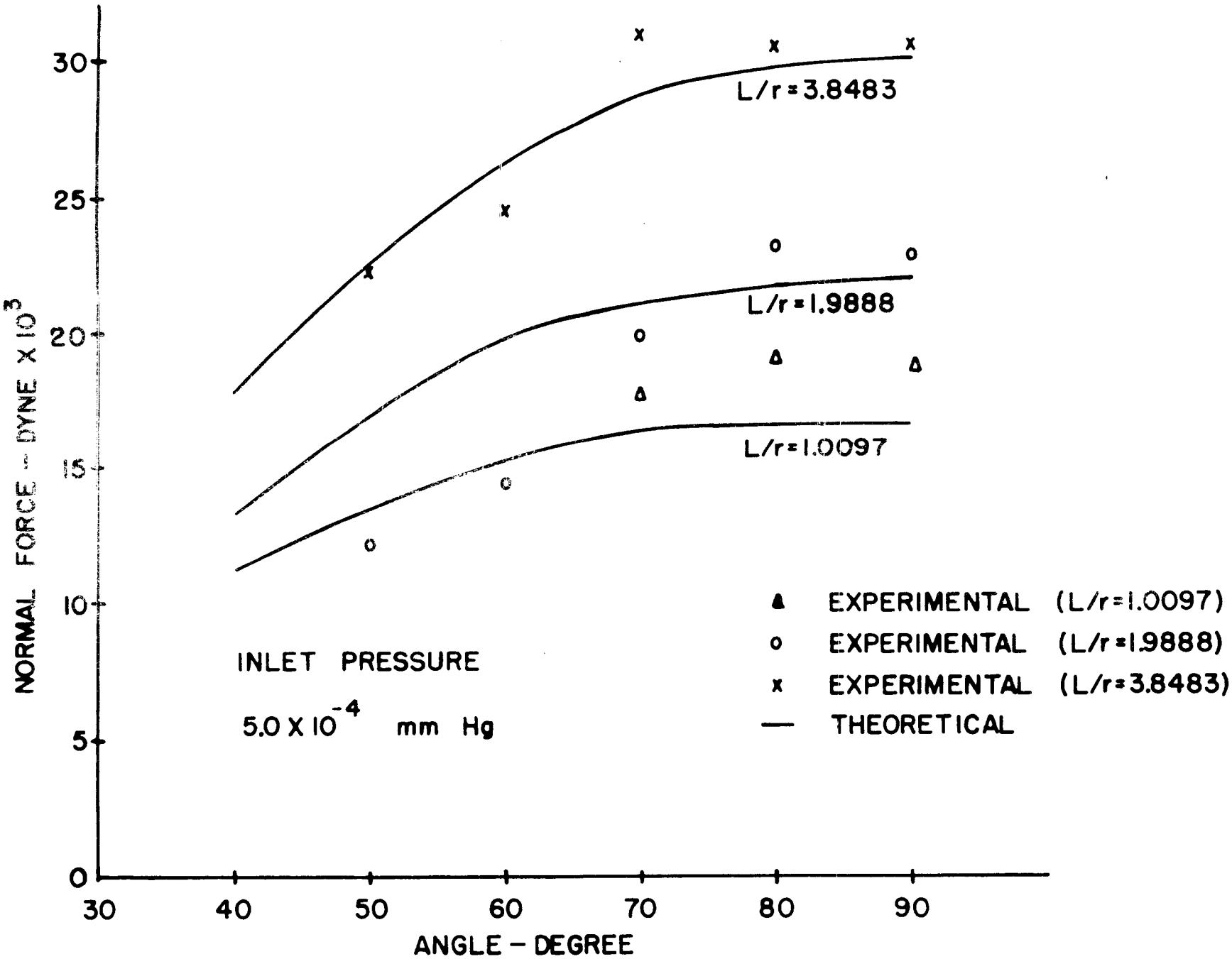

FIG. 59 NORMAL FORCE RESULTS

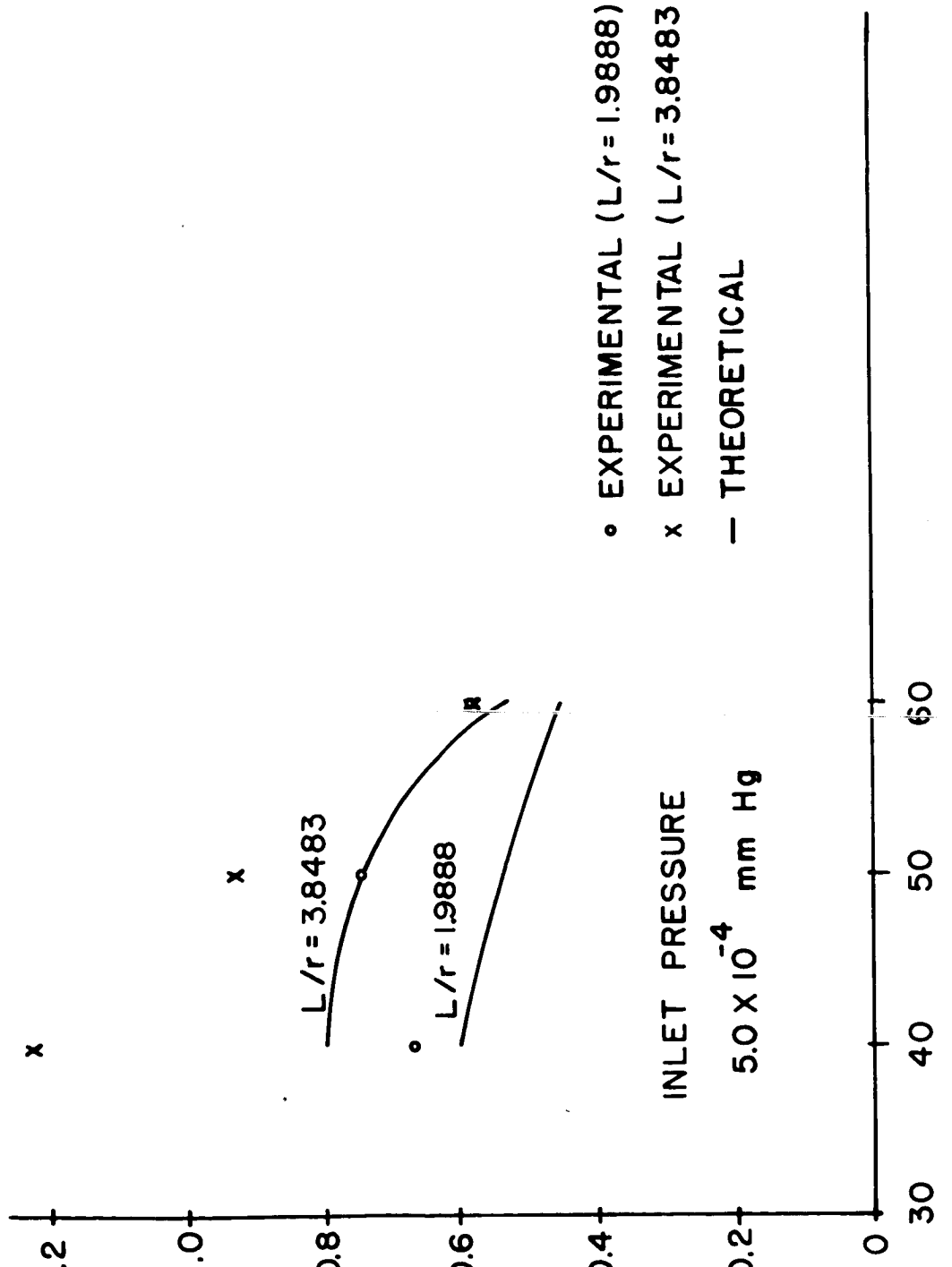

FIG.60 TANGENTIAL FORCE RESULTS

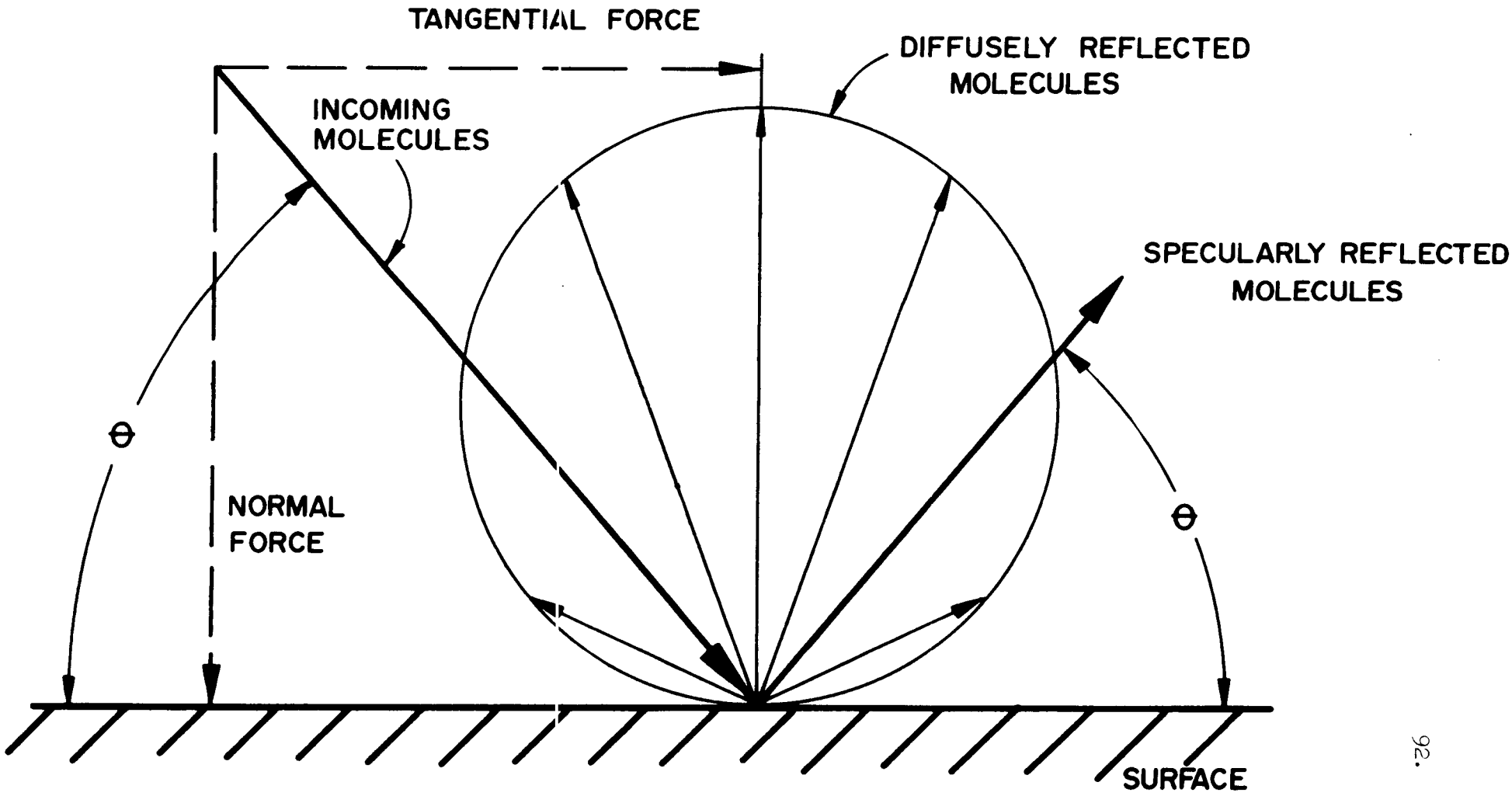

FIG. 61 MOLECULE SURFACE REACTIONS

The normal accommodation coefficient is defined as

$$\sigma' = \frac{P_i - P_r}{P_i - P_w}$$

For specular reflection σ' is equal to zero and for diffuse reflection σ' is equal to one. For this paper it will be assumed that σ equals the component of molecules diffusely reflected and $1 - \sigma$ is the component specularly reflected. This definition is not exact but has been used by a number of researchers including Knudsen.

The normal force on a surface for surface temperature equal to molecule temperature can be given as

$$F = M \sin\theta + 0.667\ \sigma' M + (1 - \sigma')\ M \sin\theta$$

where the first term represents the incoming molecules, the second term thediffusely reflected molecules (the 0.667 represents the average normal vector of diffusely reflected molecules) and the third term represents the specularly reflected molecules. For the tangential force, the same type analysis can be made resulting with

$$F_T = M_{\cos}\theta - (1 - \sigma)\ M_{\cos}\theta = \sigma M_{\cos}\theta$$

The diffusely reflected molecules have no tangential force.

It might be noted that when $\sin\theta = 0.667$ the normal force is independent of the accommodation coefficient. To eliminate errors in pressure measurement and nozzle passage probability, this point is used as a reference for some calculations. This technique also gives a calibration point for pressure on the ionization gage. The ion gage and molecular flow rate is assumed to vary linearly from this point. Some normal coefficients were calculated using an iterative technique between points. This was used when an increase in accuracy was deemed possible.

Different nozzles were used for the normal and tangential probes,

as a result the reference point could not be transferred. The data used for calculating the tangential coefficients were proved outside the required accuracy limits. Future work will include normal force points to calibrate the tangential data.

B. Results

Data has been recorded for both plastic and brass probes. Though there is some scatter in the data, normal accommodation coefficients have been calculated using both the described techniques.

The plastic was of the commercial variety used to cover printed pages. There was no excess cleaning process used on the material, but the tank and plastic were heated to about 160°F for about 8 hours to provide some degassing. This degassing reduced the available pressure level in the instrument tank by an order of magnitude. The brass was 0.003 inch shim stock and treated in the same manner as the plastic.

The swinging probe data for the plastic probe gave normal accommodation coefficients of 0.99 to 1.00 between angles of 90° to 20°. The results of the rotating plastic probe gave a slight variation with normal coefficients varying from 1.0 at 90° (θ) to .98 in the range of 80° to 60° and back to 1.0 in the range of 60° to 50°. There could be some inaccuracies in the data causing this result; however, the data was consistent with essentially no scatter.

The brass probe deflections turned out to be slightly higher than the predicted calculated values based on a iterative process between points. The deviation increased as the angle θ decreased. The excess force was a few percent near 90° with an increase to approximately 8% at an angle of 45°. A possible explanation is a slightly peaked diffuse reflected molecule distribution. This would raise the value of normal

force slightly higher than the calculated value of 0.667 for the cosine distribution. A second possibility is that the radiation absorptivity of the probe was slightly higher than the emissivity, raising probe temperature slightly above ambiant temperature, resulting in slightly higher forces.

The tangential probe data had too much scatter for reliable results and calculations showed as much as 20% deviations from realistic values. Fig. 62 shows a set of data for the plastic probe. The values increase as θ and the represented solid angle increase and again return to a minimum. The data is normalized to a constant flow rate; however, it has not been normalized for the nozzle distribution at various angles. Larger angular deflections to be used in future work should increase accuracy for a reliable set of data.

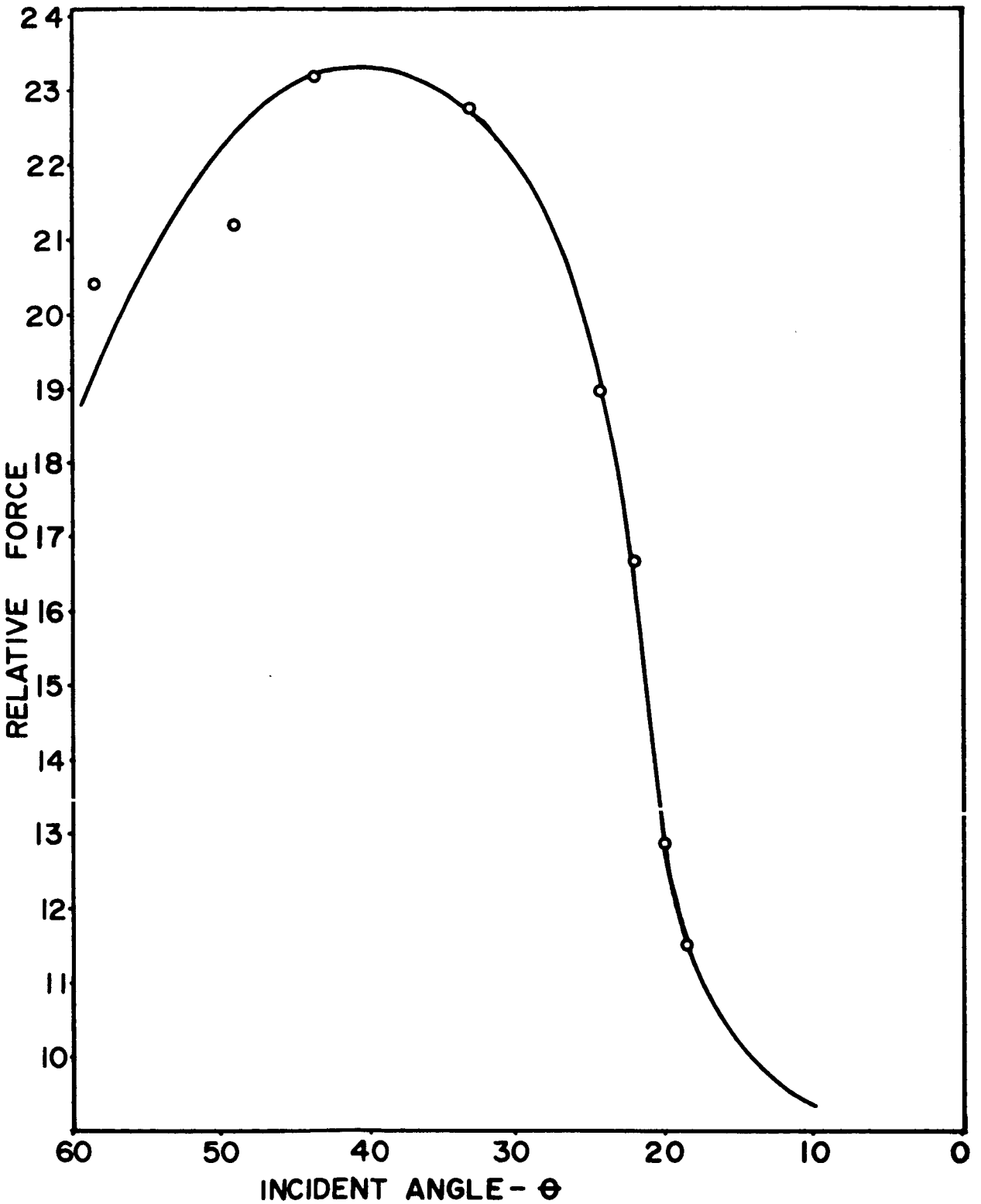

FIG. 62 TANGENT PROBE DEFLECTION

VII. FUTURE WORK

An excellent set of experimental equipment has been constructed to measure accommodation coefficients. The accelerator still requires instrumentation to precisely determine beam characteristics. The future work could consist of the following:

1. A good set of production data with the free molecular flow nozzles. (This has been initiated as a Master's Thesis and should be complete by December 1966.) The data will be recorded and placed on computer cards with the computer making the final analysis.
2. Precisely determine the properties of the high velocity molecular beam.
3. Repeat step 1 with the high velocity beam.

VIII. REFERENCES

1. Wachman, H. Y., "The Thermal Accommodation Coefficient: A Critical Survey", ARS Journal, 32, (2-12), 1962.

2. Hurlburt, F. C., "An Experimental Molecular Beam Investigation of the Scattering of Molecules from Surfaces", Ph.D. Thesis, University of California, 1954.

3. Smith, J. N. and Fite, W. L., "Recent Investigations of Gas-Surface Interactions using Modulated Atomic Beam Techniques", in Rarefied Gas Dynamics, Vol. 1, edited by J. A. Laurmann, Academic Press, 1963.

4. Jowtusch, W., "Investigation of the Scattering of Gas Molecules on Various Surfaces", in Rarefied Gas Dynamics, Vol. 1, edited by J. A. Laurmann, Academic Press, 1963.

5. Datz, S.; Moore, G.E.; and Taylor, E. H., "The Reflection of Modulated Helium and Deuterium Molecular Beams from Platinum Surfaces", in Rarefied Gas Dynamics, edited by J. A. Laurmann, Academic Press 1963.

6. Schaaf, S. A. and Chambre, P. L., "Flow of Rarefied Gases", Princeton University Press, 1961.

7. Schaetzle, W. J., "An Experimental Study of Molecular Surface Interactions at Velocities up to and Exceeding Space Probe Escape Velocities", proposal by Bureau of Engineering Research, University of Alabama, 1963.

8. Same as 7. Proposal for one-year extension, 1964.

9. Same as 7. Proposal for six-month-extension, 1964.

10. Schaetzle, W. J., "A Study of Free Molecular Flow Through Various Length Cylindrical Nozzles", in Proceedings of 3rd International Vacuum Symposium, Pergemon Press, Ltd., 1966.

11. Schaetzle, W. J., "Pumping Speeds of a Large Titanium Sublimation System", presented at 1965 American Vacuum Society Meeting.

12. Schaetzle, W. J., "Some Experimental Data on Momentum Accommodation Coefficients", presented at the 1966 International Symposium on Rarefied Gases, Oxford, England, to be published in Rarefied Gas Dynamics, Academic Press 1966.

13. Schaetzle, W. J., "An Analysis of Some Rarefied Gas Phenomena from the Molecular Approach", in Rarefied Gas Dynamics, edited by J. H. de Leeuw, Academic Press, 1965.

14. Schaetzle, W. J., "The Molecular Distributions at the Exits of Cylindrical Nozzles in Free Molecular Flow", to be published.

15. Seely, Fred B. and Smith, James O., Advanced Mechanics of Materials, John Wiley and Sons, Chapter 21.

16. ASME Boiler Construction Code Section VIII, 1950.

17. Dushman, Saul, Scientific Foundations of Vacuum Technique, John Wiley and Sons, Inc., 1961.

18. Guthrie, Andrew, Vacuum Technology, John Wiley and Sons, Inc., 1963.

19. Clausing, R. E., "A Large Scale Getter Pumping Experiment Using Vapor Deposited Titanium Films", Transactions of the American Vacuum Society, 1961, MacMillan Company.

20. Dayton, B. B., "Gas Flow Patterns at Entrance and Exit of Cylindrical Tubes", Com. on Vacuum Techniques, 1956 Vacuum Symposium Transactions.

21. Cook, Harlon, and Richley, E. A., "Measurements of Effux Patterns and Flow Rates from Cylindrical Tubes in Free Molecule and Slip Flows", NASA TN D-2480, 1964.

22. Ballance, J. A., "Transmission Probability Determination with Directed Mass Motion and with Mean Free Path Considerations," in Proceedings of the 3rd International Vacuum Symposium, Pergemon Press, Ltd., 1966.

23. Michelsen, W. R., and Kaufman, H. R., "Status of Electrostatic Thrustors for Spoa Propulsion", NASA TN D-2172, May 1964.

24. Kaufman, H. R., "An Ion Rocket with an Electron-Bombardment Ion Source", NASA TN D-585, January 1961.

25. King, H. J. and Kohlberg, I., "Low Density Arc Ion Engine Development", Interim Report No. 1 on Contract NAS8-1684, Goodrich-High Voltage Astronautics, Inc., June 1962.

26. Kaufman, H. R., "One-Dimensional Analysis of Ion Rockets", NASA TN D-261.

APPENDIX I.

PERSONNEL EMPLOYED ON PROJECT

Graduate Research Assistants

Name:	Date Employed:
Robert Irvin Balch	February 1966 - March 1966
Gerhard Paul Beduerftig	September 1964 - September 1965
Robert H. Gilbreath	May 1, 1966 - May 31, 1966
Dimitrious George Glekas	February 1964 - September 1964
Juergen Haukohl	September 1965 to February 1966
Rev. Joseph Hsiao	September 1963 - February 1964
James Edward Simmons	May 1964 - August 1965
Billy Clifford Tankersley	June 1963 - September 1963

Undergraduate Research Assistants

Name:	Date Employed:
Robert Irvin Balch	February 1965 - February 1966
Thomas James Beck	April 1965 - June 1966
James Johnson Cornelison	December 1965 - January 1966
George Donald Deerman	April 1964 - August 1965
Lawrence Edward Donahoo, Jr.	June 1965
Glennis Ray Gowens	October 1963 - May 1964
Malcolm Crawford Johnson	April 1964 - June 1965
Taylor West McLaurin	June 1965
Fred Douglas Parsons	August 1965 - June 1966
Don Patrick Reid	October 1963 - May 1964
John H. Schorn	February 1964 - May 1964

Undergraduate Research Assistants - (Continued)

Name:	Date Employed:
Jac M. Siegel	June 1965 - June 1966
James Phillip Wilson	June 1963 - September 1963

Secretaries

Name:	Date Employed:
Betty Jane Fanning	January 1964 - May 1964
Melva Jo Parsons	June 1964 - June 1966